UNIVERSITY OF URBINO "CARLO BO"

Faculty of Science and Technologies

Integrated analysis of the main environmental perturbations of the Paleogene pelagic succession in the Umbria-Marche Basin

Analisi integrata delle principali perturbazioni ambientali nella successione pelagica paleogenica del bacino umbro-marchigiano

by

Giuseppe Bancalà

XXIV CICLO - SCIENZE DELLA TERRA - GEO/01

Promoter: Prof. Rodolfo Coccioni

List of Contents

List of Figures

List of Plates

CHAPTER 1

General introduction and Summary

1.1 The Paleogene Period: a long history of environmental perturbation

The Earth planet is experiencing profound modifications. The composition of the atmosphere (e.g. greenhouse gases, reactive gases, aerosol particles) is now significantly different than it was centuries ago and global average temperatures exceed anything seen in the last thousand years. A major climatic change, probably related to the anthropogenic input of CO_2 into the atmospheric–oceanic system, is happening. The scientific interest for these profound modifications is grown with the rising awareness that human actions have an increasing influence on Earth system functioning, upon which human welfare and the future of human societies depend. But distinguishing the human from the natural impacts still remains a "grand challenge" for the scientific community. The search for successful answers will be accomplished only when we have developed a deep and real insight into the full range of natural variability of the Earth system. In fact, Earth behaves as a complex system in which the oceans, atmosphere, land, and the living and non–living parts therein, are all connected, where the endogenous and exogenous processes interact in the short and long–term.

For this reason, Earth scientists have turned increasingly to ancient time intervals, especially those in which pCO_2 was much higher than now, and in which pCO_2 changed rapidly (Zachos et al., 2008). In particular, significant interest is given to the response of the Earth system to the mechanisms involved during globally warm periods such as the early Cenozoic that represents the most recent period when a warm "greenhouse" climate prevailed on Earth. During the first ~30 Myr of the Cenozoic, Earth experienced main climatic variations from the inherited Cretaceous "greenhouse" world to the Oligocene "icehouse" world (Hambrey et al., 1991; Zachos et al., 1992, 2001).

In particular, the early Paleogene (~65–50 Ma) was characterized by high levels of CO_2 (1000–4000 ppmv), warm at high latitudes, warm in surface–and–deep oceans, and an intensified hydrological cycle (Barron et al., 1989; Lear et al., 2000; Pearson and Palmer, 2000; Tripati and Zachos, 2000; Tripati et al., 2001, 2003; Pagani et al., 2005; Jahren, 2007; Pearson et al., 2007). The early Paleogene was also a crucial interval, both for biotic evolution and environmental changes driven by this climatic long–term transition (Agnini et al., 2007). The warmest marine temperatures recorded in the latest Paleocene to early Eocene time interval (58 to 49 Ma) culminated in the Early Eocene Climatic Optimum (~53–50 Ma), when subtropical forests spread up to latitudes above 60° (Zachos et al., 2001, 2008; Pujalte et al., 2009). At that time, crocodiles, tapir–like mammals, and palm trees flourished around an Arctic Ocean with warm, sometimes brackish surface waters (Barke et al., 2011). Temperatures did not reach freezing even in continental interiors at mid to high latitudes, polar surface temperatures and global deep water temperatures were more than 10–12°C warmer than today, and polar ice sheets probably did not reach sea level, if they existed at all (Thomas et al., 2006). After that, the pCO_2 started to decline and a gradual deep–sea cooling (~7–8°C) occurred at high latitudes (Zachos et al., 2001, 2003; Wing et al., 2003; Billups

et al., 2004). The first ephemeral appearance of sea– and/or glacial–ice in the Northern Hemisphere took place at 44 Ma (Pearson and Palmer, 2000; Zachos et al., 2001; Pagani et al., 2005; Tripati et al., 2005, 2008; Moran et al., 2006). The cooling trend finally led to a major threshold at the base of the Oligocene (Miller et al., 1991), when the modern icehouse world became definitively established with the first appearance of continental ice sheets in Antarctica (oxygen isotope event Oi–1, ~33.55 Ma (e.g., Miller et al., 1991; Zachos et al., 2001, 2008; Coxall et al., 2005; Tripati et al., 2005; Lear et al., 2008).

The warming interval of the early Paleogene was interrupted by a series of transient warming events (e.g., Kennett and Stott 1991; Thomas and Zachos, 2000; Thomas et al., 2000; Bralower, 2002; Bralower et al., 2002; Cramer et al., 2003; Speijer, 2003; Hancock and Dickens, 2005; Petrizzo, 2005; Röhl et al., 2005; Bernaola et al., 2007; Kroon et al., 2007; Quillévéré et al., 2008; Bornemann et al., 2009; Coccioni et al., 2010) (Fig. 1.1). These short–lived (10^4 to 10^5 years) events, termed "hyperthermals", have been associated with changes in the carbon isotope composition of the ocean–climate system (Cramer et al., 2003). The input of carbon is evidenced by prominent negative carbon isotope excursions (CIEs) in carbonate and organic matter, as well as a deep–sea carbonate sediment dissolution interval (Zachos et al., 2004, 2005; Lourens et al., 2005; Pagani et al., 2006; Schouten et al., 2007). The presence of distinct clay layers associated with abrupt drops in carbonate content and pronounced peaks in magnetic susceptibility characterize these intervals. These levels have been interpreted as the sedimentary expression of abrupt climatic changes associated with increasing atmospheric pCO_2, substantial shoaling of the lysocline and the calcite compensation depth (CCD), and a general lowering of the carbonate saturation state (Zachos et al., 2005) potentially induced, for some events, by the dissociation of gas hydrates (Dickens et al., 1995, 1997). Accelerated hydrologic and invigorated weathering cycles inferred from more marginal settings (Bowen et al., 2004; Pagani et al., 2006; Zachos et al., 2006; Giusberti et al., 2007; Nicolo et al., 2007; Sluijs et al., 2007) might suggest an enhanced seasonality concomitant with peak humid–warming phases (Jovane et al., 2010).

Recent astronomical tuning has produced evidence showing that the maxima in short and long–term eccentricity cycles postdating prolonged minima of the very long eccentricity cycles (Lourens et al., 2005) and corresponding to insolation maxima (Galeotti et al., 2010; Jovane et al., 2010) control hyperthermal events. This implies that the hyperthermals are indeed astronomically paced. Moreover, it was suggested that the extreme seasonal contrast in both hemispheres during eccentricity maxima might have increased intermediate seawater temperatures triggering the release of methane from oceanic methane hydrates (Lourens et al., 2005). Hyperthermal events temporarily influenced foraminiferal, calcareous nannofossil, ostracod and dinoflagellate assemblages (i.e., Kelly et al., 1998; Thomas, 2003), and possibly biotic evolution may have been (at least not directly) triggered by these events (Agnini et al., 2007; Gibbs et al., 2010).

The most severe and best–studied hyperthermal was the so–called Paleocene–Eocene Thermal Maximum (PETM) occurred about 55 million years ago and lasted less than 170 kyr (Zachos et al., 2008). The PETM was so prominent that almost all the marine sedimentary records around world spanning the Paleocene–Eocene boundary have evidences of it. Among the evidences, there are a rapid and distinct decrease in the $^{13}C/^{12}C$ ratio of carbonate and organic carbon and a prominent drop in the carbonate content of deep–sea marine sediment (Zachos et al., 2005). During the PETM global temperature increased by more than 5°C in less than 10 kyr and more than 2,000 Giga tons of Carbon under the shape of CO_2 were released (Royer, 2006), leading to a 2–6‰ negative CIE in terrestrial and marine records. These findings support the hypothesis that an injection of a very large mass of ^{13}C–depleted carbon into the atmosphere or

Figure 1.1 – Global climate evolution through the Paleogene Period modified from Zachos et al. (2008) and Westerhold et al. (2011). Absolute ages are relative to GPTS2004 (Ogg and Smith, 2004). Stacked deep–sea benthic foraminiferal $\delta^{18}O$ and $\delta^{13}C$ data are based on records from Deep Sea Drilling Project and Ocean Drilling Program sites (Zachos et al., 2008). The raw data were smoothed by using a 1 million year running mean (thick red line). The $\delta^{18}O$ temperature scale was computed on the assumption of an ice–free ocean; it therefore applies only to the time preceding the onset of large–scale glaciation on Antarctica (~35 Ma). Indicated by arrows are several environmental perturbation including the Mid–Eocene Climatic Optimum, Early Eocene Climatic Optimum, and short–lived Paleocene–early Eocene hyperthermals such as for example, the PETM (ETM1) and Eocene Thermal Maximum 2 (ETM2). See Text for details about hyperthermal magneto–biostratigraphy and references. Primary components of North Atlantic Igneous Province (NAIP Phase 1–2) and Deccan Trap volcanism are adapted from Sinton and Duncan (1998) and Chenet et al. (2007), respectively. Paleogeographic reconstruction made using the Web–based software at http://www.odsn.de/odsn/index.html (Hay et al., 1999).

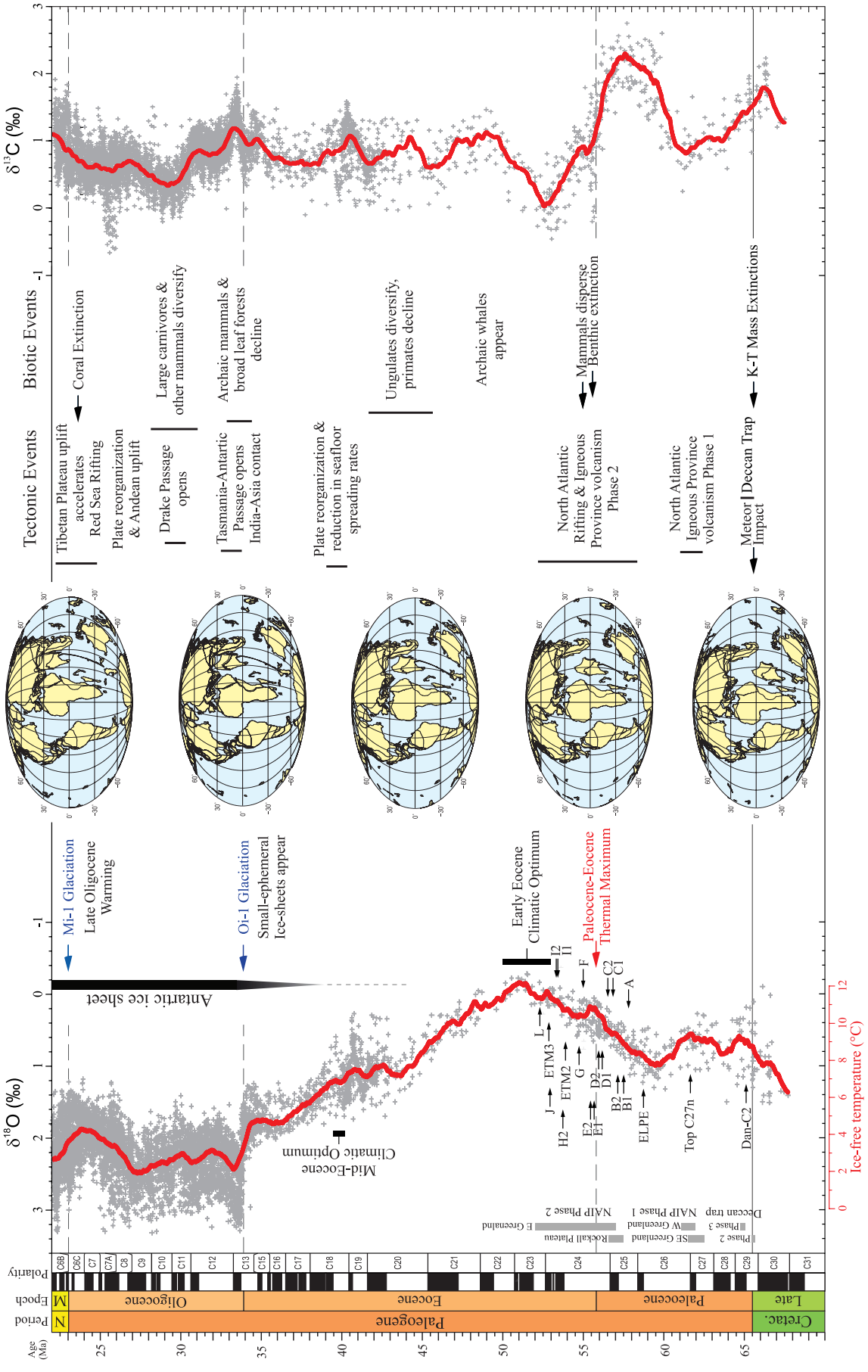
Tectonic Events
Biotic Events
δ13C (‰)
Tibetan Plateau uplift accelerates Red Sea Rifting
Coral Extinction
Plate reorganization & Andean uplift
Drake Passage opens
Large carnivores & other mammals diversify
Tasmania-Antartic Passage opens India-Asia contact
Archaic mammals & broad leaf forests decline
Plate reorganization & reduction in seafloor spreading rates
Ungulates diversify, primates decline
Archaic whales appear
North Atlantic Rifting & Igneous Province volcanism Phase 2
Mammals disperse Benthic extinction
North Atlantic Igneous Province volcanism Phase 1
Meteor Impact
Deccan Trap
K-T Mass Extinctions
Mi-1 Glaciation
Late Oligocene Warming
Oi-1 Glaciation
Small-ephemeral Ice-sheets appear
Antartic ice sheet
Early Eocene Climatic Optimum
Paleocene-Eocene Thermal Maximum
Mid-Eocene Climatic Optimum
δ18O (‰)
Ice-free temperature (°C)
Age (Ma)
Period
Epoch
Polarity
Cretac.
Late
Paleogene
Palaeocene
Eocene
Oligocene
Deccan trap
NAIP Phase 1
NAIP Phase 2
Rockall Plateau
E Greenland
SE Greenland
W Greenland
Phase 2
Phase 3

ocean, altering the composition of the global carbon cycle, while ocean acidification co–occurred. This global perturbation affected the biosphere and is also expressed in major faunal turnover. The most severe extinction event in benthic foraminifera in the last 90 Ma (Tjalsma and Lohmann, 1983) took place within the PETM with a diversification in the surface waters (Kelly et al., 1996; Crouch et al., 2001).

The PETM was preceded and followed by other transient CIEs possibly related to other warming events (e.g. Speijer, 2000, 2003a; Thomas and Zachos, 2000; Cramer et al., 2003; Lourens et al., 2005; Petrizzo, 2005; Bernaola et al., 2007; Nicolo et al., 2007; Quillévéré et al., 2008; Agnini et al., 2009; Stap et al., 2009; Coccioni et al., 2010). However, the precise number of such events, their ages and durations, and their characteristics remain uncertain. Presently, it is not obvious whether they are all truly global in nature and causally related (Cramer et al., 2003; Nicolo et al., 2007; Westerhold et al., 2007; Quillévéré et al., 2008). Since the lesser events have been mostly documented from condensed deep–sea settings, where incomplete recovery and dissolution have impacted sedimentary records (Nicolo et al., 2007), much work remains to be done to understand the nature of early Paleogene hyperthermals.

In the lower Paleogene, the most ancient hyperthermal event recognized just 300 kyr after the K/Pg Boundary, was the so–called Dan–C2 event, placed in the uppermost part of magnetochron C29r (Quillévéré et al., 2010; Coccioni e al., 2010). Severe environmental and biotic perturbations were recorded along the water column and at the seafloor while sea–surface temperatures (SSTs) rose of ~ 4°C and shoaling of the lysocline and the CCD took place (Quillévéré et al., 2008; Coccioni et al., 2010). Only few tens thousands years after the Dan–C2 event, another suspected and poorly studied hyperthermal occurred in the lower part of magnetochron C29n ("Lower C29n" event of Coccioni et al., 2010). From the Dan–C2 event to the Danian–Selandian Boundary, oxygen and carbon stable isotope values, Fe intensities and relatively lower carbonate values, show a very complex pattern, suggesting an interval of multifaceted perturbation in carbon cycle and in the climate state (Kroon et al., 2007; Westerhold et al., 2008; Coccioni et al., 2010). Recent findings provide the evidence of another suspected hyperthermal at the top of the chron C27n, in the proximity of the Danian–Selandian Boundary, named the Latest Danian Event (Speijer, 2000, 2003a; Bornemann et al., 2009; Youssef, 2009; Sprong et al., 2011). This event can be correlated to a carbon isotope excursion ("CIE–DS1") at Zumaia, Spain (Arenillas et al., 2008; Dinarès–Turell et al., 2010) and to the "top Chron C27n event", defined recently from ocean drilling sites in the Atlantic and Pacific (Westerhold et al., 2008, 2011).

In the late Paleocene, just few million years before the PETM, another severe environmental perturbation occurred. The Early Late Paleocene event (ELPE, Bralower et al., 2002; Petrizzo, 2005), also known as the Mid–Palaeocene Biotic Event (MPBE, Bernaola et al. 2007), has been recognized in several deep sea cores from the Shatsky Rise (ODP Leg 198, central Pacific), Walvis Ridge (ODP Leg 208, South Atlantic), Maud Rise (ODP Leg 113, Weddell Sea) and Black Nose (ODP Leg 171, North Atlantic) as well as in on–land Spanish sections (Zumaia and Ibaeta) (Bralower et al., 2002; Zachos et al., 2004; Petrizzo, 2005; Bernaola et al., 2007). This hyperthermal event was first described at the Shatsky Rise (ODP Sites 1209, 1210, 1211 and 1212) as a prominent 5– to 25 cm–thick clay–rich calcareous nannofossil ooze layer centered at ~58.4 Ma. It falls in the lower planktonic foraminiferal P4 Zone of Berggren et al. (1995) and coincides with the evolutionary lowest occurrence of *Heliolithus kleinpellii*, which marks the base of calcareous nannofossil Zones NP6 of Martini (1971) and CP5 of Okada and Bukry (1980) (Bralower et al., 2002). Planktonic foraminifera in the ooze layer are characterized by a low–diversity, largely dissolved assemblage dominated by representatives of the genus *Igorina* (mainly *I. pusilla* and *I. tadjikistanensis*) as described by Petrizzo (2005) at Shatsky Rise.

In the early Eocene, other several negative CIEs, including the Eocene Thermal Maximum 2 (ETM2) and the X event took place (Kennett and Stott, 1991; Thomas and Zachos, 2000; Bralower et al., 2002; Cramer et al., 2003; Lourens et al., 2005). In particular, the ETM2 (also referred to as H1 of Cramer et al., 2003, and Elmo of Lourens et al., 2005) was a distinct period of global warming at ~ 53,6 Ma, approximately 2 Myr after the PETM (Lourens et al., 2005; Stap et al., 2009, 2010a–b; Agnini et al., 2009, Galeotti et al., 2010). Similar as for the PETM, ETM2 is marked by a pronounced negative CIE, recorded in both carbonate and organic carbon sedimentary components, and by a distinct carbonate dissolution horizon in deep–sea sediments, suggesting the emission of large amounts ^{13}C–depleted carbon into the ocean–atmosphere system (Lourens et al., 2005;

Zachos et al., 2005; Sluijs et al., 2009). In particular, during the ETM2, oxygen and carbon stable isotope benthic records from the southeastern Atlantic, suggest a 3°C increase in deep–sea temperatures and a CIE of −1.4‰ (Stap et al., 2010a), both approximately half the PETM magnitude. Noteworthy, the $\delta^{13}C$ change of the exogenic carbon pool was related to warming in a similar way during both events, despite the much more gradual onset of ETM2 (Stap et al., 2010a). Along with the PETM and ETM2, a number of punctuated smaller negative CIEs (termed A to L) occurred during the Early Eocene (Cramer et al., 2003). Unfortunately, the approximate magnitude of deep–sea warming during these events has not yet been established (Cramer et al., 2003; Nicolo et al., 2007; Stap et al., 2010b). One of these events, H2, took placed ~100 kyr after the ETM2 event, and was characterized by a CIE of –0.2‰ to –0.7‰ in high–resolution bulk carbonate records from deep–sea and continental slope environments (Cramer et al., 2003; Nicolo et al., 2007; Stap et al., 2009).

In addition, Cramer et al. (2003) have identified at least six events (i.e., H1, H2, I1 I2, J, and K) in the Pacific and Atlantic Oceans in the lower–middle Eocene between the upper part of Chron C24r and Chron C24n. Some of these events have been also found and clearly correlated in South Atlantic, the Arctic Ocean and New Zealand (Zachos et al., 2004; Nicolo et al., 2007; Sluijs et al., 2008a) and perhaps in the North Sea (Sluijs et al., 2008b). This very rapid succession of events in the lower–middle Eocene between chrons C24r and C24n, still remains poorly understood (Agnini et al., 2009; Stap et al., 2010). More in details, the H1 and K events observed at DSDP Site 577 are clearly correlative to the Elmo and X events both at Site ODP 1262 (Lourens et al., 2005; Röhl et al., 2004), at the Possagno Section (Agnini et al., 2009) and at Contessa Road Section (Galeotti et al., 2010). These minor events recorded also in the Pacific (e.g., the H1, H2, I1, I2), are correlated with magnetic susceptibility spikes at Site 1262 (Nicolo et al., 2007), because of the lacking of an accurate carbon and oxygen isotopes record at this site.

As previously described, the warmest Paleogene temperatures were reached during the Early Eocene Climatic Optimum (EECO) as indicated by multiple proxy mean annual temperature estimates for sea and land surfaces (Zachos et al., 2001, 2008). The EECO onset is placed in the Chron interval C24r–C24n, and correlative to the $\delta^{18}O$ decreasing (warming) trend leading to the climax phase of the event (Zachos et al., 2008). The highest temperatures and $\delta^{18}O$ minima were reached in the Chron C23n (Agnini et al., 2006). Woodbourne et al. (2009) document an impressive plant and mammal faunal turnover related to the EECO, as a consequence of a direct primary evolutionary control played by the EECO warmth. New evolutionary trends in calcareous nannofossil assemblages took place in the marine realm, while a severe planktonic foraminiferal response to this long–term environmental perturbation has recorded (Agnini et al., 2006; Luciani et al., 2011). Beginning within C23n–C22r interval, the end of EECO is globally expressed by the onset of increasingly cooler deep–water temperatures and by the onset of the long–term cooling trend towards the icehouse world (Shackleton, 1986; Zachos et al., 2001). This trend has been attributed to the permanent removal of atmospheric CO_2 by enhanced silicate weathering (Raymo and Ruddiman, 1992; Walker et al., 1981; Smith et al., 2008) and/or enhanced burial of organic carbon (France–Lanord and Derry, 1997). New oxygen–isotope records and tropical SST reconstructions have revealed that the cooling probably largely took place at higher latitudes (Pearson et al., 2007). In particular, a relatively sudden drop in pCO_2 values during the EECO, within the interval between magnetochrons C24n.3n and C23n, was revealed by boron–based pH reconstructions (Pearson and Palmer, 2000; Bralower and Mutterlose, 1995). Moreover, a lowering of the sea level (Miller et al., 2005) as well as an increase in deep–sea strontium isotope values (Hodell et al., 2007), support the assumption of a decrease in volcanic CO_2 outgassing. Subsequently, global deep–sea benthic oxygen–isotope records reflect the onset of the long–term cooling trend at the termination of the EECO (Zachos et al., 2001). All these data might suggest that the cooling trend was driven by the combined effects of both a decline of greenhouse gases due to weathering and a decrease in CO_2 outgassing. The global cooling trend following the EECO, was non–monotonic, and was interrupted, in the middle Eocene, by a warming event, designated as the Middle Eocene Climatic Optimum (MECO) (Bohaty and Zachos, 2003; Bohaty et al., 2009). Firstly identified in the Atlantic and Indian sectors of the Southern Ocean (Barrera and Huber, 1993, Bohaty and Zachos, 2003), the MECO recently, seems to be recorded worldwide by distinct changes in $\delta^{13}C$ and $\delta^{18}O$ values and coeval oscillations in global CCD (Tripati et al., 2005; Bohaty et al., 2009). In particular, the hallmark of the event, centered at

~40.0 Ma, is a distinct negative shift in $\delta^{18}O$ values and a marked positive increase of $\delta^{13}C$ (Bohaty and Zachos, 2003; Sexton et al., 2006; Bohaty et al., 2009). During the MECO (Bohaty and Zachos, 2003; Bohaty et al., 2009), Southern Ocean deep water temperatures warmed up to 4°C and lasted for ~500 kyr before rapidly cooling. Moreover, a significant increase in pCO_2 has recently estimated by Bijl et al. (2010), leading values up to 2000–3000 ppmv. As a response, severe environmental perturbations were induced along the column water, as testified by remarkably changes in calcareous nannofossils assemblages, transient symbiont bleaching (loss of photosymbionts) of planktonic foraminifera (Edgar et al., 2011), and alteration of benthic foraminifera communities (Boscolo Galazzo et al., 2011). As partly possible triggering mechanisms differently from the PETM, Bijl et al. (2010) hypothesized the massive decarbonation, with the subduction of Tethyan Ocean pelagic carbonates under Asia as India drifted northward. The transient increase in pCO_2 has been inferred by the change in ocean chemistry as revealed by the net decline in carbonate accumulation reflecting the widespread shoaling of the lysocline in several records (Bohaty et al., 2009).

After the MECO event, the long–term cooling trend restarted, and culminating with the first appearance of permanent continental ice sheets in Antarctica (oxygen isotope event Oi–1, ~ 33.55 Ma (e.g., Miller et al., 1991; Zachos et al., 2001, 2008; Coxall et al., 2005; Tripati et al., 2005; Lear et al., 2008), leading the world into the modern icehouse climate state.

In conclusion, the Paleogene Period was characterized by a long history of environmental perturbation that had conducted the Earth complex system to the modern state where humankind grew–up. Over the last decades the research effort has shed light on this multifaceted period but much work has still to be done to deeply understand relationships between carbon cycling and climate events, feedback–mechanisms, possible causes, and biotic response to environmental changes at short– and long–term.

1.2 Possible causes of the main Paleogene environmental perturbations

Over the last decades, the possible causes and mechanisms for the long–term Paleogene climatic evolution has been a debated issue, and it is still far from being over. Most likely, during the greenhouse–icehouse transition, a complex interaction of different factors is accountable for the variations in the amount and distribution of solar radiation, heat transport and either direct or indirect, consequently reduction in pCO_2. Several mantle related large–scale processes have been also invoked to explain the greenhouse–icehouse transition. Among a number of hypotheses for possible causes, there are 1) changes in regional/global paleogeography, 2) open/closure of oceanic gateways, 3) variation in sea level related to expansion of mid–ocean ridge and/or oceanic plateau volumes, and changes in rate of mantle or volcanically emitted CO_2 (e.g., Frakes and Kemp 1972; Shackleton and Kennett 1975; Berggren and Hollister 1977; Kennett 1977; Fisher and Arthur 1977; Schnitker 1980; Owen and Rea, 1985; Barron 1985; Lasaga et al., 1985; Wise et al. 1985; McGowran 1989, 1990; Arthur et al. 1991; Zachos et al., 1993; Huber and Sloan, 2001; Lawver and Gahagan, 2003; Barker et al., 2007; Livermore et al., 2007). In particular, during the late Paleocene–Oligocene interval, when the climatic transition reached its acute phase, a series of major paleogeographic events occurred. Among them, worthy of mention, there are: coupling of the opening of the Australia–Antarctic and Drake Passage (Lawver and Gahagan, 2003) with the isolation of Antarctica, the beginning of the Arabian–Eurasian continent–continent collision, expressed as arc magmatism, the establishment of the Alpine–Himalayan chain and its subsequent aridification (Dupont–Nivet et al., 2007), and low–latitude silicate weathering (Raymo and Ruddiman, 1992) in relation to previous collisional event. Recently, based on Eocene data from the Neo–Tethys sector, Jovane et al. (2007a,b, 2009) have proposed a corollary component to this global climatic transition, the so–called "STENT" current hypothesis. Following this hypothesis, the fluctuations and final termination of a westward sub–tropical Eocene Neo–Tethys (STENT) current, played a major role in the climatic transition from greenhouse to icehouse conditions. During the Paleogene, the Neo–Tethys represented a large–scale key ocean–gateway for global circulation. Flowing through the Neo–Tethys, the STENT current constituted a global heat conveyor, able to maintain temperate high latitudes, but it was weakening in stream while increased formation of deep–water began in the North Pacific (Thomas, 2004), Southern Ocean (Scher and Martin, 2004), and North Atlantic (Via and Thomas, 2006). The concurrent tectonic closure of the gateway between the Arabian and Eurasian plates represents a threshold inducing late Eocene paleoceanographic variations in

the Neo–Tethys and as a consequence, in global ocean circulation, stopping progressively the STENT current by a switching on–and–off process (Jovane et al., 2007a,b, 2009). As previously described, at least seven transient warming events analogous in character to the PETM, but less severe in magnitude and duration, have been discovered in multiple records throughout the early Paleogene (Dan–C2 at ~65.2 Ma, ELPE/MPBE at ~58.2 Ma, ETM2/H1/ELMO at ~ 53.8 Ma, H2 at ~53.6 Ma, I1 at ~53.3 Ma, I2 at ~53.2 Ma, K/X ~52.5 Ma) (Zachos et al., 2005; Rohl et al., 2007; Zachos et al., 2008; Thomas et al., 2000; Cramer et al., 2003; Lourens et al., 2005; Petrizzo, 2005; Sexton et al., 2006; Westerhold et al., 2007; Edgar et al., 2007; Nicolo et al., 2007; Quillevere et al., 2008; Stap et al., 2010; Coccioni et al., 2010). The PETM is widely attributed to massive release of greenhouse gases from buried sedimentary carbon reservoirs (Zachos et al., 2005; Zachos et al., 2008; Lourens et al., 2005; Nicolo et al., 2007; Dickens, 2000; Dickens et al., 2003; Panchuk et al., 2008) and the other, comparatively modest, hyperthermals have also been linked to the release of sedimentary carbon Zachos et al., 2008; Lourens et al., 2005; Dickens et al., 2003; Nicolo et al., 2007; Panchuk et al., 2008). Like the PETM, hyperthermal events display evidence for Earth surface warming (including for some of them, in the deep–sea), large CIEs of surficial carbon reservoirs and dissolution of deep–sea carbonate (Zachos et al., 2010). This might be consistent with massive injections of ^{13}C–depleted carbon into the ocean–atmosphere system. These evidences coupled with the number of hyperthermals and the relative temporal spacing between some of them, suggest the existence of a possible common operative mechanism (Cramer et al., 2003; Lourens et al., 2005; Nicolo et al., 2007; Sexton et al., 2011). An important step to understanding the origin of the hyperthermals is to place them in the proper temporal context of short and longer–term variations in climate and the carbon cycle. Moreover, with recent available published data, some of these events seem coupled to orbital forcing and to have a relationship between magnitude and time (Lourens et al., 2005; Nicolo et al., 2007; Agnini et al., 2009; Stap et al., 2009, 2010; Galeotti et al., 2010; Leon–Rodriguez and Dickens, 2010; Zachos et al., 2010). Recent work has focused on elucidating the injection mechanism(s) and volume of the carbon that caused CIEs, but has also addressed the question whether the ^{13}C–depleted carbon caused the warming or acted as a positive feedback in an already warming world (Sluijs, 2008; Luhnt et al., 2011; Sexton et al., 2011). Some evidence of an orbital pacing control of the timing of carbon injection were found recently for the occurrence of PETM, ETM2 (ELMO), and ETM3 (X) events (Lourens et al., 2005; Westerhold et al. 2007, Galeotti et al., 2010). Cyclostratigraphic evidence suggests that at least these events initiated on maxima in the 100 kyr eccentricity cycle (Lourens et al., 2005; Westerhold et al., 2007, Galeotti et al., 2010). Nevertheless, there are no published explanation of how a strong imprint of orbital cycles on early Paleogene terrestrial (Abdul–Aziz et al., 2008), shallow (Sluijs et al., 2008), or deep marine sediments (Röhl et al., 2003; Westerhold et al., 2007) can arise (Lunt et al., 2011). On the whole, the real source or sources of massive carbon injections during early Cenozoic hyperthermals still remain uncertain. However, over the last decades, some hypotheses have been proposed for the ^{13}C–depleted carbon sources, including 1) methane hydrates (Dickens et al., 1995; Dickens et al., 2005; Dickens, 2011; Lunt et al., 2011), 2) oxidation of terrestrial biomass (which is suggested to have initiated the release of CO_2 to the atmosphere) (Kurtz et al., 2003), 3) thermogenic methane (Svensen et al., 2004) and more recently, 4) releases of dissolved organic carbon from the ocean by ventilation (Sexton et al., 2011). Among these hypotheses, the most controversial and widely cited explanation for this carbon input has been the thermal dissociation of methane gas hydrate (Dickens, 2011). The gas hydrate dissociation is followed by release of massive CH_4 from the seafloor and its subsequent oxidation to CO_2 in the ocean or atmosphere (Dickens et al., 1995; Dickens et al., 2005; Dickens, 2011; Lunt et al., 2011). Gas hydrates are crystalline compounds involved water and low molecular weight gas (especially CH_4) forming at relatively high pressure and relatively low temperature. It's well–known that CH_4 in modern gas hydrate systems is extremely depleted in ^{13}C (typically $<-60‰$, Milkov, 2005). The CH_4 in gas hydrates is dominantly generated by bacterial degradation of organic matter in low oxygen environments. Where sedimentation rates and the organic carbon content are high, the pore waters in the sediments are already anoxic few centimeters below the seafloor, and CH_4 is produced by anaerobic bacteria. This production of CH_4 is a rather complicated process, requires the activity of several varieties of bacteria, a reducing environment (Eh < 400 mV), and a pH between 6 and 8. High concentrations of CH_4 have accumulated in

sediment pore space along modern continental margins, where gas hydrates are largely stored (Kvenvolden, 1993; Archer, 2007). These crystalline compounds are confined within a lens–shape volume of sediments under the gas hydrate stability zone (GHSZ), between the seafloor and a sub–bottom horizon down continental slopes. The intersection of the gas hydrate–free gas phase boundary and geotherm, drives the expansion of the GHSZ and consequentially, the sediment volume dimension that contains the gas hydrates. Although several factors control the extent of the GHSZ, the seafloor temperature is invoked to play a major role at present–day, and presumably throughout geological time (Dickens, 2001). According to the gas hydrate dissociation hypothesis of Dickens et al. (1995), as first step, it is necessary that deep ocean temperatures rose rapidly since some Earth system threshold was overstepped for some reason. After that, as warmth took place and subsequently propagated into sediment on continental slopes, the base of the GHSZ shoaled, and converted large amounts of gas hydrate to large amount of free CH_4 gas (nominally 2000–3000 Gt C) (Dickens, 2003). The free CH_4 gas escaped subsequently from marine sediment through slumping or venting and diffused from bottom to top in the water column (Dickens, 2003) generating CO_2 injection by methane oxidation. In the last few years, renewed support for the overall hypothesis has been forwarded. As suggested by some stratigraphic records at several locations, environmental change might preceded the ^{13}C excursion as it was found for the PETM and other hyperthermals (Thomas et al., 2002; Sluijs et al., 2007; Harding et al., 2011; Secord et al., 2010; Coccioni et al., 2010; Handley et al., 2011). This includes increase in ocean temperature, which may have been on the order of some degrees and over several thousands of years before the onset of the CIEs that might induced the methane hydrates dissociation (Sluijs et al., 2007). More recently, based on a series of coupled climate model simulations, Lunt et al. (2011) suggest that orbitally induced changes in ocean circulation and intermediate water temperature might have triggered the destabilization of methane hydrates during the early Paleogene. More in details, the change in ocean circulation was probably caused by the shift from minimum in eccentricity to a maximum in Southern Hemisphere seasonality orbit. This transition was associated with a significant reduction in deep water formation in the Southern Ocean, and was also characterized by anomalous warming patterns of intermediate waters (Lunt et al., 2011). The intermediate water temperature, has been assumed to be critical in the stability of methane hydrate during the Paleogene (Dickens et al., 2003; Lunt et al., 2011). In this way, a plausible link between sedimentary carbon inventory, orbital changes and dissociation of methane hydrate is given (Lunt et al., 2011). However, there are some arguments against gas hydrate dissociation hypothesis. Among them, there is the idea that massive CH_4 input from the seafloor would have been a positive feedback to warming caused by other mechanisms, and could not represent the main trigger for carbon injection and consequently hyperthermal events (Dickens et al., 1995, 1997; Higgins and Schrag, 2006; Pagani et al., 2006a; Archer, 2007; Dickens, 2011; Handley et al., 2011; McInerney and Wing, 2011) Another hypothesis for the ^{13}C–depleted carbon sources has been proposed by Kurtz et al. (2003). During the early Paleogene, extensive burning of land–peat deposits might have released massive amounts of ^{13}C–depleted carbon in the order of ten thousands of Gt, potentially induced the PETM and possibly the other hyperthermals. This would require a large land–peat reservoir at least 10 times the mass of the modern peat reservoir (Higgins and Schrag, 2006; Page et al., 2011). Some evidences arise from early Paleocene, when large deposition of lignite and coal occurred throughout North America and Eurasia (Duff, 1987; Ellis et al., 1999; Nagy, 2005; Ross and Ross, 1984). Interestingly, early Paleocene coals were largely produced in coastal swamps (Warwick and Stanton, 1988). This would suggest a primarily climatic control on wetland extent and more specifically on seasonal distribution of precipitation, which in turn should be sensitive to eccentricity (Morrill et al., 2001; Valdes and Glover, 1999; Zachos et al., 2010). In particular, at low latitudes, differential land–sea heating and seasonal climate cycles have been thought to be controlled by precession which, in turn, might be able to enhance the climate effects of eccentricity (Crowley et al., 1992; Short et al., 1991). As suggested by Zachos et al. (2010), during eccentricity maxima, intense, but short wet seasons are followed by prolonged dry seasons, whereas during eccentricity minima, annual precipitation was seasonally more uniform. During eccentricity minima, low seasonality associated with uniform precipitation should be more favorable for maintaining wetlands and accumulating peat, and consequently increasing organic carbon burial. When eccentricity increased, high seasonality induces

prolonged dry seasons would overturn the trend, decreasing the accumulation of organic carbon, through desiccation and oxidation of existing peat or lignite. In this way, huge amount of CO_2 would be released, amplifying seasonality with an enhancement warming (Meehl et al., 2007), and more important, providing a potential positive feedback for fueling the hyperthermals (Kurtz et al., 2003; Wing et al., 2005; Zachos et al., 2010). A different hypothesis for a ^{13}C–depleted carbon source was suggested by Svensen et al. (2004) that postulated Intense hydrothermal vent complexes activity in the Norwegian Sea during the early Paleogene. Intrusion of voluminous mantle–derived melts in carbon–rich sedimentary strata in the northeast Atlantic may have caused an explosive release of methane transported to the ocean or atmosphere through the vent complexes–close to the Palaeocene/Eocene boundary. Even if not directly related to methane hydrates, similar volcanic and metamorphic processes may be invoked for the other abrupt hyperthermals events, associated with large igneous provinces eruption such as the Deccan Traps in the early Danian for the Dan–C2 event (Coccioni et al., 2010) More recently, Sexton et al. (2011) reported at least 13 negative excursions of $\delta^{18}O$ values indicative of short–term warming (~2–4°C) through the early Eocene–middle Eocene transition (47.6–50.0 Myr ago) based on a very long benthic and planktonic foraminifer stable isotope record from Demerara rise in the tropical western Atlantic Ocean (Ocean Drilling Program Site 1258). At the same time, these excursions are accompanied by a shift to lower $\delta^{13}C$ planktonic and benthic foraminifer values, suggesting probably a whole–ocean decrease in $\delta^{13}C$ total dissolved inorganic carbon. In addition, each short–warming event lasted ~40 kyr, and spaced ~100–400 kyr apart. They also shared a very rapid development phase (5–10 kyr) and a more slowly recovery phase to background temperatures values (over ~30 kyr). Since the duration of these hyperthermals is similar to the 41–kyr obliquity cycle, Sexton et al. (2011) hypothesized that the forcing for individual events was related to obliquity pacing of high latitude surface ocean stratification, which in turn controlled carbon ventilation (via oxygenation), as proposed for the last deglaciation (Sigman et al., 2007). Since the recharge times of the abyssal, are rapid compared to the slow, multi–million–year filling of sedimentary methane hydrate reservoirs, carbon dioxide ventilation might represent a more plausible mechanism with which to sustain the repeated, frequent carbon releases that define hyperthermals over the early Paleogene (Sexton et al., 2011). This might represent an alternative potential source. Furthermore, Sexton et al. (2011) hypothesized that hyperthermals seems to be mutually exclusive to external sedimentary carbon sources. The ^{13}C–depleted carbon that fuelled the hyperthermals was probably redistributed within the readily exchangeable reservoirs at Earth's surface, although some of this carbon may have come from the terrestrial biosphere, possibly acting as a feedback to a primary source (Sexton et al., 2011).

In conclusion, the mechanisms and possible causes of the main early Paleogene environmental perturbations still remain answered. Much work has been done to reveal nature, timing, causes and effects of hyperthermals and other events, but there is still a long way to go to get a real deep insight.

1.3 Objectives and outline of this study

The principal aim of this PhD project was to investigate some main environmental perturbations in the Paleogene pelagic succession of the Umbria–Marche basin from the Cretaceous–Paleogene boundary to the early Eocene. To reach this objective, several integrated analyses were performed on some critical intervals to constrain where these environmental perturbations are expected to occur. Each integrated analysis was based on abiotic (carbonate content, $\delta^{13}C$ and $\delta^{18}O$ stable isotopes, magnetic susceptibility, environmental magnetism) and biotic (quantitative analysis on calcareous nannofossils, planktonic and benthic foraminifera) parameters, in order to have a real deep insight into the whole paleoceanographic and paleoecological conditions. Integrated analyses results are utilized not only to identify possible environmental perturbations, but also to reveal and estimate potential environmental effects along the water column and on biotic communities (calcareous nannofossil and foraminifera) and finally, to discuss global implications. More details about materials and methods utilized for this Phd project are given in each following chapters.

To follow, a summary of the main aspects of each chapter is given.

In **Chapter 2,** it is presented and discussed a high–resolution biochronostratigraphic and magnetic susceptibility data and geochemical records from the western Tethyan Contessa

Highway section (Gubbio, Italy), which provide the first direct evidence of the Dan–C2 event beyond the Atlantic Ocean and point to the supra–regional, possibly global, significance thereof. At Contessa Highway, the Dan–C2 event exhibits stressed ecological responses among calcareous nannoplankton and foraminifera, which highlight marked environmental perturbation affecting the geobiosphere and resulting in enhanced eutrophication of the sea surface waters and carbonate dissolution, as well as lowered oxygen content along the water column and at the sea bottom. As for other early Paleogene hyperthermal events, the cause of the Dan–C2 event might likely to be found in changes, potentially astronomically paced, in the distribution of carbon within surface biosphere reservoirs. However, the role played by the concurrent third and last phase of Deccan volcanism with its huge release of greenhouse gases into the atmosphere would be also taken into account.

In addition, first evidence of a further short–lived (~38 kyr) hyperthermal event (here termed the "Lower C29n" event) not known up to now are provided.

In **Chapter 3,** a ~250 kyr long event of environmental disruption during the Paleocene, here named Selandian–Thanetian Transition Event (STTE), has been recognized in the Western Tethys Contessa Road section (Gubbio, Italy). The uppermost part of the STTE includes the suspected short–lived hyperthermal event known as the early late Paleocene event (ELPE) or mid–Paleocene biotic event (MPBE), which therefore would become part of a more complex scenario. It is presented and discussed high–resolution biochronostratigraphic and geochemical records, and magnetic susceptibility and environmental magnetism data from the western Tethyan Contessa Road section (Gubbio, Italy). The STTE falls within the middle–lower part of the planktonic foraminiferal Zone P4b and calcareous nannofossils Zone NP6 with its onset placed in the uppermost part of Chron C26r. The STTE exhibits peculiar stressed ecological responses among calcareous nannofossils and foraminifera, which highlight marked environmental perturbation affecting the geobiosphere. The environmental instability is not confined within the photic zone but extends to the seafloor leading to little more trophic conditions of the sea surface waters with an enhanced, but of short measure, nutrient availability on the seafloor under almost unchanged warm–water conditions and marked rise of lysocline. Further studies are needed to understand whether the STTE represents a regional or global event. However, an abrupt environmental perturbation close to the Selandian–Thanetian transition has been observed in other Tethyan as well as open ocean sites suggesting that the STTE might be a possible global prelude to the PETM.

In **Chapter 4,** it is presented and discussed detailed analyses of calcareous nannofossils and foraminiferal assemblages, and high–resolution geochemical, isotopic and magnetic records across the middle Ypresian at Contessa Road (Gubbio, Italy) that allow to better constrained the Eocene Thermal Maximum 3 (K or X) and four minor (I1, I2, J, L) suspected hyperthermals. At Contessa Road, the ETM3 is characterized by prominent and short–live negative excursions in both $\delta^{13}C$ and $\delta^{18}O$ and marked changes in the rock magnetic properties. The ETM3 testifies stressed ecological responses among calcareous nannoplankton and foraminifera, which highlight marked environmental perturbation affecting the geobiosphere and resulting in warmer and more oligotrophic sea surface waters and carbonate dissolution. Although, the magnitude and effect of ETM3 appear less intense then the well–known PETM and ETM2, the input of a large mass of isotopically depleted carbon into the ocean and atmosphere may have altered the deep–sea pH, triggering a rapid and transient shoaling of the lysocline and contributing to a greenhouse warming. As for other early Paleogene hyperthermal events, the cause of the ETM3 event is likely to be found in changes, in the distribution of carbon within surface biosphere reservoirs, likely controlled by orbital cycles.

In **Chapter 5**, it is presented and discussed, a high–resolution study of the Tethyan Contessa Highway reference section (Gubbio, Italy), that has produced a detailed, well–constrained and more complete pattern of the gradual evolutionary origin of the foraminiferal genus *Hantkenina* from *Clavigerinella* than hitherto shown. A nine–stage pattern is presented for this evolutionary lineage and the related time−frame and duration are assessed using the astronomical calibration of the Contessa Highway record. The evolution of *Clavigerinella caucasica* to *Hantkenina gohrbandti*, the real ancestor of *Hantkenina*, occurred in 333 kyr with the *H. gohrbandti* first

appearance dated at 45.564 Ma. These findings show that during the middle Eocene, from 46 to 45.5 Ma and with a major pulse centered at 45.521 Ma deep−mesopelagic planktonic foraminifera may have developed different morphological modifications, principally related to poorly oxygenated and usually food−poor waters, to tolerate temporary exceptionally stressful environmental conditions. This suggests that sustained and expanded oxygen minimum zone conditions and associated enhanced eutrophication might have occurred during that time.

In **Chapter 6,** synthetic conclusions are presented.

1.4 General geological and stratigraphic setting

One of the most studied Tethyan Paleogene sequence is located in the Umbria–Marche Basin (UMB) (northeastern Apennines of central Italy) and is characterized by a remarkable record of many crucial aspects of Earth history from the Cretaceous/Paleogene (K/Pg) boundary through to the Upper Oligocene including hyperthermals events (e.g., Coccioni et al., 1986, 1988, 1989, 1994, 2008, 2009, 2010; Cresta et al., 1989; Bellagamba and Coccioni, 1990; Mattias et al., 1992; Brinkhuis and Biffi, 1993; Premoli Silva and Jenkins, 1993; Lowrie and Lanci, 1994; Montanari et al., 1994, 1997; Galeotti et al., 1998, 2000, 2004, 2010; Montanari and Koeberl, 2000; Spezzaferri et al., 2002; Coccioni and Galeotti, 2003; Bodiselitsch et al., 2004; Jovane et al., 2006, 2007a, 2007b, 2009, 2010; Brown et al. 2009; Giusberti et al., 2009; Hyland et al. 2009; Pross et al., 2010; and reference therein). Extensive outcrops in the UMB provide a complete sequence of Paleogene carbonate sediments, which have offered an unusual opportunity to stratigraphers. The deposition was continuous through the Paleogene Period, in a pelagic setting at middle to lower bathyal depths (1000–1500 m) (Galeotti et al., 2004; Jovane et al., 2007a Giusberti et al., 2009; Coccioni et al., 2010), above the CCD with a rather modest tectonic overprint and at ~30°N paleolatitude (Jovane et al., 2010) (Fig. 1.2) These exceptionally oceanographic conditions have led to the availability of an excellent age control through magneto–, bio–, chemostratigraphy, that have allowed to construct an integrated stratigraphic framework for the Paleogene period, here summarized in the Figure 1.3.

The Umbria–Marche succession represents a continuous record of the geotectonic evolution of an epeiric sea from the Late Triassic to the Pleistocene. During the Late Triassic and Early Jurassic, at the time of the opening of the North Atlantic, rifting took place between Europe and Africa within formerly continuous continental crust at the southern margin of Europe (Centamore et al., 1980; Bosellini, 1989). This rifting formed some oceanic basins ancestral to the present Alpine mountain chains, including the Pennine–Liguride Ocean. This new ocean, perhaps connected with part of the ancient Tethyan Ocean to the east, outlined a northward–pointing promontory of African continental crust, commonly referred to as Adria or the Adriatic Promontory (Channell et al., 1979) (Fig. 1.2). The Adriatic Promontory was isolated from inputs of clastic sediments. As a large, and nearly isolated passive continental margin, Adria underwent extensional faulting. Normal faults defined a complex of subsiding blocks leading to an irregular topography of structural highs (horsts) and adjacent depocenters (grabens and/or half–grabens). In cases where shallow water carbonate deposition could keep up with subsidence, and where the faulted blocks where large enough to support productive carbonate platform environments, very thick sequences of shallow water carbonates developed on the Adria's crust. In other regions, subsidence and complex block faulting carried the sea floor down, below the photic zone and out of the zone of shallow–water carbonate production. Areas with this history became pelagic basins, such as the Umbria–Marche Basin, in which the Paleogene carbonate succession was deposited recording, the geologic, biologic and oceanographic evolution of this region with remarkable continuity and completeness. The Paleogene pelagic sequence is represented by three distinct formations (from bottom to top): Scaglia Rossa (early Turonian to middle Eocene), Scaglia Variegata (middle to late Eocene) and Scaglia Cinerea (late Eocene to earliest Miocene). The Italian terms "Rossa", "Variegata" and "Cinerea" refer respectively to the red, variegated and ashy color and "Scaglia" to the scaly, conchoidal fracture of the rocks. The Paleogene Scaglia Rossa corresponds to the R3 and R4 members of Alvarez and Montanari (1988) and is made up of well–bedded, pink to red limestones with red marly interbeds in the middle–lower Danian, at the Selandian–Thanetian transition and from the upper Thanetian to middle Ypresian. Chert occurs from the middle Ypresian to

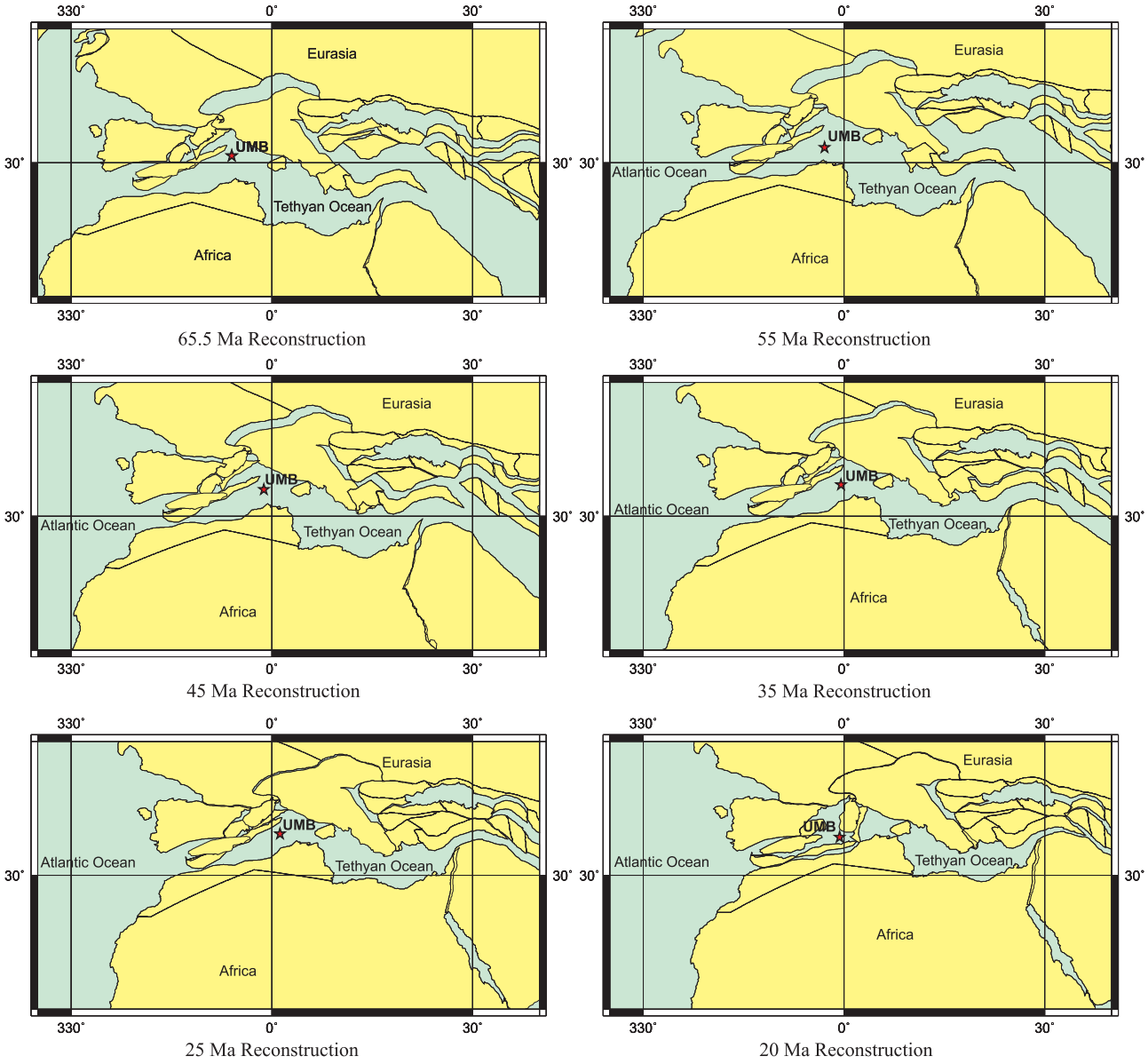

Figure 1.2 – Paleogeographic Reconstructions of Tethyan Ocean during the Paleogene Period. Red star marks the approximated position of the Umbria–Marche Basin (UMB) within the Tethyan Ocean. Reconstruction made using the Web–based software at http://www.odsn.de/odsn/index.html (Hay et al., 1999).

the lower Lutetian. The Paleogene Scaglia Rossa varies in thickness between 80 and 100 m. Beginning in the middle Eocene, clay input became increasingly important. The Scaglia Variegata represents a transitional interval between the Scaglia Rossa and Scaglia Cinerea and consists of alternation of white, greenish–grey and pink to red marly limestones and calcareous marls. Its lower boundary is marked by the last occurrence of nodular chert (Lowrie et al., 1982). The top of the Scaglia Variegata is conventionally placed at the top of the uppermost reddish–violet interval (Monaco et al., 1987).

Geological and stratigraphic details related to the studied intervals and sections are given in each following chapters.

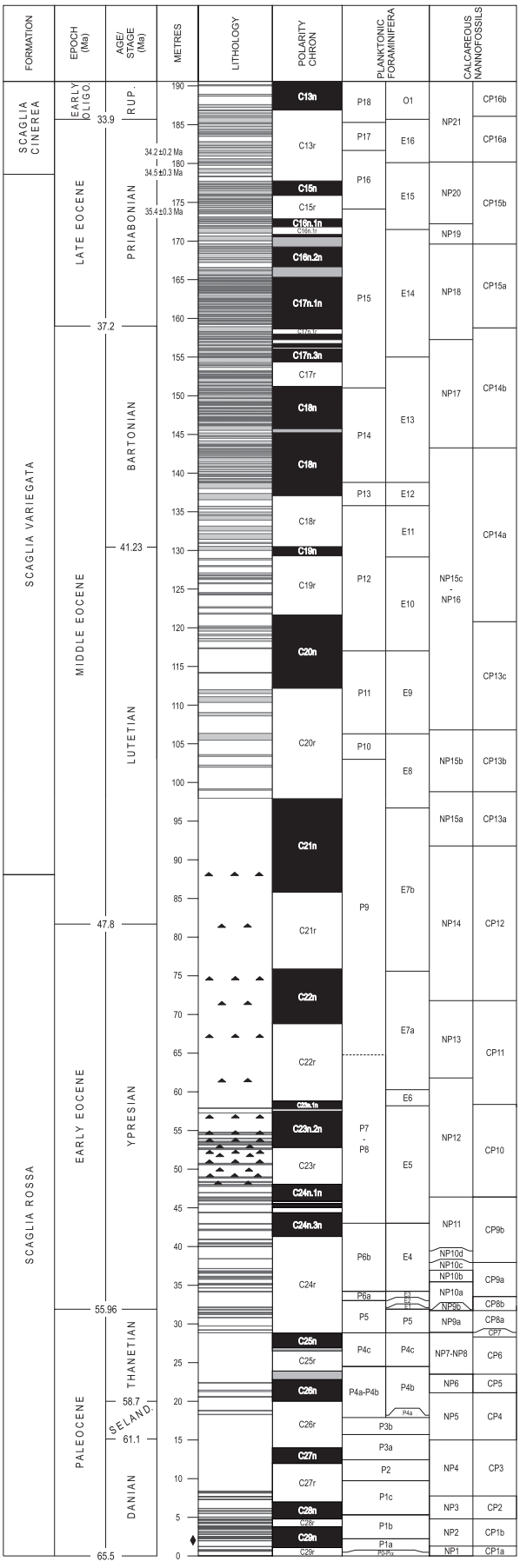

Figure 1.3 – Integrated stratigraphy of the Paleogene pelagic sequence of the Umbria–Marche Basin. Chronostratigraphy is after Coccioni et al. (2008), Ogg et al. (2008), Jovane et al. (2010) and Molina et al. (2011). Planktonic foraminiferal Zones and Subzones are after Berggren et al. (1995) (codified as P and M) and Berggren and Pearson (2006) and Wade et al. (2011) (codified as O and M). Calcareous nannofossil Zones and Subzones are after Martini (1971) (codified as NP) and Okada and Bukry (1980) (codified as CP).

CHAPTER 2

The Dan-C2 hyperthermal event at Gubbio (Italy): Global implications, environmental effects, and cause(s)

2.1 Introduction

Recent findings from some deep–sea ocean sections (Shatsky Rise, Central Pacific; Demerara Rise, equatorial Atlantic; Walvis Ridge, Southeast Atlantic), have highlighted the existence of several prominent carbonate dissolution levels interspersed in lower Paleogene carbonate sediments (Bralower et al., 2002; Hancock and Dickens, 2005; Lourens et al., 2005; Petrizzo, 2005; Edgar et al., 2007; Kroon et al., 2007).

Abrupt climate changes associated with increased greenhouse gas levels (Bralower et al., 2002; Lourens et al., 2005; Zachos et al., 2005) may have probably induced these carbonate dissolution as for the Paleocene–Eocene Thermal Maximum (Kennett and Stott, 1991; Zachos et al., 1993).

More recently, Quillévéré et al. (2008) investigated the large–scale variations in climate and the associated cycle dynamics during the early Danian, over the ~400 kyr that followed the Cretaceous-Paleogene Boundary. Their framework was based on highly time–resolved whole sediment bulk and foraminiferal shell $\delta^{18}O$ and $\delta^{13}C$ changes from the western North Atlantic Ocean (Ocean Drilling Program, hole 1049C on the Blake Nose margin off Florida), and from the eastern South Atlantic Ocean, (Deep Sea Drilling Project, holes 527 and 528 on Walvis Ridge). At Hole 1049C, after an interval characterized by a low planktonic–to–benthic $\delta^{13}C$ gradient, throughout the Danian part of magnetochron C29r, as expected in an open ocean ecosystem altered by the Cretaceous–Tertiary mass extinction, planktonic and benthic foraminifera $\delta^{13}C$ bulk sediment values show a fairly symmetrical, conspicuous double negative excursion (Quillévéré et al., 2008). These remarkable changes in stable isotopic values are placed in the uppermost part of Chron C29r, within the planktonic foraminiferal Zone P1a and the calcareous nannofossil Zone CP1a (Norris et al., 1998, 1999; Huber et al., 2002). The lower $\delta^{13}C$ spike is larger than the upper one, which occurs in the uppermost part of magnetochron C29r. These two carbon isotope excursions (CIEs) are followed by rapid return to values that prevailed before the isotopic anomaly. The CIEs are different in magnitude among the studied localities and the studied material (bulk, planktonic and benthic foraminifera). In particular, the CIEs are the largest in bulk sediment (~1.3‰), intermediate in benthic foraminifera (~1‰), and smaller in planktonic foraminifera (~0.7‰). This conspicuous double negative excursion in stable isotope values was named the Dan–C2 event by Quillévéré et al. (2008). This event is also associated with a major double negative excursion in $\delta^{18}O$, significant magnetic susceptibility increases and some distinctive coloration changes across the horizons characterized by negative $\delta^{13}C$ and $\delta^{18}O$ values (Quillévéré et al., 2008). Assuming no ice–volume change, Quillévéré et al. (2008) inferred an increase in sea surface temperature of ~4°C, based on a ~1‰ decrease in oxygen stable isotope values measured on *Praemurica taurica*. Interestingly, there is no significant shift in the benthic $\delta^{18}O$ record, suggesting that there were no changes in bottom water temperatures. At Walvis Ridge, (DSDP Holes 527 and 528), bulk sediment carbon isotope data show a similar double negative spike in $\delta^{13}C$ value, that resembled the Dan–C2 event recorded at

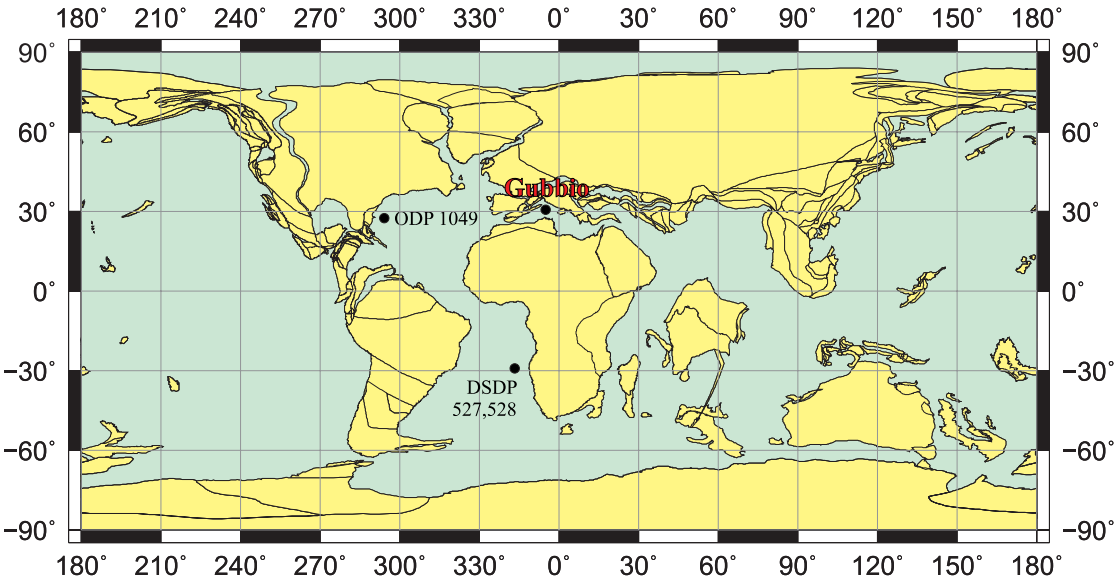

Figure 2.1 – Paleogeographic reconstruction at the time of the K/Pg boundary and location of DSDP Sites 527 and 528, and ODP Site 1049, and Contessa Highway Section (Gubbio). Reconstruction made using the Web–based software at http://www.odsn.de/odsn/index.html (Hay et al., 1999).

Blake Nose, between ~65.24 Ma and ~65.14 Ma. These double negative CIEs are placed at the top of magnetochron C29r (Ogg and Bardot, 2001), within planktonic foraminiferal Zone P1a and calcareous nannoplankton Zone CP1a (Norris et al., 1998, 1999; Huber et al., 2002) strongly suggesting that the Dan–C2 event at Hole 1049C is stratigraphically correlative with the depletions recorded on Walvis Ridge. On the basis of the extrapolated sedimentation rates between this magnetic reversal and the Cretaceous–Tertiary boundary, Quillévéré et al. (2008) suggested a ~100 kyr duration for the Dan–C2 event. In particular, these authors estimated that the older and younger spikes persisted each for ~40 kyr (from ~65.24 Ma to ~65.20 Ma and from ~65.18 to ~65.14 Ma, respectively) and the intervening positive $\delta^{13}C$ excursion had a duration of ~20 kyr. The wide geographic coverage (~58° latitude) between sites 1049C on the Blake Nose (North Atlantic Ocean) and 527, 528 on Walvis Ridge (eastern South Atlantic Ocean) suggests the likely global significance of the Dan–C2 event (Quillévéré et al., 2008). Previously, at sites 1049C and 528, D'Hondt et al. (1996) and Speed and Kroon (2000) reported a relative decrease in carbonate content in the levels where Quillévéré et al. (2008) found the Dan–C2 event. At site 1262 (Walvis Ridge), recent analyses show analogous significant decreases in both carbonate content and abundance in residue <63 μm (Kroon et al., 2007). These changes are associated with depleted bulk sediment $\delta^{13}C$ values in levels correlative to the Dan–C2 event suggesting that enhanced carbonate dissolution and shoaling of the lysocline/CCD may have also occurred (Kroon et al., 2007). During the previously documented early Paleogene hyperthermals, like the PETM (e.g. Zachos et al., 2005), the ELMO event (Lourens et al., 2005) and middle Eocene C19r event (Edgar et al., 2007), similar pattern were recognized. Noteworthy, a long–term rise in global $\delta^{13}C$ of marine carbonates and deep water temperatures starting during the mid–Maastrichtian (e.g. Norris et al., 2001), preceded the Dan–C2 event. This rise, coupled with the increase of deep water temperature, probably may reflect carbon burial and CO_2 sequestration at the same time (Zachos et al., 1989; Stott and Kennett, 1990). Since the benthic $\delta^{13}C$ values are similar to those of the bulk sediment within the negative excursions of the Dan–C2 event, Quillévéré et al., (2008) interpreted the isotopic event to be a reservoir signal representing a massive exhumation of carbon buried during the long–term rise in global $\delta^{13}C$. The rapid recovery of $\delta^{13}C$ and the transient nature of the Dan–C2 event suggest that the CO_2 was probably derived from redistribution of carbon that was already in the ocean–atmosphere–biosphere system either in the form of carbon stored in deep anoxic ocean water, although the source of ^{12}C remains unknown (Quillévéré et al., 2008). Unfortunately, the environmental effects and the cause(s) of the Dan–C2 event are still not completely deciphered, though potentially astronomically paced

(Lourens et al., 2005) disturbances in the global carbon cycle may have had an effect.

2.2 Objectives

The main goals of this study are (1) to document for the first time the Dan–C2 event beyond the Atlantic Ocean in the western Tethyan realm, (2) to support evidence of the supra–regional, possibly global, significance thereof, (3) to document stressed ecological responses during this event, (4) to provide first evidence of a further short–lived (~38 kyr) hyperthermal event not known up to now and that we term the "Lower C29n" event.

To this end, we explore the features of the Dan–C2 event through a high–resolution, multidisciplinary (litho–, bio–, magneto–, chemostratigraphy and mineralogy) integrated study at the Contessa Highway section (Gubbio, Italy), in the Umbria–Marche basin.

2.3 Stratigraphical setting

At Contessa Highway (lat. 43°22′47″N; long. 13°33′49″E, Figs. 2.1–2.2), the lower Danian belongs to the Scaglia Rossa Formation of the Umbria–Marche Basin, which is predominantly composed of pelagic, coccoliths–foraminiferal limestones with subordinated marls deposited at middle to lower bathyal depths (Kuhnt, 1990; Galeotti et al., 2004; Jovane et al., 2007; Giusberti et al., 2009). This study is focused on the 1.5 m–thick stratigraphic interval immediately overlying the Cretaceous–Paleogene (K–Pg) boundary, which is characterized by three 3 cm–thick calcareous marly beds at 0.63–0.66 m, 0.81–0.84 m and 1.23–1.26 m, respectively (Fig. 2.3). The studied section spans from the base of indistinct planktonic foraminiferal Zones P0−Pα to the middle part of Zone P1a of Berggren and Pearson (2005), and from the calcareous nannofossil Zone NP1 to the lowermost part of Zone NP2 of Martini (1971), the calcareous nannofossil Zone *Biantholithus sparsus* to the middle part of Zone *Cruciplacolithus primus* of Romein (1979), the calcareous nannofossil Zone CP1a to the lowermost part of Zone CP1b of Okada and Bukry (1980), and the calcareous nannofossil Zone *Biantholithus sparsus*, barren interval–*Biscutum*? *romeinii* Subzone, to the middle part of Zone *Cruciplacolithus primus* and *Toweius petalosus* Subzone of Perch–Nielsen (1985).

According to Lowrie et al. (1982), the C29r/C29n magnetochron boundary is placed at 1.3 m above the K–Pg boundary. However, these authors used a ~30 cm spacing for sampling with four samples in the first 1.3 m. Following this, the base of magnetochron C29n might confidently be placed close to 1 m above the K–Pg boundary (Fig. 2.3), which is in agreement with the available magnetobiostratigraphy for the lower Danian (e.g., Romein, 1979; Smit, 1982; Cresta et al., 1989; Keller, 1989; D'Hondt and Keller, 1991; Wei and Pospichal, 1991; Preisinger et al., 1993; Berggren et al., 1995; Pospichal, 1995, 1996; Molina et al., 1996; Rögl et al., 1996; Norris et al., 1998, 1999; Huber et al., 2002; Dinarès–Turell et al., 2003; Galbrun and Gardin, 2004; Bernaola and Monechi, 2007; Ogg et al., 2008; Westerhold et al., 2008; Ogg and Lugowski, 2009).

Figure 2.2 – The Contessa Highway Section, on the right the K/Pg boundary.

2.4 Materials and Methods

A total of seventy–one bulk rock samples was collected at 5 cm intervals through the basal 0.4 m of the Danian (P0−Pα indistinct Zone), and at 1–2 cm intervals through the rest of the section. All the material studied is housed in the laboratory of the Dipartimento di Scienze dell'Uomo, dell'Ambiente e della Natura, Università di Urbino, Italy.

2.4.1 *Calcium carbonate*

The bulk rock samples were reduced to fine powder in agate mortar. Calcium carbonate content measurements were obtained using a Dietrich–Frühling calcimeter. The method is based on the measurement of CO_2 volume produced by the complete dissolution of pre–weighted samples (300 ± 1 mg each), in 10 % vol. HCl. Total carbonate contents (wt.% $CaCO_3$) with a precision of 1% were computed using formulae that take into account pressure and temperature of the lab environment, amount of bulk sample used, and the volume of CO_2 developed in the calcimeter. Standards of pure calcium carbonate (i.e., Carrara Marble) were measured every ten samples to ensure proper calibration.

2.4.2 *Stable isotopes*

Stable isotope analyses were conducted on sixty–six bulk samples. They were produced using an automated continuous–flow carbonate preparation GasBenchII device (Spötl and Vennemann, 2003) and a ThermoElectron Delta Plus XP mass spectrometer in the geochemistry laboratories at the IAMC–CNR Institute of Naples. The acidification of samples was performed at 50 °C. An internal standard (Carrara Marble with $\delta^{18}O = -2.43$ versus Vienna Peedee belemnite [VPDB] and $\delta^{13}C = 2.43$ versus VPDB) was run for every six samples, and for every thirty samples the NBS19 international standard was measured. Standard deviations of carbon and oxygen isotope measurements were estimated at 0.1‰ and 0.08‰, respectively, on the basis of replicate measurements of 20% of analyzed samples. All of the stable isotope data are reported in per mil (‰) relative to the VPDB standard.

2.4.3 *Magnetic susceptibility*

A total of sixty–six samples was used for paleomagnetic analyses in the magnetically shielded laboratory at the Istituto Nazionale di Geofisica e Vulcanologia (INGV), Rome. A range of rock magnetic measurements was used to investigate the magnetic mineralogy throughout the investigated section. The low field mass–specific magnetic susceptibility (χ) was measured with a Kappabridge KLY–2 magnetic susceptibility meter.

2.4.4 *Calcareous nannoplankton*

Samples were prepared from unprocessed material as smear slides, and were examined using a light microscope at 1250x magnification. Throughout the studied interval, calcareous nannofossils are generally rare and poorly preserved. As for biostratigraphy, all samples were studied while a quantitative analysis was performed on nineteen selected samples. In this study the calcareous nannofossil zonations of Martini (1971), Romein (1979), Okada and Bukry (1980), and Perch–Nielsen (1985) were applied. Nannofossils were counted using the methods described by Backman and Shackleton (1983) and Rio et al. (1990): 1) counting species versus total assemblage, taking into account at least 300 nannofossils and 2) counting the number of species in 1 mm^2. An expanded area of about 6–7 mm^2 was used to count *Cruciplacolithus primus*. For the counting of the calcareous dinoflagellate, *Thoracosphaera* spp., Gardin and Monechi's (1998) approach was followed by the counting fragments larger than 4 μm as a single specimen. Species concepts largely follow Romein (1979), Perch–Nielsen (1985) and Van Heck and Prins (1987). In the material used for this study there were some problems in distinguishing *Neobiscutum romeinii* and *Neobiscutum parvulum*, which have consequently been combined.

2.4.5 *Foraminifera*

Samples were treated following the cold acetolyse technique of Lirer (2000) by sieving through a 32 μm mesh and drying at 50°C. Foraminifera are generally abundant and well preserved, although evidence of enhanced dissolution can be observed between 0.6 and 1.3 m.

2.4.5.1 *Planktonic foraminifera*

All samples were studied to determine the biostratigraphy, while the quantitative analysis was

focused on nineteen selected samples, the same ones used for the calcareous nannoplankton studies. The planktonic foraminiferal zonation of Berggren and Pearson (2005) was followed. Probably due to stratigraphical condensation, the biostratigraphical interval corresponding to Zone P0 (*Guembelitria cretacea* Zone), and characterized by the partial range of the nominate taxon between the last occurrence of Cretaceous taxa and the first occurrence of *Parvulorugoglobigerina eugubina,* which defines the base of the next Zone Pα (*P. eugubina* Zone), is not recognized at Contessa Highway, because this species is already present at the base of the studied section. This is probably due to vertical mixing caused by bioturbation as indicated by burrows and impact spherules found in the basal 5 cm of the Danian, immediately above the K–Pg boundary clay (Montanari and Koeberl, 2000). Accordingly, in the biostratigraphy here presented, it is not possible to separate Zones P0 and Pα, which have consequently been combined. A representative split of at least 300 planktonic foraminiferal specimens was picked from the >32 μm fraction. All specimens were mounted on micro–slides for permanent record and identification purposes. Largely following Pardo and Keller (2008, and references therein), planktonic foraminiferal were grouped in *Guembelitria* spp., and low–oxygen tolerant taxa (small biserial forms, which include *Heterohelix*, *Chiloguembelina*, *Woodringina*, and *Zeuvigerina*). The percentages of planktonic foraminiferal fragments or partially dissolved tests (Fragmentation index) have been determined for estimating the effect of carbonate dissolution. Following Hancock and Dickens (2005) and Luciani et al. (2007), these data were calculated using about 300 planktonic foraminifera, including the whole test, fragments and dissolved tests.

2.4.5.2 *Benthic foraminifera*

The quantitative study was performed on the same selected samples as for calcareous nannoplankton and planktonic foraminifera. A representative split of the >63 μm fraction was used to pick approximately 300 specimens. The fraction >63 μm has been chosen since it can be regarded as the most appropriate for investigating the benthic community, and, following Schroeder et al. (1987), the study of larger fractions would be not suitable for inferring environmental variations with accuracy. The sample–split weight used to pick benthic foraminifera was determined so that the foraminiferal density (FD, the number of foraminifera per gram of dry sediment) was calculated. Significant benthic foraminiferal taxa were identified mainly following the taxonomy outlined by Tjalsma and Lohmann (1983), Van Morkhoven et al. (1986), Bolli et al. (1994), Alegret and Thomas (2001), Sztrakós (2005) and Kaminski and Gradstein (2005). Percentages of agglutinans and abundances (number of specimens per gram of dry sediment) of paleoecological–diagnostic taxa (*Spiroplectammina* spp., *Reophax* spp., *Subreophax* spp., *Repmanina charoides*, *Aragonia aragonensis*, *Dorothia* spp., *Marssonella* spp., and *Remesella* spp.) were determined. In order to calculate the infaunal percentages, all taxa were allocated to infaunal and epifaunal morphogroups, largely following Corliss (1985), Alegret et al. (2003) and Kaminski and Gradstein (2005).

2.5 Results and discussion

2.5.1 *The Dan–C2 event at Contessa Highway: Supra–regional to global implications*

The studied section is characterized by three discrete intervals containing lower carbonate contents and higher magnetic susceptibility (χ) values, which are linked to the marly beds (Fig. 2.3). The bulk carbonate $\delta^{13}C$ record displays background values of 1.3‰–2.2‰, with three short–distinct CIEs, which correspond or are close to the marly beds (~0.8‰, ~0.4‰ and ~0.7‰, respectively) (Fig. 2.3). Although the two major CIEs coincide with marly beds, adjacent limestone and marly limestone beds exhibit similar $\delta^{13}C$ values, suggesting that these are primarily signals in carbonate rather than manifestations of a different lithology.

Following Corfield et al. (1991), the Paleogene Scaglia sediments at Contessa Highway might be affected by diagenesis, and oxygen isotope values have, therefore, been disregarded. The χ variation can be due to the changes in the concentration of magnetic minerals, which in turn could be related to changes in terrigenous influx or carbonate dissolution, or changes in magnetic mineralogy, which might be related to redox conditions on the seafloor–magnetite vs. hematite– or it might be related to the nature of the weathering in the continental search area.

On the basis of magnetobiochronostratigraphy, and the comparison of variations and the structure of $\delta^{13}C$, $CaCO_3$, and χ among the different sites, findings here

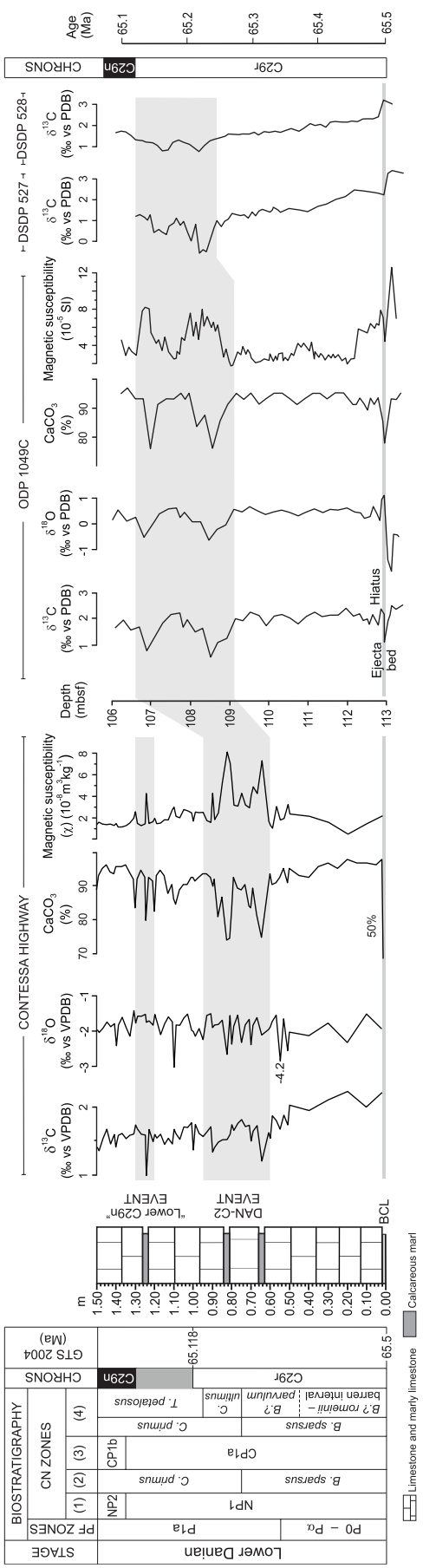

Figure 2.3 – Changes in $\delta^{13}C$ and $\delta^{18}O$ of bulk sediments, $CaCO_3$ content, and magnetic susceptibility (χ) in the lowermost Danian at Contessa Highway, plotted with changes in $\delta^{13}C$ and $\delta^{18}O$ of bulk sediments, $CaCO_3$ content, and magnetic susceptibility from the equivalent stratigraphic interval at ODP Hole 1049C (Black Nose, NW Atlantic) and DSDP Holes 527 and 528 (Walvis Ridge, SE Atlantic), where the Dan–C2 event was first recognized by Quillévéré et al. (2008). Reliable correlation of these changes among locations shows the occurrence of the Dan–C2 event, here represented by the lower gray shaded area, at Contessa Highway. The upper gray shaded area marks the "Lower C29n" event. The new biostratigraphy of the early Danian at Contessa Highway is based on the planktonic foraminiferal (PF) Zones of Berggren and Pearson (2005) and calcareous nannoplankton (CN) Zones of Martini (1971) (1), Romein (1979) (2), Okada and Bukry (1980) (3), and Perch–Nielsen (1985) (4). Magnetostratigraphy is from Lowrie et al. (1982). BCL: K–Pg boundary clay layer. Stage and numerical ages (GTS, Geological Time Scale 2004) are from Gradstein et al. (2004).

Figure 2.4 – The Contessa Road Section, outcrop enlargement. Shaded areas mark the Dan–C2 and Lower C29n events.

presented, show that the lower Danian critical interval between 0.6–0.95 m above the K–Pg boundary at the Contessa Highway is confidently correlative with the Dan–C2 interval of Quillévéré et al. (2008), and is, therefore, the sedimentary expression of the Dan–C2 event in this part of the western Tethyan Ocean (Figs. 2.3 and 2.4).

This would also implicate that the interval between 1.2–1.3 m above the K–Pg boundary including the upper marly bed centered at ~65 Ma might be the sedimentary expression of a further short–lived (~38 kyr) hyperthermal event not known up to now and that we term the "Lower C29n" event.

The Dan–C2 event recognized at Contessa Highway and in the Atlantic Ocean Sites together with "Lower C29n" event might correspond to the lower part of the interval with high Fe intensities and relatively lower carbonate values documented by Kroon et al. (2007) in the South Atlantic Sites 1262 and 1267, which matches the lower part of the expanded interval labeled as "strange interval" by Westerhold et al. (2008) at Sites 1209 (Shatsky Rise, NW Pacific Ocean). In the same interval, on the basis of magnetostratigraphic correlation between Leg 198 (Shatsky Rise, North Pacific, Sites 1209, 1210, 1211) and Leg 208 (Walvis Ridge, South Atlantic, Sites 1262, 1267), Westerhold et al. (2008) identified several prominent peaks in magnetic susceptibility and iron intensity that they labeled Pa through Pq (see Additional Figure F1 in Westerhold et al., 2008). In particular, the oldest two peaks (Pa1 and Pa2, respectively) match well with those linked to the Dan–C2 and "Lower C29n" events, respectively. Moreover, at ODP Site 1262 these spikes are associated with major changes in $\delta^{13}C$, $\delta^{18}O$, and $CaCO_3$ (Kroon et al., 2007).

On the whole, the presented results, together with these records, would extend the latitudinal and longitudinal range over which the Dan–C2 event has been documented, lending new support to its interpretation as a potentially global event.

2.5.2 *Biotic changes across the Dan–C2 event and inferred environmental effects*

In accordance with the work of Fornaciari et al. (2007), the investigated section is subdivided into discrete intervals reflecting the nannofossil recovery pattern in the aftermath of the K–Pg boundary event (Fig. 2.4). The first 10 cm interval following the K–Pg extinction event represents the coccolithophore "Dead Zone" *sensu* Erwin (2001), and is characterized by the almost total absence of persistent Cretaceous taxa (except for the calcareous dinoflagellates, *Thoracosphaera*) and by the total absence of incoming species (Fig. 2.5).

The subsequent survival interval initially shows low diversity, dominated by *Thoracosphaera* and persistent Cretaceous taxa, followed by a gradual rise in relative abundance of the incoming taxa like *Fuytania petalosa* (Fig. 2.5). A sharp increase in the total abundance of calcareous nannofossil assemblage occurs shortly below the onset of the Dan–C2 event. Notably, the increase in relative abundance of the persistent Cretaceous taxa (not taking into

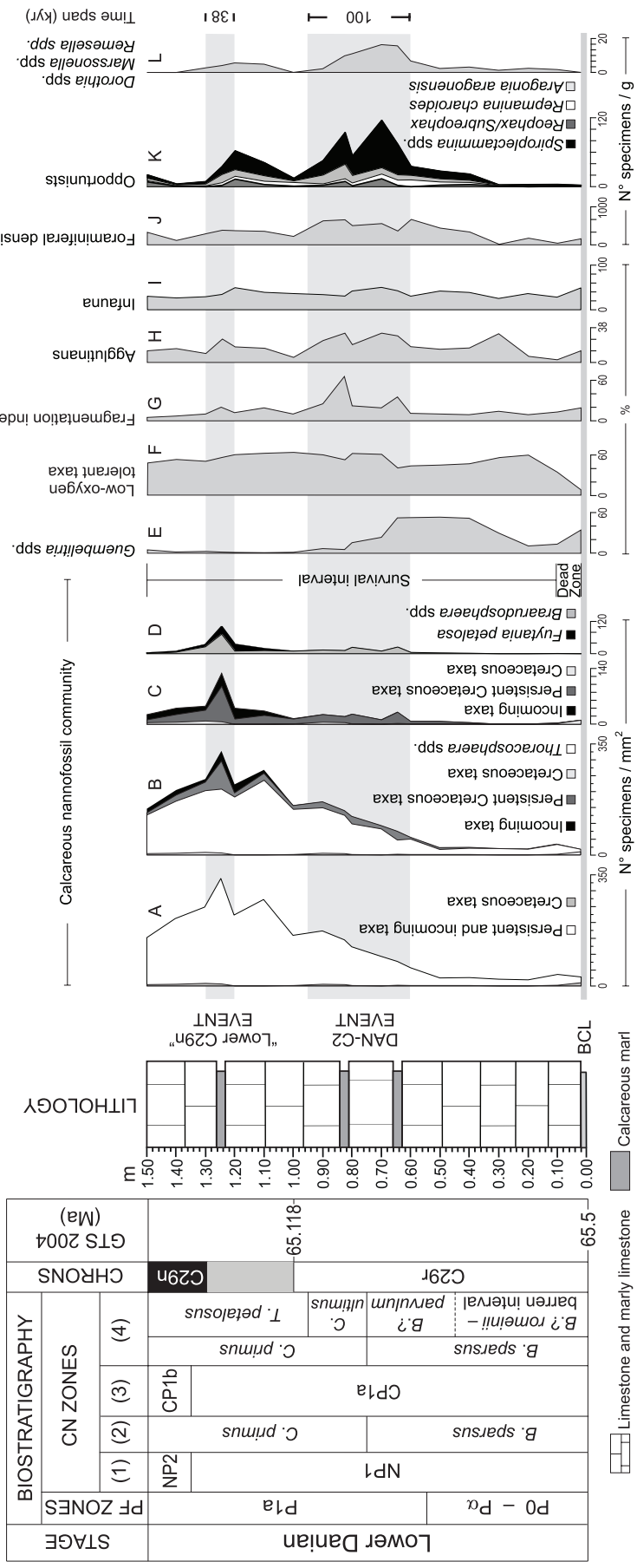

Figure 2.5 – Magnetobiochronostratigraphy and lithology, as seen in Fig. 2.3 plotted with selected calcareous nannofossil (A–D), planktonic (E–G) and benthic (H–L) foraminiferal abundances and parameters. The lower gray shaded area represents the Dan–C2 event with an assumed time span of ~100 kyr according to Quilléveré et al. (2008). The upper gray shaded area marks the "Lower C29n" event. Based on magnetostratigraphy provided by Lowrie et al. (1982) and the numerical ages from Gradstein et al. (2004), the "Lower C29n" event would span ~38 kyr.

account *Thoracosphaera*) and *Braarudosphaera* is linked to the onset of the Dan–C2 event (Fig. 2.5). *Braarudosphaera*, which blooms within the marly beds, is commonly regarded as an opportunistic taxon that proliferates either in response to reduced competition or eutrophication, and is currently flourishing in warm waters (Takano et al., 2006; Bartol et al., 2008). *Fuytania petalosa*, a very small–sized opportunistic coccolith, which is thought to thrive under unstable paleoceanographic conditions and enhanced productivity (e.g. Gardin and Monechi, 1998), increases in abundance in the marly bed related to the "Lower C29n". It must be noted that the *Braarudosphaera* spikes (when expressed as percentages), and the *F. petalosa* peak mimic the major negative $\delta^{13}C$ excursions.

Up to the onset of the Dan–C2 event and within the rapid initial phase of the evolutionary recovery from the K–Pg mass extinction (e.g., Coxall et al. 2006), the planktonic foraminiferal assemblages are dominated by the stress tolerant and opportunistic genus *Guembelitria*, which thrives in the aftermath of the K–Pg event (Pardo and Keller, 2008) (Fig. 2.5). As the environmental conditions became more stable after the K–Pg event, this taxon retreats, vacating niches for other ecological generalists such as the low–oxygen tolerant small biserial taxa (*Heterohelix*, *Chiloguembelina*, *Woodringina*, *Zeuvigerina*), which slightly increase in abundance during the Dan–C2 event (Fig. 2.5). Relatively higher values of the planktonic fragmentation index and increasing percentages of agglutinated foraminifera, both of which indicate significant changes in the ocean chemistry and suggest an intensification of dissolution, are also recorded during the Dan–C2 and "Lower C29n" events (Fig. 2.5).

Increased food supply to the seafloor during the Dan–C2 event is indicated by higher values of benthic foraminiferal density and infaunal morphogroups, which may suggest a recovery of the food web and/or enhanced eutrophication (Fig. 2.5). Several benthic taxa (*Reophax, Subreophax*, *Spiroplectammina*, *Repmanina charoides*, *Aragonia aragonensis*), which are normally recognized as opportunists, also exhibit higher abundances during the Dan–C2 event (Fig. 2.5). *Reophax*, *Subreophax* and the disaster taxon *Spiroplectammina* are regarded as re–colonization taxa that are linked to increased organic flux (Kuhnt and Kaminski, 1996). Increases in the abundance of *Repmanina charoides*, a form feeding on organic detritus, has been found during episodes of environmental instability, low oxygenation, rapid changes in productivity, and severe carbonate dissolution (e.g. Coccioni et al., 1994; Kaminski and Gradstein, 2005). *Aragonia aragonensis,* which has been related to hyperthermal events (Ortiz and Thomas, 2006), shows peaks in relative abundance in some post–extinction intervals at several ODP sites in correspondence with minimum bulk carbonate $\delta^{13}C$ values (Thomas, 1998). Finally, a marked increase in the abundance of the elongated subcylindrical taxa (*Dorothia, Marssonella,* and *Remesella*), which typically dominate in low–oxygen environments and are adapted to proliferate in more eutrophic areas with higher levels of organic flux (Kaminski and Gradstein, 2005), is recorded during the Dan–C2 event (Fig. 2.4).

2.5.3 *The cause(s) of the hyperthermal Dan–C2 event*

According to Quillévéré et al. (2008), the short–lived early Danian Dan–C2 hyperthermal event may reflect amplification, potentially astronomically paced, of a regular cycle in the size and productivity of marine biosphere and balance between burial of organic and carbonate carbon. Significant shoaling of the lysocline and the CCD took place as predictable consequences of perturbation to the global carbon cycle (Zachos et al. 2005; Zeebe and Zachos, 2007) leading to ocean acidification with diminished carbonate production and/or seafloor carbonate dissolution documented during the Dan–C2 event by the increasing fragmentation of foraminifera and the numbers of agglutinans. A sea surface temperature rise of ~4°C has been evaluated for the Dan–C2 event (Quillévéré et al., 2008), which is about half of the high–latitude sea surface temperature changes estimated for the PETM, but nearly equivalent to those recorded in the tropical Ocean (Zachos et al., 2003). The lack of changes in bottom water temperatures during the Dan–C2 event and of severe biotic response at the sea floor induced by this event also support the interpretation that the Dan–C2 event was a Danian partial analog for the PETM of less intensity than the PETM.

However, at the time of the Dan–C2 event, the last and third phase of the Deccan volcanism concurrently took place. In fact, geochronological and magnetostratigraphic (Chenet et al., 2007, 2009), petrological and volcanological (Self et al., 2008), and paleontological (Keller et al., 2008)

studies show that the primary structures of Deccan trap emplacement were actually three gigantic pulses consisting of a number of discrete, short (~kyr), but huge eruptive events (Chenet et al., 2009). The third and last mega–phase, which started in the upper part of magnetochron C29r and ended in the lowermost part of magnetochron C29n (Chenet et al., 2009), is confidently correlated with the magnetostratigraphic interval constraining the Dan–C2 event (Fig. 2.3). It was estimated for the last Deccan megapulse that there was a release of ~200 Gt of SO_2 and ~400 Gt of CO_2 (Chenet et al., 2009). This is also supported by the rise of atmospheric pCO_2 to moderately high levels (up to 1500 ppmV) in the early Danian (Nordt et al., 2003; Royer, 2006; Retallack, 2009). Although the inferred magnitude and duration of warming cannot be readily explained as the result of the direct addition of volcanic CO_2 (Caldera and Rampino, 1990), the estimated large sulfate aerosol and CO_2 release might have additionally contributed, at some extent, to ocean carbonate chemistry, climate and environmental changes.

2.6 Conclusions

These high–resolution biochronostratigraphic and magnetic susceptibility data and geochemical records from the Contessa Highway section (Gubbio, Italy) provide the first direct evidence of the early Danian Dan–C2 hyperthermal event beyond the Atlantic Ocean. This suggests a supra–regional, possibly global, nature of this transient warming event with a carbon cycle perturbation.

At Contessa Highway, biotic changes, as recorded across the Dan–C2 event by calcareous nannoplankton and foraminifera, are interpreted as a consequence of significant environmental instability. This situation involves a change to eutrophic conditions, the enhanced dissolution of carbonates and planktonic foraminiferal fragmentation relating to shoaling of lysocline/CCD, and depletion of oxygen along the water column and at the seafloor. The enhanced fertility would have been induced by global mechanisms such as an intensified hydrological cycle driven by the expanded greenhouse conditions and the consequent input of nutrients. The increases in relative abundance exhibited by calcareous nannoplankton eutrophic indicators and infaunal opportunistic and low–oxygen tolerant foraminiferal taxa are consistent within this scenario.

As for other early Paleogene hyperthermal events, the cause of the Dan–C2 event is likely to be found in changes, in the distribution of carbon within surface biosphere reservoirs, possibly controlled by orbital cycles. However, the third and last phase of Deccan volcanism, with its huge release of greenhouse gases into the atmosphere during the Dan–C2 event would be also taken into account.

CHAPTER 3

Is the scenario for the Early Late Paleocene Event (ELPE) more complex than hitherto supposed? Evidences from the Selandian-Thanetian transition at Gubbio (Italy)

3.1. Introduction

The early late Paleocene hyperthermal event (ELPE, Bralower et al., 2002), also known as the mid-Palaeocene biotic event (MPBE, Bernaola et al. 2007), has been recognized in several deep sea cores from the Shatsky Rise (ODP Leg 198, central Pacific), Walvis Ridge (ODP Leg 208, South Atlantic), Maud Rise (ODP Leg 113, Weddell Sea) and Black Nose (ODP Leg 171, North Atlantic) as well as in on–land Spanish sections (Zumaia and Ibaeta) (Bralower et al., 2002; Zachos et al., 2004; Petrizzo, 2005; Bernaola et al., 2007) (Fig. 3.1). This hyperthermal event was first described at the Shatsky Rise (ODP Sites 1209, 1210, 1211 and 1212) as a prominent 5– to 25 cm–thick clay–rich calcareous nannofossil ooze layer centered at ~58.4 Ma. It falls in the lower planktonic foraminiferal P4 Zone of Berggren et al. (1995) and coincides with the evolutionary lowest occurrence (LO) of *Heliolithus kleinpellii*, which marks the base of calcareous nannofossil Zones NP6 of Martini (1971) and CP5 of Okada and Bukry (1980) (Bralower et al., 2002). The clay-rich layer contains common phillipsite crystals, fish teeth and phosphatic micronodules, and corresponds to a prominent peak in magnetic susceptibility that most likely reflects the Fe–Mn coating of grains. Planktonic foraminifers in the ooze layer are characterized by a low-diversity, largely dissolved assemblage dominated by representatives of the genus *Igorina* (mainly *I. pusilla* and *I. tadjikistanensis*). In contrast, *Igorina albeari*, morozovellids, acarininids, globanomalinids, subbotinids, and chiloguembelinids are common below the clay–rich layer, almost disappear within it and reappear in low abundances above it (Petrizzo, 2005). Although this author concluded that the planktonic foraminiferal shifts might have been the result of differential dissolution, based on nannofossil assemblages Bralower et al. (2006) suggested that the event might correspond to surface water warming. Moreover, at Site 1209 an increased abundance of benthic foraminifera has been documented within the event (Petrizzo, 2005). Marked changes in benthic foraminiferal morphogroups were also evidenced at Maud Rise (Sites 689 and 690), explained by the formation of warm saline bottom waters (Thomas, 1990). On the basis of the planktonic/benthic ratio and the percentages of planktonic foraminiferal fragments or partially dissolved tests (fragmentation index, FI), Hancock and Dickens (2005) extended the dissolution interval at Sites 1209 and 1211 beyond the biotic event previously defined by Petrizzo (2005) and highlighted that the event marks a short extreme within the context of a longer 1–2 Myr interval of odd conditions. This supports the hypothesis of a prominent change in ocean circulation as also corroborated by the occurrence of an unusual black shale-condensed interval at Mead Stream, found within the Waipawa Formation deposited under dysaerobic conditions and surface-water warming (Killops et al., 2000), falling within Zone P4 of Berggren et al. (1995) and correlated throughout New Zealand (Hollis et al., 2005). This event has also been identified at Walvis Ridge as a prominent 10– to 30 cm–thick dark brown clay-rich calcareous nannofossil ooze at Sites 1262 and 1267, and a 10 cm–thick brown nannofossil chalk at Site 1266 (Zachos et al., 2004). These layers show pronounced magnetic susceptibility peaks that

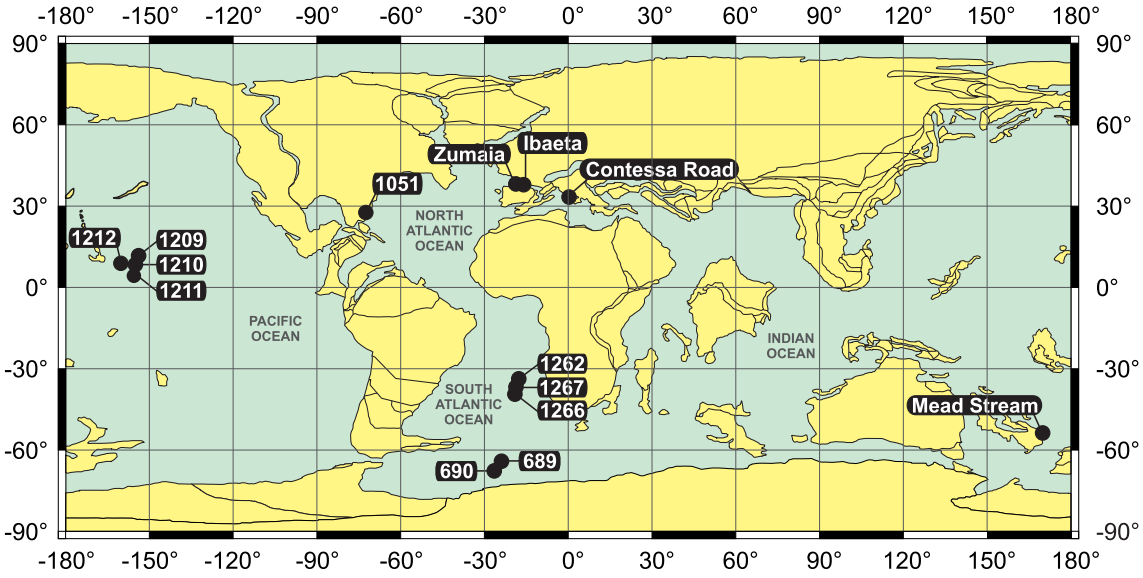

Figure 3.1 – Palaeogeographic reconstruction at 60 Ma and location of the Shatsky Rise (ODP Leg 198, Sites 1209, 1210, 1211, 1212), Walvis Ridge (ODP Leg 208, Sites 1262, 1266, 1267), Maud Rise (ODP Leg 113, Sites 689, 690), Black Nose (ODP Leg 171, Site 1051) and Zumaia, Ibaeta, Contessa Road and Mead Stream on–land sections. Reconstruction made using the web–based software at http://www.odsn.de/odsn/services/paleomap/paleomap.html.

reflect an increase in clay content (paramagnetic). In the Shatsky Rise an impoverished-highly dissolved planktonic foraminiferal assemblage is dominated by the genus *Igorina* (Zachos et al., 2004). A relationship between the consecutive appearances of the genera *Heliolithus*, *Discoasteroides* and *Discoaster*, and ELPE was demonstrated by Agnini et al. (2007) at Site 1262, with these evolutionary impulses being related to environmental perturbations leading to the onset of the ELPE (the emergence of *Heliolithus*) and to the critical conditions during (the emergence of *Discoasteroides*) and after (the emergence of *Discoaster*) the transient event. The onset of the ELPE has been constrained to the uppermost part of magnetochron C26r and its end to the middle part of magnetochron C26n (Agnini et al., 2007).

The Zumaia section represents the first land–based locality where the MPBE was documented and described in detail (Bernaola et al., 2007). Here, it is represented by a distinct clay–rich interval characterized by a significant drop in both carbonate content and $\delta^{13}C$, pronounced values of magnetic susceptibility and significant changes in calcareous nannofossil and foraminiferal assemblages. This interval is located ~4.5 m above the LO of *H. kleinpellii*, ~2 m below the base of Chron C26n and within Zone P4 of Berggren et al. (1995), and its duration is estimated to be ~52–53 kyr (Bernaola et al., 2007). On the basis of micropaleontological analyses, a shift from relatively cooler mesotrophic to warmer oligotrophic conditions, probably induced by an input of isotopically depleted carbon triggering a rapid shoaling of the lysocline, was suggested (Bernaola et al., 2007). The *Igorina* dominance, which characterizes the ELPE both at the Atlantic and Pacific Ocean sites, was not recognized at Zumaia. Instead a distinct peak in abundance of *Subbotina* genus, which corresponds to the main CIE and to the core of the event, was found (Bernaola et al., 2007). Anomalous peaks in Fe intensity were documented in different ODP Sites (1262, 1267, 1209, 1210, 1211, and 1051) by Röhl et al. (2003) and Westerhold et al. (2008). Despite some discrepancies in the magnetostratigraphic position of the ELPE, Westerhold et al. (2008) place the recognized peaks in Fe intensity within the same eccentricity cycle (labelled as $Pc_{405}16$ and $Pc_{100}67$), with their onset and end at the top of magnetochron C26r and in the middle part of magnetochron C26n, respectively. Conversely, at Zumaia, the MPBE is located ~8 precession cycles below the base of magnetochron C26n and at $Pc_{100}65$ (Dinarès–Turell et al., 2007). The cyclostratigraphic reinterpretation of records from ODP Legs 198 (Sites 1209, 1210 and 1211) and 208 (Sites 1262 and 1267), and the Zumaia section place the ELPE event at the 405–kyr cycle number 17 (Hilgen et al., 2010). According to Westerhold et al. (2008), magnetochron C26n is difficult to identify in any record of the past,

and the high quality paleomagnetic signal in Leg 208 should be considered the best available up to now.

3.2 Objectives

The goals of this study are (1) to document and characterize the significant abiotic and biotic changes across the Selandian–Thanetian transition in the Western Tethys Contessa Road reference section (Gubbio, Italy) (2) to provide lines of evidence throughout the comparison with analogous deep–sea sites and land–based sections that the ELPE might be part of a more complex scenario than previously supposed. To this end, we performed at first a high–resolution biostratigraphic, geochemical, and rock–magnetic property data analysis and then, we characterize the biotic changes using quantitative analysis of calcareous nannofossils, planktonic and benthic foraminifera.

3.3 Location and stratigraphic setting

Located near Gubbio (central Italy) is one of the best studied Tethyan Mesozoic–Cenozoic successions which is characterized by a remarkable record of many crucial aspects of the Earth's history (e.g., Luterbacher and Premoli Silva, 1964; Alvarez et al., 1977; Lowrie et al., 1982; Premoli Silva et al., 1988; Coccioni et al., 1989, 1995, 2006, 2008, 2010; Ingram et al., 1994; Coccioni, 1996; Montanari et al., 1997; Galeotti et al., 2000, 2004, 2010; Coccioni and Luciani, 2004; Scopelliti et al., 2006; Jovane et al., 2007, 2010; Musavu–Moussavou et al., 2007; Giusberti et al., 2009; Robinson et al., 2009; Turchyn et al., 2009).

In particular, the Contessa Road section (lat. 43°22′47″N; long. 13°33′49″E) represents a continuous, complete and undisturbed record suitable for correlating the early–middle Paleogene biostratigraphy to the geomagnetic polarity history (Fig. 3.1). This ~120 m−thick section of pelagic sediments belongs to the "Scaglia"−type facies (Lowrie et al., 1982) and is made up of well−stratified coccolith−foraminiferal limestones with subordinated marls deposited at lower middle to lower bathyal depths (1000–1500 m) (Coccioni et al., 2010). This study focuses on a 4 m thick stratigraphic segment located from 18 to 22 m above the Cretaceous–Paleogene (K–Pg) boundary characterized by the occurrence of five marly beds at 18.37–18.47 m, 20.05–20.09 m, 20.15–20.17 m, 20.75–20.95 m and 21.88–21.92 m (Fig. 3.3). Following Coccioni et al. (2006), significant biotic and abiotic changes compared to the underlying and overlying beds are identified. According to Galeotti et al. (2000), the studied segment spans from the upper part of magnetochron C26r to the uppermost part of magnetochron C26n with a duration of ~720 kyr and an average sedimentation rate of ~0.55 cm/kyr following the numerical ages of Gradstein et al. (2004).

3.4 Material and methods

A total of forty–eight bulk rock samples for calcium carbonate, bulk isotopic, rock magnetic and micropaleontological analyses were collected throughout the studied segment (Fig. 3.3) at an average spacing of ~8 cm, corresponding to ~14 kyr. For low field mass–specific magnetic susceptibility, two hundred samples were collected at 2 cm intervals corresponding to ~3.6 kyr. All the materials studied are housed in the laboratory of the Dipartimento di Scienze della Terra, della Vita e dell'Ambiente, Università di Urbino, Italy. Further details, including about the materials and methods used in this study, are summarized in the following paragraphs.

3.4.1 *Calcium carbonate analysis*

Analyses of carbonate content were performed at the geochemistry laboratory of the Dipartimento di Scienze della Terra, della Vita e dell'Ambiente, Università di Urbino, Italy. The bulk rock samples were reduced to fine powder in an agate mortar. Calcium carbonate content measurements were obtained using a Dietrich–Frühling calcimeter. The method is based on the measurement of CO_2 volume produced by the complete dissolution of pre−weighted samples (300±1 mg each) in 10% vol. HCl. Total carbonate contents (wt.% $CaCO_3$) were computed with a precision of 1% using formulae that take into account pressure and temperature of the lab environment, amount of bulk sample used, and the volume of CO_2 developed in the calcimeter. Standards of pure calcium carbonate (i.e., Carrara Marble) were measured every ten samples to ensure proper calibration.

3.4.2 *Stable isotope analyses*

Stable isotope analyses ($\delta^{18}O$ and $\delta^{13}C$) were conducted using an automated continuous−flow carbonate preparation GasBenchII device (Spötl and Vennemann, 2003) and a ThermoElectron Delta Plus XP mass spectrometer in the geochemistry laboratories at the IAMC–CNR Institute of Naples.

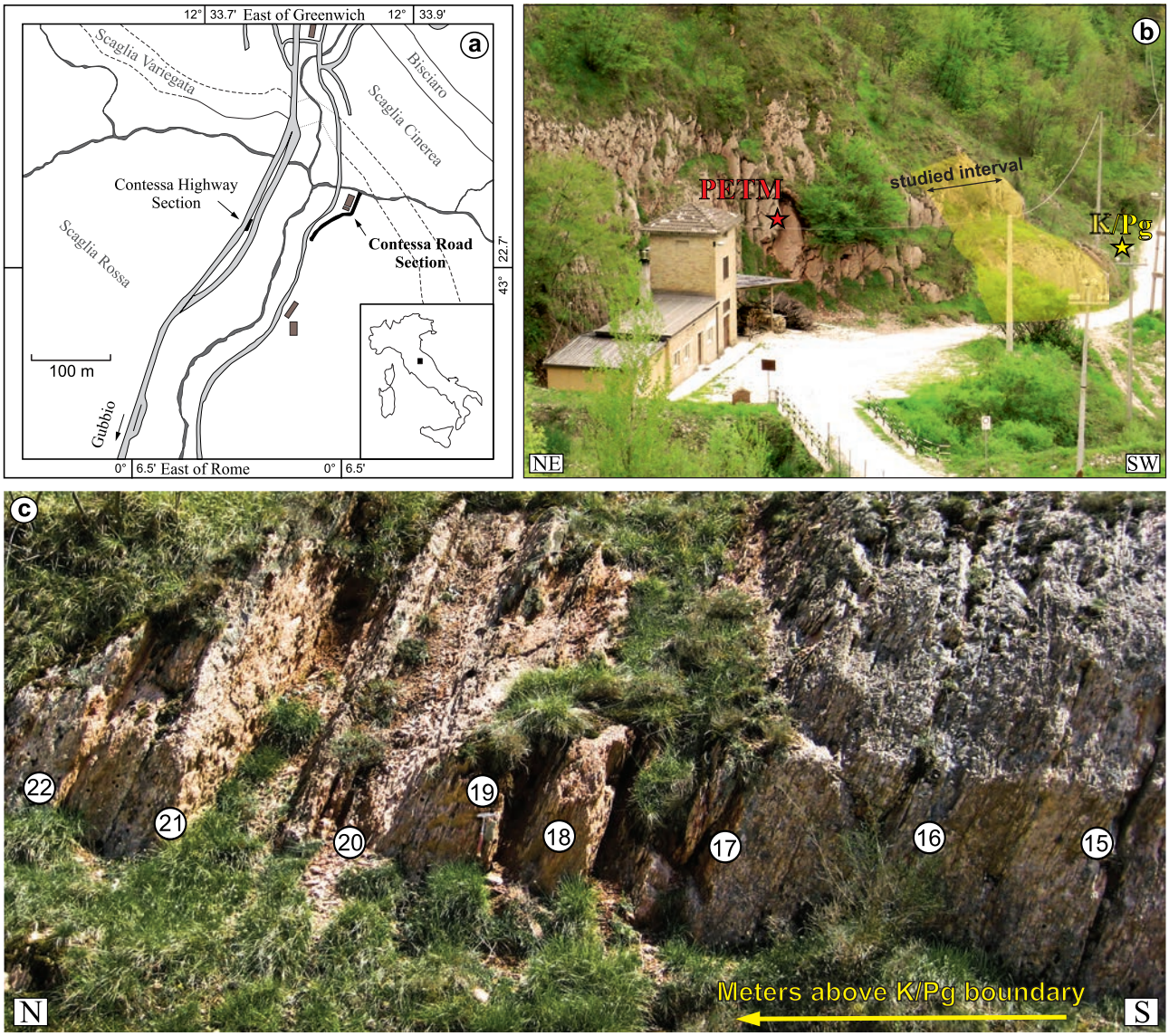

Figure 3.2 – (a) Location map and (b) panoramic view of Contessa Road Section. (c) Detailed view of the studied interval from ca. 15 m to ca. 22 m.

The acidification of samples was performed at 50 °C. An internal standard (Carrara Marble with δ18O=−2.43 versus Vienna Pee Dee Belemnite [VPDB] and $\delta^{13}C$=2.43 versus VPDB) was run every six samples while the NBS19 international standard was measured every thirty samples. Standard deviations of carbon and oxygen isotope measurements were estimated at 0.1‰ and 0.08‰, respectively, on the basis of replicate measurements of 20% of the analyzed samples. All of the stable isotope data are reported in per mil (‰) relative to the VPDB standard.

3.4.3 *Magnetic susceptibility and environmental magnetic analyses*

Magnetic susceptibility and environmental magnetism analyses were completed at the National Oceanography Centre, Southampton (NOCS), University of Southampton, UK. The low field mass–specific magnetic susceptibility was measured with a Kappabridge KLY–4 magnetic susceptibility meter. Artificial remanences, including the anhysteretic remanent magnetization, (ARM) imparted in a 100 mT AF, with a superimposed 0.05 mT direct current (DC) bias field, the isothermal remanent magnetization (IRM) imparted in a field of 0.9 T, and back–field demagnetization of the IRM at 0.1

T and 0.3 T were also measured. These data were used to determine the S–ratio$_{300}$ (IRM$_{-0.3T}$ / IRM$_{0.9T}$) and the HIRM$_{300}$ (HIRM = [IRM$_{0.9T}$ + IRM$_{-0.3T}$] / 2). Natural and artificial remanences were measured using a 2G Enterprises automated pass–through cryogenic magnetometer (Model 755R) with in–line AF demagnetization capability. Environmental magnetic properties (concentration, composition, and dimension of magnetic grains) were defined by investigating ARM, IRM and other indirect parameters from them. ARM magnetically excites only finer magnetic minerals, while IRM excites all magnetic minerals (concentration). Backfield magnetizations allow us to define HIRM$_{300}$ and S–ratio$_{300}$, which give information about coercivities (composition) of the magnetic minerals.

3.4.4 *Calcareous nannofossil*

Samples were prepared from unprocessed material as smear slides and were examined using a light microscope at 1250x magnification. Throughout the studied segment, calcareous nannofossils are generally rare and poorly preserved. As for biostratigraphy, all samples were studied with a quantitative analysis performed on thirty–one selected samples. In this study the calcareous nannofossil zonations of Martini (1971) and Okada and Bukry (1980) were applied. Nannofossils were counted using the methods described by Backman and Shackleton (1983) and Rio et al. (1990) counting species versus total assemblage, taking into account at least 300 nannofossils. In order to infer probable temperature and trophic variations of the surface waters, most calcareous nannofossils were, whenever possible, allocated into groups of environmental affinities, largely following Haq and Lohman (1976), Aubry (1992), Gardin and Monechi (1998), Bralower (2002), Tremolada and Bralower (2004), Persico and Villa (2004), Gibbs et al. (2006), and Raffi et al. (2009). Thus, according to the aforementioned literature, the following environmental groups have been used: warm (*Coccolithus pelagicus, Discoaster, Discoasteroides, Ericsonia, Fasciculithus, Heliolithus, Sphenolithus*), cold (*Chiasmolithus, Cruciplacolithus, Prinsius, Toweius*), eutrophic (*Chiasmolithus, Cruciplacolithus, Prinsius*), mesotrophic (*Toweius*), meso–oligotrophic (*Heliolithus*), and oligotrophic (*Coccolithus pelagicus, Discoaster, Discoasteroides, Ericsonia, Fasciculithus, Sphenolithus*).

3.4.5 *Foraminifera*

Samples were treated following the cold acetolyse technique of Lirer (2000) by sieving through a 63 μm mesh and drying at 50 °C. The cold acetolysis method enabled extraction of generally easily identifiable foraminifera even from indurated limestones. This technique offered the possibility of accurate taxonomic determination and detailed analysis of foraminiferal assemblages.

3.4.5.1 *Planktonic foraminifera*

All samples were studied for biostratigraphical and quantitative analyses. A representative split of at least 300 specimens was picked from the >63 μm fraction, mounted on micro–slides for permanent record and identification purposes, and taxonomically classified at the genus level. However, for the *Igorina* genus, a species–level classification was adopted following the taxonomic and morphological criteria of Petrizzo (2005). Following Hancock and Dickens (2005), the FI has been calculated using at least 300 specimens and including the whole test, fragments and dissolved tests for estimating the effect of carbonate dissolution. The planktonic foraminiferal zonation of Wade et al. (2011) was followed. Inferred life strategies, environmental affinities and depth ranking of the Paleocene planktonic foraminifera, which derived from latitudinal distribution, environmental inferences (morphology and biogeographic distribution) and stable isotope data, are from Luciani et al. (2007) and references therein.

3.4.5.2 *Benthic foraminifera*

A quantitative study of thirty–four selected samples was performed. A representative split of the >63 μm fraction was used to pick approximately 300 specimens. The >63 μm fraction was chosen because it can be regarded as the most appropriate for the investigation of the benthic community and because following Schroeder et al. (1987) the study of larger fractions would not be suitable for accurately inferring environmental variations. The sample–split weight used to pick benthic foraminifera was determined so that the foraminiferal density (FD), expressed as the number of foraminifera per gram of dry sediment, could be calculated. The planktonic to planktonic and benthic (P/P+B) ratio, expressed as a percentage, and the percentages of agglutinans and the opportunistic

"disaster species" *Spiroplectammina* spp. were also calculated. In order to calculate the infaunal percentages all taxa were allocated to infaunal and epifaunal morphogroups largely following Corliss (1985), Alegret et al. (2003) and Kaminski and Gradstein (2005).

3.4.6 *Weight percent coarse fraction*

The entire >63 μm residue obtained for all the samples was dried and weighted. The weight percent ratio of the >63 μm size fraction to the weight of the bulk sample (~100 g for each sample) is here referred to as the coarse fraction according to Broecker and Clark (1999, 2001). This index, calculated instead using the >38 μm size fraction, has been largely used as a possible indicator of dissolution (i.e., Hancock and Dickens, 2005; Colosimo et al., 2006; Leon–Rodriguez and Dickens, 2010; Luciani et al., 2010).

3.5 Results

3.5.1 *Biostratigraphy*

Also following previous findings (Coccioni et al., 2006), several calcareous nannofossil and planktonic foraminiferal events were recognized in the studied segment as well as just below and above it. They are as follows: LOs of *Morozovella occlusa* and *Morozovella velascoensis* (16 m), LO *Globanomalina pseudomenardii* (17 m), highest occurrence (HO) of *Parasubbotina variospira* (17.5 m), LO of *Heliolithus cantabriae* (18 m), LO of *Sphenolithus anarrhopus* (19.4 m), LO of *H. kleinpellii* (20.6 m), LO *Discoasteroides bramlettei* (21 m), LOs of *Discoaster mohleri* and *Heliolithus bukry* (23 m), and LO of *Acarinina soldadoensis* (24 m). The LO of *H. cantabriae* predates the LO of *H. kleinpellii*, but a transitional–intergraded form between them has been observed that sometimes hampers the correct identification of these two species. The LOs of *H. kleinpellii* and *D. mohleri* define the bases of calcareous nannofossil Zones NP6 and NP7 of Martini (1971), respectively, which correspond to the lower zonal boundaries of Zones CP5 and CP6 of Okada and Bukry (1980). The LO of *G. pseudomenardii*, the HO of *P. variospira* and the LO of *A. soldadoensis* mark the bases of planktonic foraminiferal Zones P4a, P4b and P4c of Wade et al. (2011), respectively. Therefore, the studied segment spans from the lowermost part of planktonic foraminiferal Zone P4b to the upper part of Zone P4b of Wade et al. (2011) and from the lower part of calcareous nannofossil Zone NP5 to the middle part of NP6 of Martini (1971), that is from the lower part of Zone CP4 to the middle part of Zone CP5 of Okada and Bukry (1980) (Fig. 3.3).

3.5.2 *$CaCO_3$ content, bulk, $\delta^{13}C$ and $\delta^{18}O$ isotopes, and paleomagnetic records*

The calcium carbonate content record has an average value of ~82% (minimum ~69.2% and maximum ~93.6% at 20.85 m and 22 m, respectively) (Fig. 3.3). Five discrete intervals containing lower carbonate contents and higher values of low–field magnetic susceptibility linked to the marly beds are recognized (Fig. 3.3). Magnetic susceptibility and calcium carbonate records show a significant negative correlation (r=−0.72). Relatively high values of magnetic susceptibility are related to low values of $CaCO_3$ and correspond to peaks in abundance of paramagnetic (e.g., increased amount of clay minerals) and ferromagnetic minerals in the sediments. The carbonate $\delta^{13}C$ record displays background values of 1.6‰–3.0‰ with three short, distinct CIEs at 20.15 m, 20.81 m and 21.88 m, which fall within three discrete marly beds (Fig. 3.3). However, adjacent limestone and marly limestone beds exhibit similar $\delta^{13}C$ values suggesting that these are primarily carbonate signals rather than manifestations of a different lithology. According to Corfield et al. (1991) the Paleogene Scaglia–type sediments near Gubbio might be affected by diagenesis and the oxygen isotope values have, therefore, been disregarded. The measured carbon isotope values oscillate around a natural variability range of biogenic calcite precipitated in marine environments ruling out significant effects of burial diagenesis on the carbon isotope signature. Post–depositional carbonate precipitation associated with mineralization of organic matter (low carbon isotope values) may influence the $\delta^{13}C$ values of the studied bulk sediments. However, the contribution of highly organic–rich sediments in the studied sedimentary context could be reasonably excluded because of the overwhelming dominance of pelagic carbonate.

The rock magnetic properties exhibit marked changes along the studied segment (Fig. 3.3). The IRM ranges from 1.81×10^{-5} to 8.93×10^{-4} Am^2/kg with an arithmetic mean of 7.82×10^{-5} Am^2/kg. The ARM shows an average value of 5.74×10^{-7} Am^2/kg (minimum of 1.55×10^{-7} and maximum of 2.35×10^{-6} Am^2/kg). The $HIRM_{300}$ (HIRM = [$IRM_{0.9}$T +

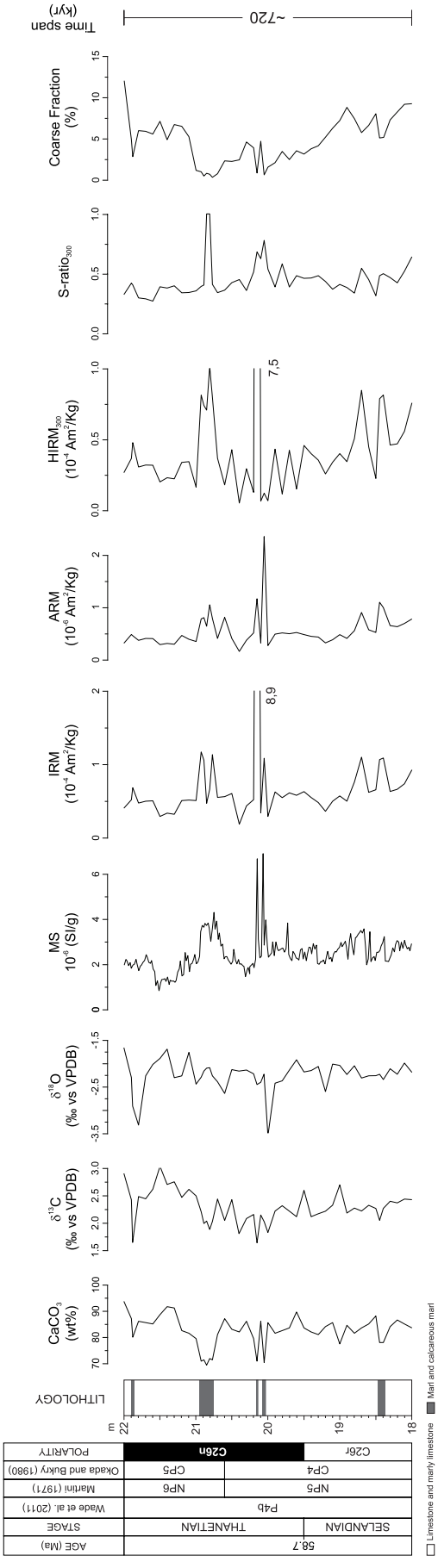

Figure 3.3 – Changes in $CaCO_3$ content, $\delta^{13}C$ and $\delta^{18}O$ of bulk sediments, magnetic susceptibility (MS), rock magnetic properties (isothermal remanent magnetization, IRM; anhysteretic remanent magnetization, ARM; hard isothermal remanent magnetization, $HIRM_{300}$; S–$ratio_{300}$), and coarse fraction across the 4 m–thick studied segment spanning the Selandian–Thanetian transition at Contessa Road. Biostratigraphy is based on the planktonic foraminiferal Zones of Wade et al. (2011) and calcareous nannoplankton Zones of Martini (1971) and Okada and Bukry (1980). Magnetostratigraphy is from Galeotti et al. (2000). The position of the Selandian–Thanetian boundary and the relative age is according to Gradstein et al. (2004) and Ogg et al. (2008). Based on magnetostratigraphy and the numerical ages of Gradstein et al. (2004) the segment spans ~720 kyr.

$IRM_{-0.3}T$] / 2) ranges from 4.99 x 10^{-6} to 7.51 × 10^{-4} Am^2/kg with an arithmetic mean of 5.48 × 10^{-5} Am^2/kg (Fig. 3.3). The S–$ratio_{300}$ ($IRM_{-0.3}T$ / $IRM_{0.9}T$) varies from 0.27, at 21.60 m, to 1.00 at 20.79–20.87 m with an arithmetic mean of 0.46. The ARM parameter shows spikes with high concentration of finer magnetic grains, whereas spikes IRM activate the entire magnetic component (concentration), and HIRM provides information about the magnetic coercivity of the magnetic carriers. The presence of low coercivity magnetic mineral (i.e., magnetite) is indicated by the value of S–$ratio_{300}$ close to unity (20.79–20.87 m). In contrast, low S–$ratio_{300}$ values and high values of $HIRM_{300}$ indicate the presence of high–coercivity magnetic minerals (i.e., hematite). The two latter parameters indicate both a subtle variation in the composition of magnetic minerals as well as a non–significant variation in grain size and concentration. The coarse fraction record shows a marked decrease from 19.3 to 21 m (Fig. 3.3).

3.5.3 *Biotic changes*

3.5.3.1 *Calcareous nannofossil*

Calcareous nannofossils assemblages are rich and well diversified. In most of the studied samples calcareous nannofossils exhibit moderate to good preservation, but enhanced dissolution has been observed from 19.2 to 20.95 m based on the preservation criteria proposed by Roth and Thierstein (1972). Assemblages are characterized by large abundances of *C. pelagicus*, *Sphenolithus* spp. and *Toweius* spp. (mostly *T. pertusus* and *T. eminens*), with subordinate numbers of *Fasciculithus* spp., *Heliolithus* spp., and *Prinsius* spp. (Fig. 3.4). Populations are dominated by warm–water indices without significant changes throughout the studied segment, oligo–mesotrophic taxa (Fig. 3.4). From 19.2 to 20.95 m, the trophic groups undergo remarkable changes. In particular, the eutrophic indices exhibit an overall decrease abundance from 19.2 to 20.75 m, while the meso–oligotrophic and mesotrophic indices show a concomitant increase that is more pronounced from 20.05 to 20.95 m with the highest values in correspondence of the marly layer at 20.75–20.95 m (Fig. 3.4).

3.5.3.2 *Planktonic foraminifera*

Planktonic foraminifera are abundant, generally well diversified and preserved from 18 to 19.2 m and from 21 to 22 m where they are mainly composed, in similar proportions, of different representatives of the genera *Acarinina*, *Igorina*, *Morozovella*, *Subbotina* and *Parasubbotina* with subordinate numbers of *Chiloguembelina*, *Zeauvigerina* and *Globanomalina* (Fig. 3.5).

From 19.2 to 20.95 m populations are relatively less diversified and largely dissolved, particularly within the marly layer at 20.75–20.95 m. In addition, they exhibit a gradual increase in the relative abundance of *Igorina* (especially represented by *I. tadjikistanensis*, *I. pusilla* "high trochospire" and *I. albeari* "chubby") and a concomitant gradual decline in the relative abundance of *Morozovella*, *Acarinina*, *Subbotina* and *Parasubbotina* together with a larger number of *Chiloguembelina* and *Zeauvigerina* and a lower number of *Globanomalina* (Fig. 3.5). However, according to their relative abundances, *Acarinina* suffered a minor decline with respect to *Morozovella* from 19.2 to 20.05 m (Fig. 3.5). Interestingly, within the marly layer at 20.75–20.95 m, *Igorina* (mainly *I. albeari* "chubby" and *I. tadjikistanensis)* peaks in abundance and occurs together with *Acarinina* that returns to increase in abundance and low numbers of *Acarinina*, *Chiloguembelina*, *Zeauvigerina*, subbotinids, and scattered specimens of *Morozovella* (Fig. 3.5). The FI displays a clear increasing trend from 18.6 m to 20.95 m with higher values within the marly layers at 20.05–20.09 m, 20.15–20.17 m and 20.75–20.95 m (up to ~80% at 20.85 m) (Fig. 3.5).

3.5.3.3 *Benthic foraminifera*

Assemblages are generally well diversified and preserved throughout the segment, except within the marly layer at 20.75–20.95 m where some evidence of dissolution is observed (Fig. 3.6). Populations are dominated by calcareous–hyaline forms with variable percentages of agglutinans that normally peak in correspondence with the marly layers (Fig. 3.6). Interestingly, *Spiroplectammina* spp. occur, although in different percentages, only within the marly layers at 20.05–20.09 m, 20.15–20.17 m and 20.75–20.95 m (Fig. 3.6). Infaunal and epifaunal taxa are present in different proportions within the assemblages. Infaunal and epifaunal taxa are present in different proportions within the assemblages. However, epifaunal taxa prevail in most of the samples, with higher percentages from 20.05 to 20.95 m (Fig. 3.6). There epifaunal taxa first gradually increase in

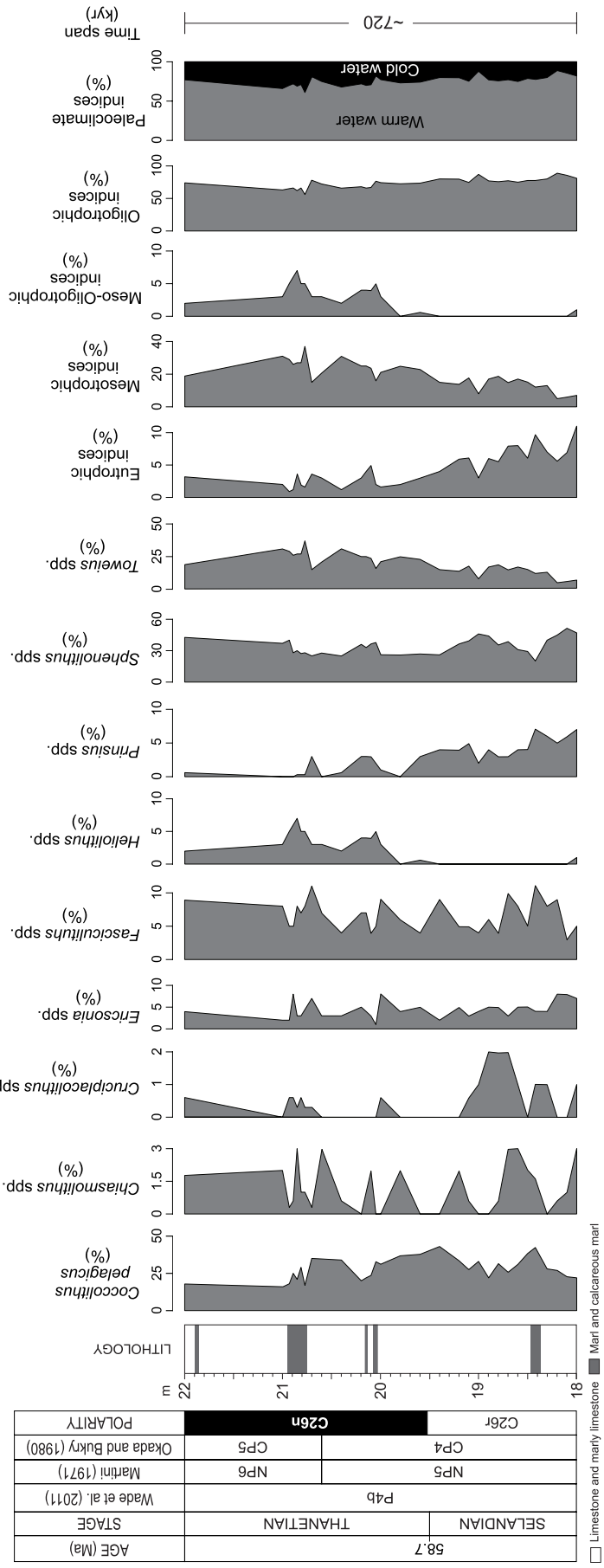

Figure 3.4 – Changes in selected calcareous nannofossil genera, species, and ecological groups across the studied segment at Contessa Road. Magnetobiochronostratigraphy and time span as in Figure 3.3.

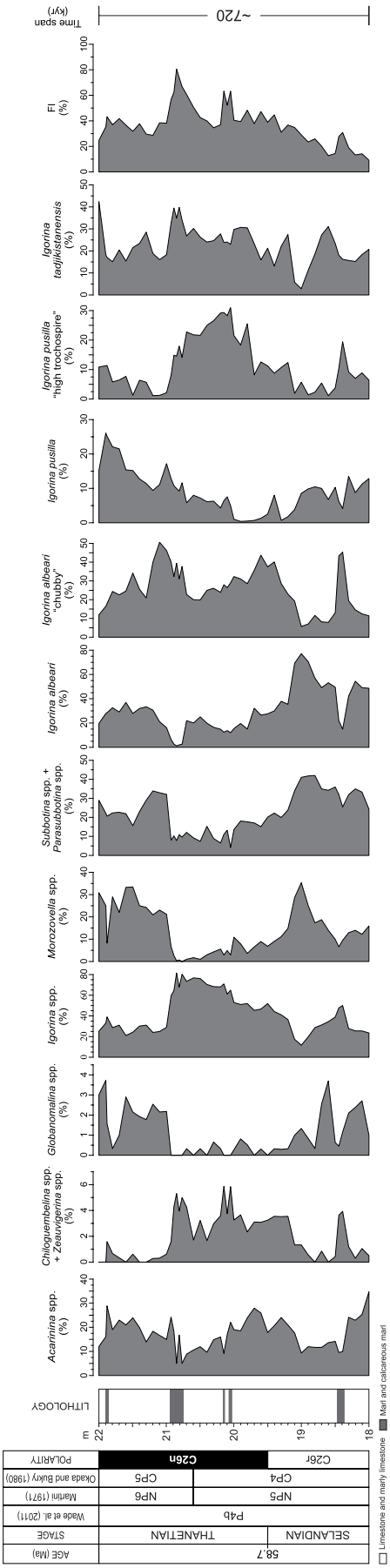

Figure 3.5 – Changes in selected planktonic foraminiferal genera, species, and morphospecies and fragmentation index across the studied segment at Contessa Road. Magnetobiochronostratigraphy and time span as in Figure 3.3.

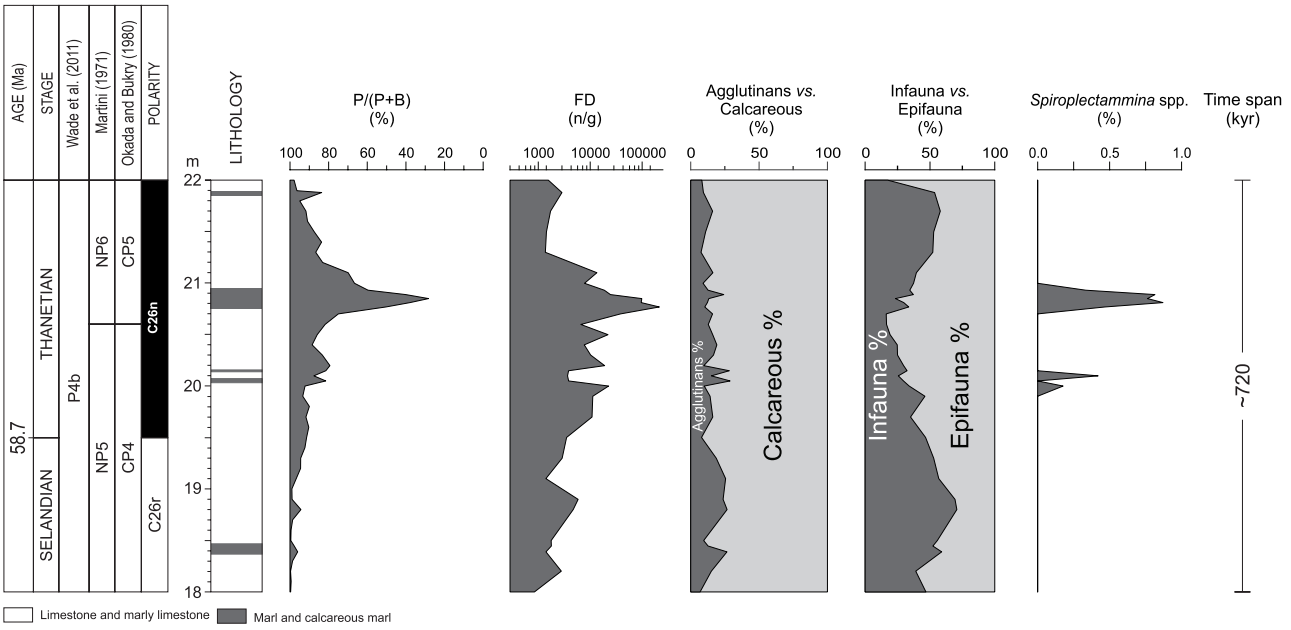

Figure 3.6 – Changes in selected benthic foraminiferal parameters [P/(P+B) ratio, foraminiferal density (FD), agglutinans vs. calcareous ratio, and infauna vs. epifauna ratio] and the relative abundance of Spiroplectammina spp. across the studied segment at Contessa Road. Magnetobiochronostratigraphy and time span as in Figure 3.3.

abundance reaching the highest percentage and then slightly decline just within the marly layer at 20.75–20.95 m that also corresponds to the highest values of FD. The P/(P+B) ratio fluctuates throughout the studied segment with decreasing values from 19.2 m upwards and lower percentages from 20.05 to 21.3 m. The lowest value (~30%) is found at 20.85 m (Fig. 3.6). The fluctuations of the P/(P+B) ratio are well mirrored by the FD.

3.6 Discussion

3.6.1 *Defining and constraining the age and duration of STTE and ELPE at Contessa Road*

Significant changes, both in the surface water and at the seafloor, took place across the Selandian–Thanetian transition as revealed by several rock parameters and by calcareous nannofossils and foraminifera documented in the Contessa Road section. On the basis of the biotic and abiotic changes, the 4 m–thick studied segment can be subdivided into five discrete intervals of different durations following the numerical ages of Gradstein et al. (2004). They are as follows interval 1 (18–19.2 m, ~360 kyr), interval 2 (19.2–20 m, ~145 kyr), interval 3 (20–20.75 m, ~80 kyr), interval 4 (20.75–20.95 m, ~25 kyr) and interval 5 (20.95–22 m, ~110 kyr) (Fig. 3.7).

Intervals 2 to 4 are characterized by significant pronounced changes, which testify that significant, stepped environmental and ecological perturbations took place during their deposition (Figs. 3.3–3.7). In particular, interval 4, which corresponds to a discrete marly layer, starts just after (~16 kyr) the evolutionary LO of *H. kleinpellii*, and falls in the middle part of Zone P4b and the lower part of Chron C26n. Magnetobiostratigraphically, interval 4 might be confidently correlated with the ELPE of Bralower et al. (2002, 2006), Zachos et al. (2004) and Agnini et al. (2007), which would, therefore, be the sedimentary expression of this event at Contessa Road. In such a scenario, intervals 2 to 4 at Contessa Road would represent the sedimentary expression of a relatively long lasting (~250 kyr) event that we here name the Selandian–Thanetian Transition Event (STTE) (Fig. 6). Interval 4, which would be the ~25 kyr long lasting ELPE equivalent, would represent the climax phase of the STTE. Based on the magnetostratigraphy provided by Galeotti et al. (2000) and the numerical ages from Gradstein et al. (2004), the STTE is centered at ~ 58.67 Ma.

3.6.2 *Carbon isotope and magnetic records of the STTE at Contessa Road*

The STTE at Contessa Road is characterized by a decreasing trend in $\delta^{13}C$ values with an abrupt negative CIE (~0.6‰) in correspondence with the ELPE equivalent, as well as drops in carbonate content, enhanced carbonate dissolution, and pronounced peaks in magnetic susceptibility (Figs. 3.3, 3.7). This could be ascribed to massive additions of ^{13}C–depleted carbon to the ocean–atmosphere system from an external carbon reservoir that is associated with substantial shoaling of the lysocline and accelerated hydrologic and weathering cycles (Dickens et al., 1995; Lourens et al., 2005; Nicolo et al., 2007). Enhanced values of magnetic susceptibility and other magnetic parameters occur throughout the STTE, with the highest values in correspondence with the marly layers and particularly during the ELPE equivalent (Figs. 3.3, 3.7). $S–ratio_{300}$ values approaching unity, as documented during the ELPE equivalent at Contessa Road, testify to the presence of magnetite. On the other hand, the presence of hematite is indicated by low $S–ratio_{300}$ values and high values of $HIRM_{300}$. The magnetic susceptibility variations may be due to the changes in the concentration of mainly ferromagnetic and subordinately paramagnetic minerals, which could be related to changes in terrigenous influx, carbonate dissolution or magnetic mineralogy, which in turn might be related to redox conditions on the seafloor–low coercivity (i.e., magnetite) vs. high coercivity magnetic minerals (i.e., hematite) – or to the nature of the weathering in the continental search area (Jovane et al., 2004). Higher values of magnetic susceptibility have been related to warmer and wetter climates, with associated enhanced chemical weathering and continental runoff (Jovane et al., 2010). Variations in magnetic susceptibility and Fe content, which reflect changes in clay contents, have been documented during prominent events (i.e., K/Pg, ELPE, PETM) both in the Pacific and Atlantic oceans (Westerhold et al., 2008; Hilgen et al., 2010). These changes appear to be controlled by carbonate dissolution (Zachos et al., 2003; Hancock and Dickens, 2005) driven by the expansion and contraction of biosphere productivity in response to changes in solar insolation (Pälike et al., 2006). At the deep sites of Walvis Ridge and Shatsky Rise, a lowering of sedimentation rate was documented during the ELPE and their equivalents that might be related to changes in productivity and/or preservation (Westerhold et al., 2008). The higher sedimentation rate at the shallower Atlantic ODP Site 1051 and the condensed sequences at Shatsky Rise confirm lysocline shoaling during the ELPE and its equivalents (Westerhold et al., 2008).

3.6.3 *Reading the biotic changes induced by the STTE at Contessa Road: which scenario for this environmental perturbation?*

The remarkable changes in the relative abundances, preservation and taxonomical composition of calcareous nannofossil and foraminiferal assemblages recognized across the studied segment at Contessa Road show that during the STTE, and particularly in correspondence with the ELPE equivalent where these changes appear to be more prominent, an abrupt environmental perturbation took place in the photic zone and at the seafloor following a period of relatively stable environmental conditions characterized by essentially warm and oligo–mesotrophic surface waters (Figs. 3.5–3.6). Although the response of calcareous nannofossils to multiple environmental factors is fairly complex and still largely unclear (i.e., Raffi et al., 2009), the increase in abundance of the cold–water and meso–oligotrophic to mesotrophic taxa suggests slightly less warm surface waters and little more trophic conditions during the STTE (intervals 2 to 4) with slightly more pronounced nutrient availability in correspondence of the ELPE equivalent (interval 4) (Figs. 3.4, 3.7).

Higher FI and lower P/(P+B) ratio values during the STTE (Figs. 3.4 and 3.5) strongly reflect the effect of enhanced carbonate dissolution, most likely induced by an impressive shallowing of the lysocline caused by acidification of the oceans, that reaches its climax during the ELPE equivalent, where impoverished and largely dissolved planktonic foraminiferal assemblages occur. The genera *Igorina*, *Acarinina* and *Morozovella* have widely been inferred to be an oligotrophic, warm–water surface–dweller taxa (i.e., Luciani et al., 2007 and references therein). Among these genera, the symbiont–bearing *Igorina*, which is believed to have occupied a depth habitat between the shallower photosymbiotic morozovellids and the relatively deeper photosymbiotic acarininids, might have benefited the most from the changing environmental conditions during the STTE, most likely replacing the ecological niches vacated by *Acarinina*, *Globanomalina*, *Morozovella* and subbotinids. However, according to their relative

abundances, *Acarinina* suffered a minor decline with respect to *Morozovella* in the early phase (interval 2) of the STTE and partially recovered during the ELPE equivalent (Fig. 3.5). It cannot be excluded, therefore, that in this phase the ecological niches vacated by the morozovellids were first filled by the acarininids in agreement with a similar life strategy documented by Luciani et al. (2007) and Agnini et al. (2009) during the PETM and the K hyperthermal event. The dominance of *I. tadjikistanensis*, *I. pusilla* "high trochospire" and *I. albeari* "chubby" during the STTE could be interpreted as a morphologic response to a relative change in surface water productivity, which enhanced species competition forcing the igorinids to modify their morphologies to cope. *Subbotina*, *Parasubbotina* and *Globanomalina* are considered opportunistic genera that prefer deeper, colder and more eutrophic waters (i.e., Luciani et al., 2007 and references therein). Their decline in abundance during the STTE might be essentially driven by ecological competition and differential dissolution, the latter probably more significant since *Subbotina* and *Parasubbotina* are known to be prone to that process (i.e., Luciani et al., 2007 and references therein). The increase in abundance of the opportunistic, intermediate dwellers *Chiloguembelina* and *Zeauvigerina* that thrive in low–oxygen environments (i.e., Luciani et al., 2007 and references therein) during the STTE, may document a weakly developed oxygen minimum zone in the depositional environment of that time (Figs. 3.5, 3.7). Moreover, the slight increase in *Acarinina*, a meso–oligotrophic genus, and in low–oxygen tolerant *Chiloguembelina* and *Zeauvigerina* along with the drop in abundance of the oligotrophic morozovellids during the ELPE equivalent might be interpreted as a slight increase in the trophic levels. This scenario is consistent both with the suggestion of Agnini et al. (2009) for the K event at Farra, where the surface dwelling acarininids were able to temporarily proliferate in nutrient enriched waters previously occupied by subbotinids and to better tolerate these conditions than morozovellids and with the calcareous nannofossil data.

The relatively higher numbers of the benthic agglutinated foraminifera in correspondence with the marly layers within the STTE could suggest a further shallowing of the lysocline during their deposition (Figs. 3.6, 3.7). No clear sign of oxygen deficiency at the seafloor has been documented at Contessa Road. The higher abundance of epifaunal taxa during the STTE might be interpreted as a lowering of nutrient availability at the seafloor. In agreement with the calcareous plankton data, however, differential dissolution probably played a major role in determining lowered values of the epifauna to infauna ratio (Figs. 3.6, 3.7). In oligotrophic environments, all metabolizable nutrients are consumed at the sediment surface and the underlying sediment layers contain small quantities of nutrients and lower infaunal species as depicted in the TROX model (Jorissen et al., 1995). Following Herguera and Berger (1991), the higher values of FD during the STTE that are particularly pronounced during the ELPE equivalent suggest enhanced food supply at the seafloor, although a complex interplay of increasing and differential dissolution susceptibility in planktonic foraminifera when compared to their benthic counterparts may have played a major role (Hancock and Dickens, 2005). Moreover, the marked changes affecting the planktic ecosystem might have determined changes in quality and quantity of the food flux to the seafloor, thus triggering changes in the benthic communities. Finally, the occurrence of *Spiroplectammina*, which is known to be an opportunistic "disaster taxon" indicating a stressed environment (Kuhnt and Kaminski, 1996), would mark significant environmental disturbance at the seafloor (Figs. 3.6, 3.7). If we also speculate that the relative abundance of *Spiroplectammina* is proportional to the strength of the environmental perturbation (Fig. 3.6), the ecological disruption related to the STTE would be confirmed to have been more severe in the late phase (intervals 3 and 4) of that event and particularly during the ELPE equivalent (interval 4), which can be considered as the climax of the STTE.

At the end of the STTE (interval 5) a rapid environmental and ecological recovery occurs, with the relative abundances, preservation and composition of the main components of calcareous nannofossil and foraminiferal assemblages moving towards features similar to those of the pre–STTE conditions (interval 5).

Interestingly, no major biotic extinctions occurred among calcareous nannofossils and foraminifera during the STTE, even though it represents a significant event inducing severely stressed surface water and seafloor environments. In particular, the complex interplay of the enhancing surface productivity and dissolution, which involved changes in relative abundances, preservation and composition of primary producers (calcareous nannoplankton) and zooplankton (planktonic foraminifera), may have

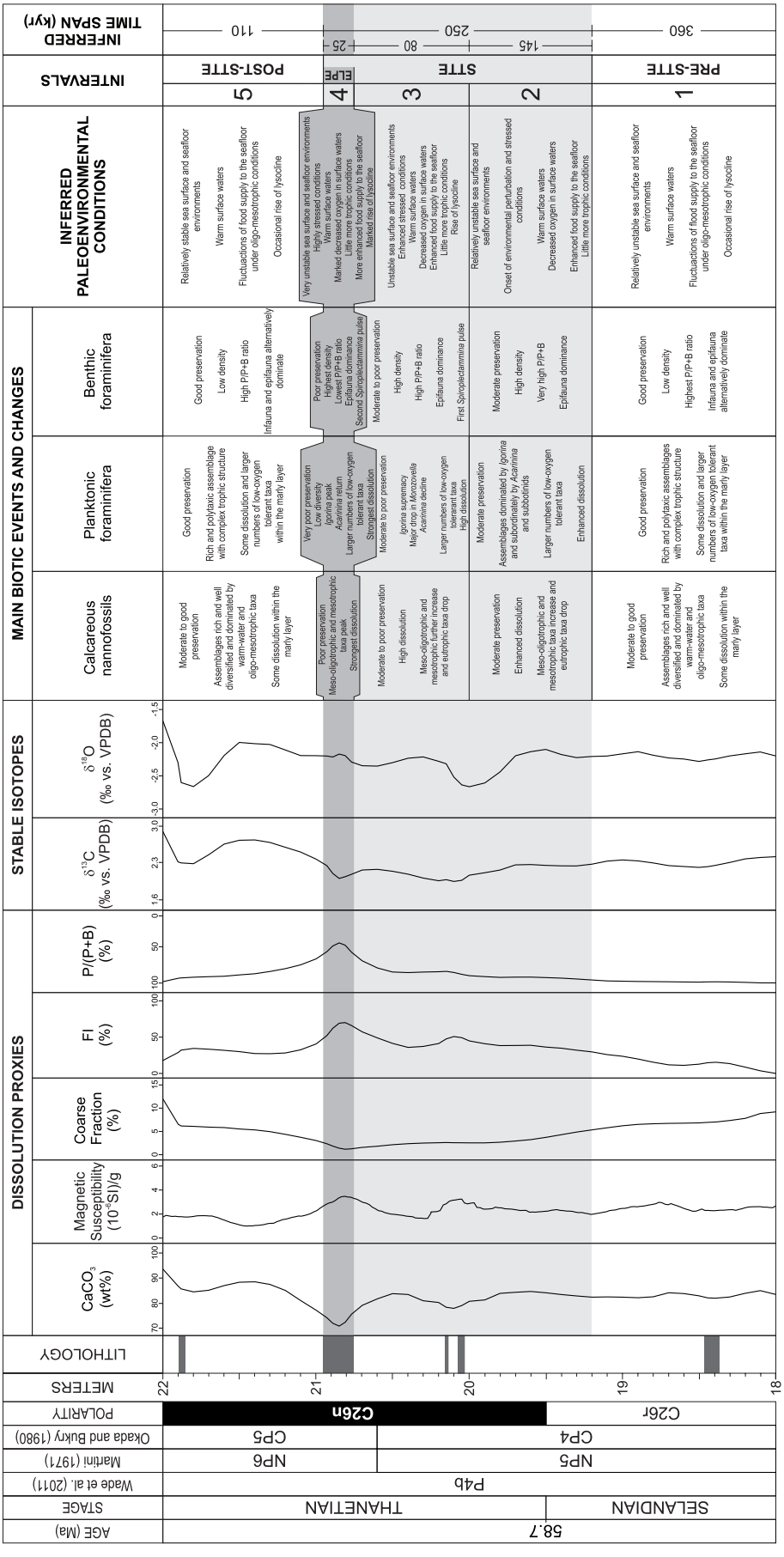

Figure 3.7 – Summary of the main dissolution proxies, stable isotopes, main biotic events and chnges, and inferred paleoenvironmental conditions across the 4 m–thick studied segment spanning the Selandian–Thanetian transition at Contessa Road. Calcium carbonate, magnetic susceptibility, coarse fraction, fragmentation index, P/(P+B) ratio, and stable isotopes have been smoothed by an adjacent moving average with a five–point window. Magnetobiochronostratigraphy as seen in Figure 3.3. The light gray shaded area highlights the Selandian–Thanetian transition event (STTE) event and the dark gray area marks the early late Paleocene hyperthermal event (ELPE) equivalent. In the basis of the biotic and abiotic changes, the studied segment can be subdivided into five discrete intervals, which have a different duration according to the available magnetostratigraphy at the Contessa Road and following the numerical ages from Gradstein et al. (2004).

been affected by the reorganization of the planktic ecosystem. These changes may have, in turn, altered the food flux (i.e., type and quantity) to the seafloor, thus triggering changes in the benthic communities. The biotic and abiotic variations that took place during the STTE indicate gradual changes in paleoenvironmental conditions rather than a sudden event both in the photic zone and at the seafloor. These major changes suggest a scenario that provides for an enhanced, but of short measure, nutrient availability during the STTE, which peaks during the ELPE equivalent.

In addition, no significant climate changes have been recorded throughout the studied segment except for hardly less warm conditions during the STTE. This is well in agreement with the recent findings of Westerhold et al. (in press) who provided a continuous high–resolution benthic foraminiferal stable isotope record for the Paleocene at ODP Site 1209 where slight increasing values of $\delta^{18}O$, probably accompanied by a small decrease in temperature, and a $\delta^{13}C$ complex record have been detected across the ELPE.

3.6.4 *Implications for a more complex scenario for the ELPE than hitherto supposed*

The variations in the planktonic foraminiferal assemblages recognized before (intervals 2 and 3), during (interval 4) and after (interval 5) the deposition of the marly layer equivalent to the ELPE (Fig. 3.7) well mirror those recorded before, during and after the ELPE at Shatsky Rise by Petrizzo (2005) and also support the suggestion of Hancock and Dickens (2005) that the ELPE at Sites 1209 and 1211 might have marked only a brief period within the context of a 1–2 Myr long interval of unusual conditions. Furthermore, a prolonged ELPE interval of enhanced calcareous nannofossil dissolution was observed at site 1262 by Agnini et al. (2007).

At Zumaia, which is the first land–based locality where the ELPE equivalent was recognized (Bernaola et al., 2007), we observe magnetobiostratigraphic mismatches and uneven biotic response when compared with deep–sea cores and the Contessa Road section that represents the Tethyan analogue of the Spanish section. In fact, according to Bernaola et al. (2007), the ELPE equivalent is placed well after (~273 kyr based on cycle–counting) the LO of *H. kleinpellii* and in the upper part of C26r (~168 kyr prior the Chron C26r/C26n boundary). Moreover, within the planktonic foraminiferal assemblages of the core of the ELPE equivalent, *Igorina* declines while *Subbotina* largely and concurrently increases in abundance. Therefore, the biotic response of the planktonic foraminiferal assemblages of the ELPE equivalent at Zumaia is significantly different from that documented at Shatsky Rise, Walvis Ridge and Contessa Road. This different biotic response could partially reflect a different depositional setting while environment, and the magnetobiochronostratigraphic discrepancy might be explained by the occurrence of transitional forms (intergrades) between *H. kleinpellii* and its ancestor *H. cantabriae* that sometimes may hamper precise identification (Agnini et al., 2007). Moreover, the pinpointing of the exact position of Chron C26n in deep–sea cores is hampered by its proximity to the ELPE (Röhl et al., 2004; Bralower et al., 2006; Westerhold et al., 2008).

All of these data and remarks from different ocean and land–based sites suggest a more complex character for the ELPE than previously supposed, which the considerable body of diverse analytical data we provide from the Contessa Road strongly confirms.

3.7 Conclusion

Detailed analyses of calcareous nannofossils and foraminiferal assemblages, and high–resolution geochemical, isotopic and magnetic records across the Selandian–Thanetian transition at Contessa Road (Gubbio, Italy) allow us to recognize and accurately document a 250 kyr–lasting interval of environmental perturbations that we here name the Selandian–Thanetian Transition Event (STTE). These changes clearly outline a complex paleoenvironmental evolution in the western central Tethys across the Selandian–Thanetian stages. The Contessa Road represents the first land–based section where the STTE is recognized and its effects documented. The remarkable changes in the relative abundances, preservation and composition of calcareous nannofossils and foraminiferal assemblages show that during the STTE an abrupt environmental perturbation took place and reached its climax during the ELPE equivalent, where these changes appear to be more prominent. The environmental instability is not confined within the photic zone but extends to the seafloor resulting in little more trophic conditions of the sea surface waters with an enhanced, but of short measure, nutrient availability on the seafloor

under almost unchanged warm–water conditions and marked rise of lysocline.

Further studies are needed to understand whether the STTE represents a regional or global event. However, an abrupt environmental perturbation close to the Selandian–Thanetian transition has been observed in other Tethyan as well as open ocean sites suggesting that the STTE might be a possible global prelude to the PETM.

The comparison of our biotic and abiotic records throughout the Selandian–Thanetian transition with available data across the ELPE and related remarks from former investigated ocean and land–based sites provides lines of evidence that this event is part of a more complex scenario than hitherto supposed.

CHAPTER 4

The Eocene Thermal Maximum 3 (K or X) hyperthermal event: Reading the environmental perturbations at Gubbio (Italy)

4.1 Introduction

Recently, at least five early Eocene hyperthermal events, presently called H1, H2, I1, I2, and K (after Cramer et al., 2003), have been documented in several records at approximately 53.7, 53.6, 53.3, 53.2, and 52.5 Ma (Dickens, 2011). Although different in magnitude, with deep-sea temperatures rise of 5–6°C during the PETM, about 4°C during Eocene Thermal Maximum 2 (ETM2) and about 2.5°C during Eocene Thermal Maximum 3 (ETM3) (Thomas et al., 2011), these five hyperthermal events seem to share similar characteristics. In particular, the ETM3, also informally known as K or "X" event has been recognized in several deep-sea cores from Shatsky Rise (DSDP Site 577, central Pacific), Goban Spur (DSDP Site 550, North-west Atlantic), Walvis Ridge (ODP Leg 208 Sites 1262-1267, South Atlantic), Demerara Rise (ODP Leg 207, Site 1258, central Atlantic), Hawaii (ODP Leg 199, Site 1215, central Pacific) as well as in on–land Italian (Contessa Road, Farra and Possagno), French (Corbières Hills), New Zealand (Mead Stream), Egyptian (Bir Dakhl and Wadi Tarfa) sections and in Kallo core (Belgium) (Cramer et al., 2003; Röhl et al., 2004, 2005, 2009; Zachos et al., 2004, 2010; Agnini et al., 2006, 2009, Sexton et al., 2006; Thomas et al., 2006; Kroon et al., 2007; Pirkenseer et al., 2009; Westerhold and Röhl, 2009; Galeotti et al., 2010; Leon-Rodriguez and Dickens, 2010, Höntzsch et al., 2011; Lunt et al., 2011; Slotnick et al., 2011; Speijer et al., 2011, Thomas et al., 2011) (Fig. 4.1). The ETM3 was, at first, identified by DSDP Site 577 in magnetochron C24n and middle-upper part of calcareous nannofossils Zone NP11 of Martini et al. (1971) and at DSDP Site 550 at the base of Zone NP12 (Cramer et al., 2003) (Fig. 4.2). It is there marked by a ~0.3-1.0‰ negative CIE and increase values of magnetic susceptibility (χ). It was then documented at Walvis Ridge Sites (1262, 1263, 1265, 1266 and 1267) where it represents a prominent clay–rich layer and characterizes by magnetic susceptibility spikes occurring in the planktonic foraminiferal Zone P7 of Berggren et al. (1995) and in the calcareous nannofossil Zone CP10 of Okada and Bukry (1980) (Röhl et al., 2004; Zachos et al., 2004; Kroon et al., 2007) (Fig. 4.2). Although varying with the paleodepth, the negative CIEs in bulk, planktonic and benthic foraminifera are comprised between 0.5 and 1.0‰ (Röhl et al., 2004, 2005; Thomas et al., 2006). At Walvis Ridge Sites poorly diversified benthic foraminiferal assemblages mainly dominated by small specimens of the epifaunal *Nuttallides truemphy* and different abyssaminids have been documented (Röhl et al., 2004, 2005; Thomas et al., 2006). These variations are accompanied by changes in calcareous nannofossil assemblages. In particular, across the ETM3, robust taxa like *Discoaster, Tribrachiatus orthostylus*, and *Sphenolithus* increase in abundance, whereas *Zygrablithus* decreases during the event, followed by a significant increase in abundance at the end of the event (Thomas et al., 2006). In the same sites, a lower food supply to the seafloor has been inferred, probably in response to decreased open-ocean productivity and enhanced ocean stratification (Thomas et al., 2011). Moreover, on the basis of benthic foraminiferal assemblages, the same authors documented no expansions of Oxygen Minimum Zone (OMZ) during the ETM3. At ODP

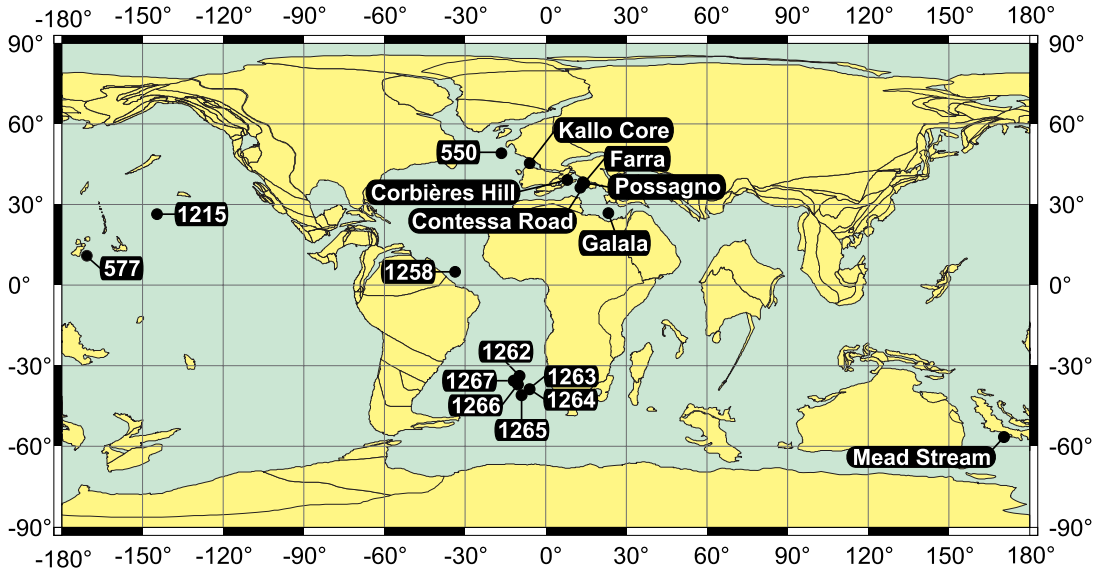

Figure 4.1 – Palaeogeographic reconstruction at 52 Ma and location of the Shatsky Rise (DSDP Site 577, central Pacific), Goban Spur (DSDP Site 550, North-west Atlantic), Walvis Ridge (ODP Leg 208 Sites 1262-1267, South Atlantic), Demerara Rise (ODP Leg 207, Site 1258, central Atlantic), Hawaii (ODP Leg 199, Site 1215, central Pacific), Contessa Road, Farra, Possagno, Corbières Hills, and Mead Stream on-land sections, Galala succession and Kallo core. Reconstruction made using the web-based software at http://www.odsn.de/odsn/services/paleomap/paleomap.html.

Site 1262, the ETM3 has been constrained in the middle part of Chron C24n.1n? and in the lowermost part of calcareous nannofossil Zones NP12 of Martini (1971) and CP10 of Okada and Bukry (1980) and is associated with enhanced calcareous nannofossil dissolution and increase iron (Fe) intensity (Agnini et al., 2007, Zachos et al., 2010) (Fig. 4.2). Increase Fe intensity for the ETM3 has been documented at Site 1258, where the event has been well-constrained in the lower part of Chron C24n.1n and is represented by precession cycles 146 and 147, and lies in the middle of $Ec_{100}32$, and in the middle of $Ec_{405}8$ (Westerhold and Röhl, 2009) (Fig. 4.2). In the same site, on the basis of benthic foraminiferal isotopic data Sexton et al. (2006) document a negative excursion, centered at ~52.6 Ma, in both $\delta^{13}C$ and $\delta^{18}O$ of ~1‰ and ~0.8‰, respectively. The $\delta^{18}O$ excursion provides compelling evidence of a ~4°C rapid warming in the upper abyssal tropical Atlantic (Sexton et al., 2006). The Contessa Road section (Umbria–Marche Basin, Italy) represents the first land-based locality where the ETM3 was identified (Coccioni et al., 2006; Galeotti et al., 2010) (Fig. 4.2). In particular, the ETM3, which was well-constrained in the middle part of Chron C24n.1n and a the NP11/NP12 transition, is associated with ~0.5‰ CIE and drop in calcium carbonate content and corresponds to insolation maxima within a very long modulation period of eccentricity (~1.2 Myr) (Galeotti et al., 2010). The most comprehensive paleoclimatological investigation was performed at Possagno and Farra sections (Venetian pre–Alps, Italy), where micropaleontological and geochemical analyses were carried out across several hyperthermals including the ETM3 (Agnini et al., 2009). At both Possagno and Farra sections, the ETM3 has been identified in the uppermost part of Chron C24n.1n and in the lowermost part of NP12 and is marked by ~0.4‰ and ~0.6‰ CIEs, respectively (Fig. 4.2). Moreover at Farra, on the basis of micropaleontological analyses, a rapid warming and enhanced eutrophic of sea surface water were documented (Agnini et al., 2009). At ODP site 1215 the ETM3 has been constrained in the middle part of Chron C24n.1n, very close to NP11/NP12 transition and in the planktonic foraminiferal zone E4 of Wade et al. (2011) (Leon–Rodriguez and Dickens, 2010) (Fig. 4.2). The same authors documented a ~1.0‰ CIE associated with drops of $\delta^{18}O$ and carbonate content, and an increase in the fragmentation index and P/B ratio. More recently, the ETM3 has been recognized in the southern Tethyan carbonate platform of Galala (Egypt) in the lowermost part of indistinct zone NP12–13 and is associated with marked calcium carbonate content and increase Total Organic Carbon (TOC) (Höntzsch et al., 2011).

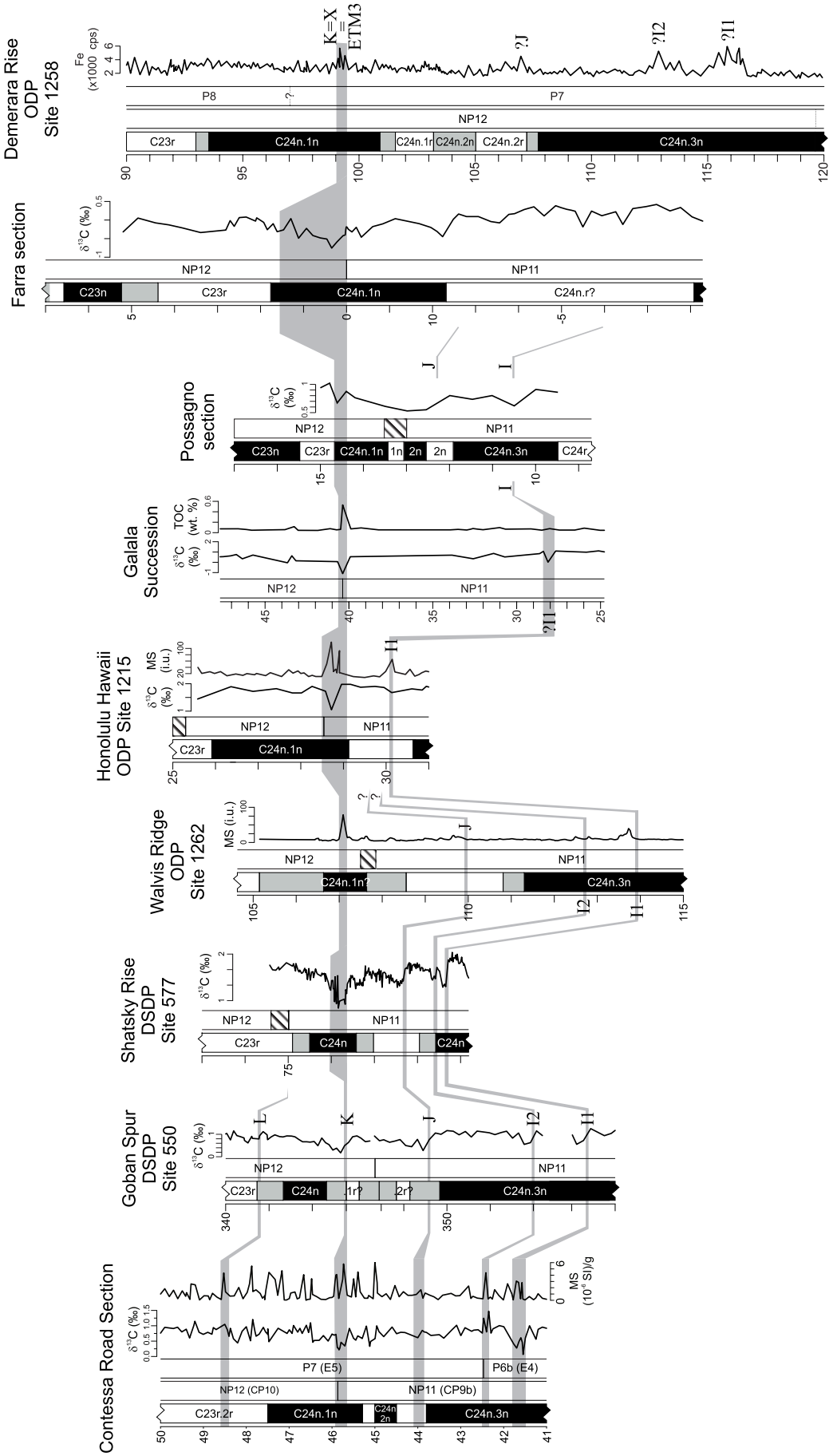

Figure 4.2 – Correlation between Contessa Road, Farra and Possagno sections, Galala succession, DSDP Sites 550 and 577, and ODP Sites 1215, 1258, and 1262. Calcareous nannofossil schemes of Martini et al. (1971) and Okada and Bukry (1980), planktonic foraminiferal scheme of Berggren et al. (1995) and Wade et al. (2011). Data from DSDP 550 and 577 are from Cramer et al. (2003). Magnetostratigraphy and biostratigraphy from ODP Site 1262 are from Bowles (2006) and Agnini et al. (2007), respectively, while MS is from Zachos et al. (2004). Magnetostratigraphy and biostratigraphy from ODP Site 1215 are from Shipboard Scientific Party Leg 199 (2002), Raffi et al. (2005) and Leon-Rodriguez and Dickens (2010), whereas $\delta^{13}C$ is from Leon–Rodriguez and Dickens (2010). Biostratigraphy and $\delta^{13}C$ of Galala succession are from Höntzsch et al. (2011). Data from Possagno and Farra sections are from Agnini et al. (2009). Magnetostratigraphy and biostratigraphy from ODP Site 1258 are from Suganuma and Ogg (2006). Iron intensity is from Westerhold and Röhl (2009) and I1, I2 and J events are tentatively placed.

4.2 Objective

The main aims of this study are (1) to better constrained the main early Eocene hyperthermals with a refinement of the available biostratigraphy in the Western Tethys Contessa Road reference section (Gubbio, Italy); (2) to identify and characterize the significant biotic and abiotic changes across the ETM3; (3) to document and characterize the paleoenvironmental and paleoecological effects induced by ETM3 the response of calcareous nannofossil and foraminifera across from available records at different paleodepth.

4.3 Stratigraphical setting

Located near Gubbio (central Italy) is one of the best studied Tethyan Mesozoic–Cenozoic successions which is characterized by a remarkable record of many crucial aspects of the Earth's history (e.g., Luterbacher and Premoli Silva, 1964; Alvarez et al., 1977; Lowrie et al., 1982; Premoli Silva et al., 1988; Coccioni et al., 1989, 1995, 2006, 2008, 2010; Coccioni, 1996; Montanari et al., 1997; Galeotti et al., 2000, 2004, 2010; Coccioni and Luciani, 2004; Scopelliti et al., 2006; Jovane et al., 2007, 2010; Musavu-Moussavou et al., 2007; Giusberti et al., 2009; Robinson et al., 2009; Turchyn et al., 2009) (Fig. 4.3). In particular, the Contessa Road section (lat. 43°22′47″N; long. 13°33′49″E) represents a continuous, complete and undisturbed record suitable for correlating the early-middle Paleogene biostratigraphy to the geomagnetic polarity history. This ~120 m−thick section of pelagic sediments belongs to the "Scaglia"−type facies (Lowrie et al., 1982) and is made up of well−stratified coccolith−foraminiferal limestones with subordinated marls deposited at lower middle to lower bathyal depths (1000-1500 m) (Coccioni et al., 2010). This study focuses on a 9-m thick stratigraphic segment located from 41 to 50 m above the Cretaceous-Paleogene (K–Pg) boundary (Figs. 4.3 and 4.4). Following Coccioni et al. (2006), significant biotic and abiotic changes compared to the underlying and overlying beds are identified. According to Galeotti et al. (2010), the studied segment spans from the lowermost part of magnetochron C24n.3n to the uppermost part of magnetochron C23r.2r with a duration of ~1500 kyr and an average sedimentation rate of ~0.59 cm/kyr following the numerical ages of Gradstein et al. (2004) (Fig. 4.4).

4.4 Materials and Methods

A total of one–hundred and twenty-eight bulk rock samples was collected at ~7 cm intervals corresponding to ~10 kyr through the 41-50 m interval at Contessa Road. All the material studied is housed in the laboratory of the Dipartimento di Scienze del Terra, della Vita e dell'Ambiente, Università di Urbino, Italy.

4.4.1 *Calcium carbonate*

Analyses of carbonate content were performed on sixty-one samples at the geochemistry laboratory of the Dipartimento di Scienze della Terra, della Vita e dell'Ambiente, Università di Urbino, Italy. The bulk rock samples were reduced to fine powder in agate mortar. Calcium carbonate content measurements were obtained using a Dietrich-Frühling calcimeter. The method is based on the measurement of CO2 volume produced by the complete dissolution of pre-weighted samples (300 ± 1 mg each), in 10 % vol. HCl. Total carbonate contents (wt.% CaCO3) with a precision of 1% were computed using formulae that take into account pressure and temperature of the lab environment, amount of bulk sample used, and the volume of CO2 developed in the calcimeter. Standards of pure calcium carbonate (i.e., Carrara Marble) were measured every ten samples to ensure proper calibration.

4.4.2 *Stable isotopes*

Stable isotope analyses ($\delta^{18}O$ and $\delta^{13}C$) were conducted on a hundred and eleven bulk samples. They were produced using an automated continuous-flow carbonate preparation GasBenchII device (Spötl and Vennemann, 2003) and a ThermoElectron Delta Plus XP mass spectrometer in the geochemistry laboratories at the IAMC-CNR Institute of Naples. The acidification of samples was performed at 50 °C. An internal standard (Carrara Marble with δ18O = −2.43 versus Vienna Peedee belemnite [VPDB] and δ13C = 2.43 versus VPDB) was run for every six samples, and for every thirty samples the NBS19 international standard was measured. Standard deviations of carbon and oxygen isotope measurements were estimated at 0.1‰ and 0.08‰, respectively, on the basis of replicate measurements of 20% of analyzed samples. All of the stable isotope

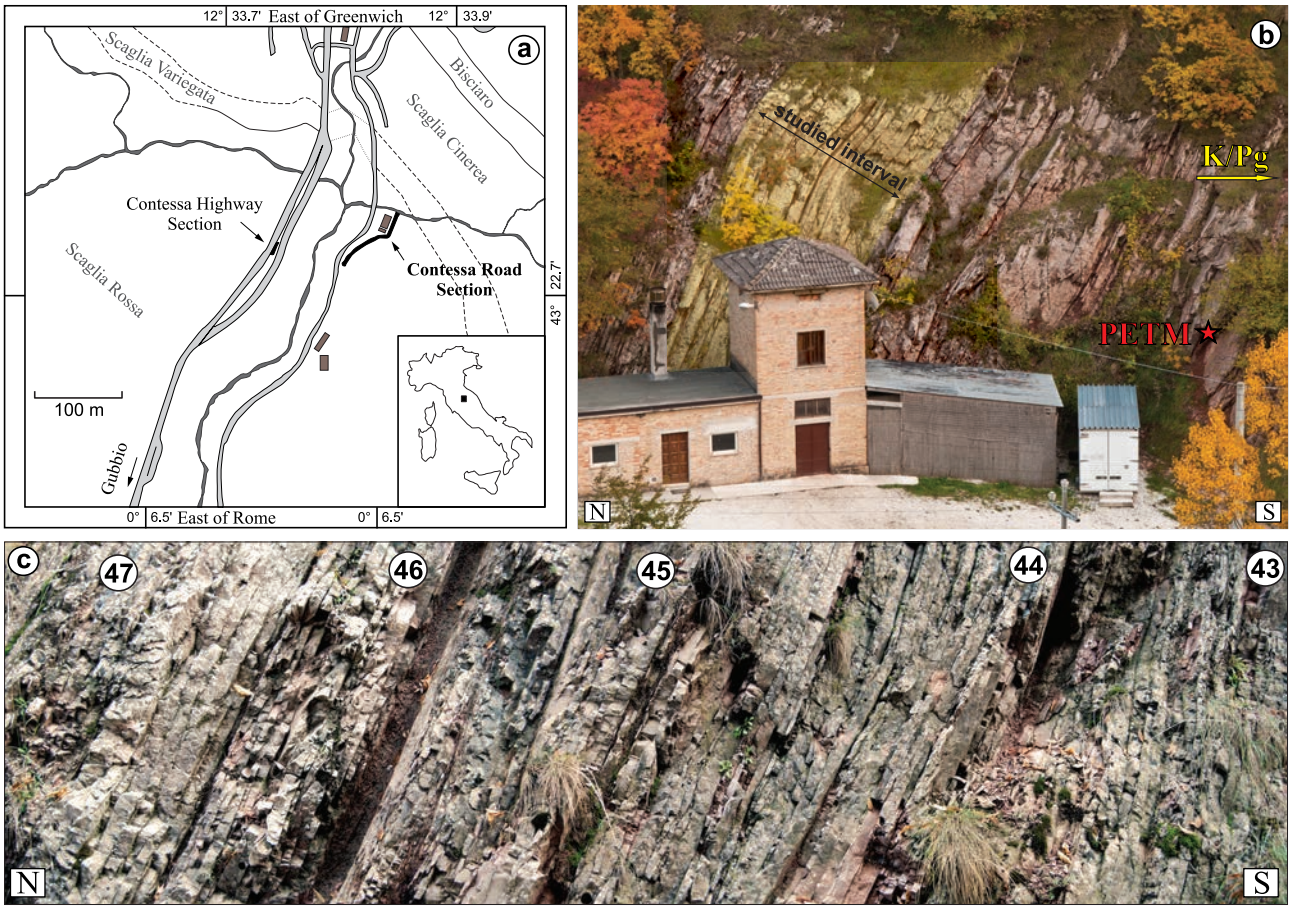

Figure 4.3 – (a) Location map and (b) panoramic view of Contessa Road Section. (c) Detailed view of the studied interval from ca. 43 m to ca. 47 m.

data are reported in per mil (‰) relative to the VPDB standard.

4.4.3 *Environmental magnetism and magnetic susceptibility*

A total of a hundred and twenty-six samples was used for paleomagnetic analyses. These analyses were carried out at National Oceanography Centre Southampton (NOCS), University of Southampton, UK. The low field mass-specific magnetic susceptibility (χ) was measured with a Kappabridge KLY-2 magnetic susceptibility meter. A range of rock magnetic measurements was used to investigate the magnetic mineralogy throughout the investigated section. Artificial remanences were also measured, including the anhysteretic remanent magnetization (ARM) imparted in a 100 mT AF, with a superimposed 0.05 mT direct current (DC) bias field, the isothermal remanent magnetization (IRM) imparted in a field of 0.9 T, and back−field demagnetization of the IRM at 0.1 T and 0.3 T. These data were used to determine the S−ratio (IRM–0.3T/IRM0.9 T) and the HIRM (HIRM = [IRM0.9 T + IRM–0.3 T]/2). Natural and artificial remanences were measured using a 2G Enterprises automated pass−through cryogenic magnetometer (Model 755) with in−line AF demagnetization capability. Environmental magnetic properties (concentration, composition, and dimension of magnetic grains) were defined by investigating ARM, IRM and other indirect parameters from them. ARM magnetically excites only finer magnetic minerals, while IRM excites all of them (concentration). Backfield magnetizations allow us to define HIRM and S−ratio 300, which give information about coercivities (composition) of the magnetic minerals.

4.4.4 *Calcareous nannoplankton*

Samples were prepared from unprocessed material as smear slides, and were examined using a light microscope at 1250x magnification. As for biostratigraphy, all samples were studied while a quantita-

tive analysis was performed on ten selected samples in the 43–47 m interval. In this study the calcareous nannofossil zonations of Martini (1971), and Okada and Bukry (1980) were applied. Quantitative analyses were performed by counting species and genera on a fixed area (100 fields). In order to infer probable temperature and trophic variations of the surface waters, most calcareous nannofossils were, whenever possible, allocated into groups of environmental affinities, largely following Haq and Lohman (1976), Aubry (1992), Gardin and Monechi (1998), Bralower (2002), Tremolada and Bralower (2004), Persico and Villa (2004), Gibbs et al. (2006), Villa et al. (2008), Raffi et al. (2009) and Agnini et al. (2011). Thus, according to the aforementioned literature, the following environmental groups have been used: warm (*Discoaster, Ericsonia, Sphenolithus, Zygrablithus bijugatus*), temperate (*Coccolithus*), cold (*Chiasmolithus, Cruciplacolithus, Toweius*), eutrophic (*Chiasmolithus, Cruciplacolithus*), mesotrophic (*Toweius*), and oligotrophic (*Coccolithus, Discoaster, Ericsonia, Sphenolithus, Z. bijugatus*).

4.4.5 *Foraminifera*

Samples were treated following the cold acetolyse technique of Lirer (2000) by sieving through a 63 μm mesh and drying at 50°C. The cold acetolysis method enabled extraction of generally easily identifiable foraminifera even from indurated limestones. This technique offered the possibility of accurate taxonomic determination and detailed analysis of foraminiferal assemblages.

4.4.5.1 *Planktonic foraminifera*

All samples were studied to determine the biostratigraphy, while the quantitative analysis was focused on thirty-one selected samples in the 43–47 m interval. The residues were studied with a binocular microscope to characterize assemblages and identify biostratigraphic marker species. A representative split of at least 300 specimens was picked from the >63 μm fraction, mounted on micro-slides for permanent record and identification purposes, and classified following the taxonomic criteria of Pearson et al. (2006). The planktonic foraminiferal standard zonation schemes of Berggren et al. (1995) and Wade et al. (2011) were followed. Inferred life strategies, environmental affinities and depth ranking of the Paleocene planktonic foraminifera, which derived from latitudinal distribution, environmental inferences (morphology and biogeographic distribution) and stable isotope data, are from Luciani et al. (2007, 2010) and references therein. Thus, according to the aforementioned literature, the following environmental groups have been used: warm-water taxa (*Acarinina, Morozovella*, and *Igorina*), cool-water taxa (subbotinids, *Globorotaloides, Globanomalina*, and *Planorotalites*). Following Hancock and Dickens (2005), the FI has been calculated using at least 300 specimens and including the whole test, fragments and dissolved tests for estimating the effect of carbonate dissolution.

4.4.5.2 *Benthic foraminifera*

The quantitative study was performed on twenty selected samples in the 43–47 m interval. A representative split of the >63 μm fraction was used to pick approximately 300 specimens. The sample–split weight used to pick benthic foraminifera was determined so that the foraminiferal density (FD), expressed as the number of foraminifera per gram of dry sediment, could be calculated. The planktonic to planktonic and benthic (P/P+B) ratio, expressed as a percentage, and the percentages of agglutinans and the opportunistic *Glomospira* spp. were also calculated. In order to calculate the infaunal percentages all taxa were allocated to infaunal and epifaunal morphogroups largely following Corliss (1985), Alegret et al. (2003) and Kaminski and Gradstein (2005).

4.4.6 *Weight percent coarse fraction*

The entire >63 μm residue obtained for all the samples was dried and weighed. The weight percent ratio of the >63 μm size fraction to the weight of the bulk sample (~100 g for each sample) is here referred to as the coarse fraction according to Broecker and Clark (1999, 2001). This index, calculated instead using the >38 μm size fraction, has been largely used as a possible indicator of dissolution (i.e., Hancock and Dickens, 2005; Colosimo et al., 2006; Leon-Rodriguez and Dickens, 2010; Luciani et al., 2010).

4.5 Results

4.5.1 *Biostratigraphy*

Also following previous findings (Coccioni et al., 2006; Galeotti et al., 2010; Coccioni et

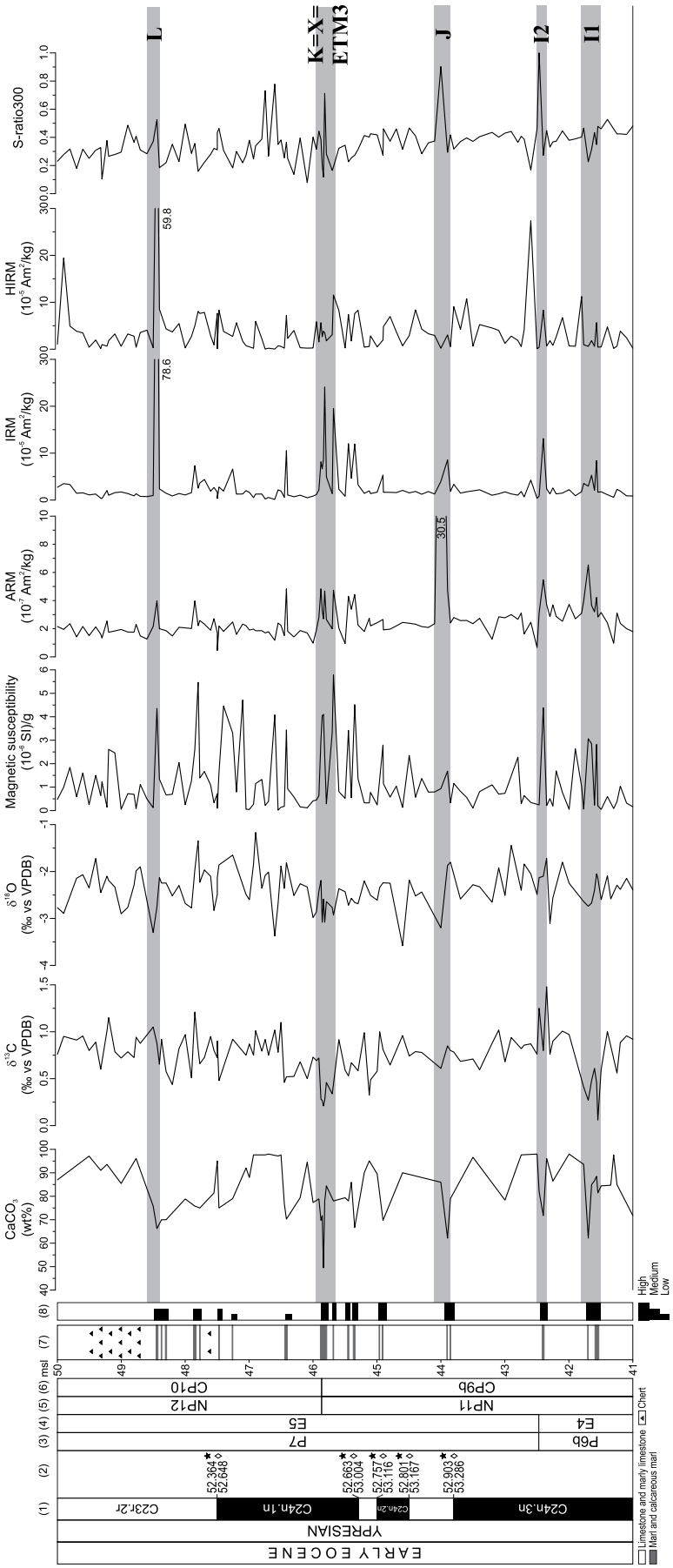

Figure 4.4 – Changes in $CaCO_3$ content, $\delta^{13}C$ and $\delta^{18}O$ of bulk sediments, magnetic susceptibility, and rock magnetic properties (anhysteretic remanent magnetization, ARM; isothermal remanent magnetization, IRM; hard isothermal remanent magnetization, HIRM; and S-ratio$_{300}$) across the 9 m-thick studied segment at Contessa Road. Magnetostratigraphy (1) is from Galeotti et al. (2010). Numerical ages (2) are from Cande and Kent (1995) (stars) and Gradstein et al. (2004) (diamonds). Biostratigraphy is based on the planktonic foraminiferal Zones of Berggren et al. (1995) (3) and Wade et al. (2011) (4) and calcareous nannoplankton Zones of Martini (1971) (5) and Okada and Bukry (1980) (6). Lithostratigraphy is from Galeotti et al. (2010), and this study. The gray shaded areas mark the recognized hyperthermal events.

al., submitted), several calcareous nannofossil and planktonic foraminiferal events were recognized in the studied segment as well as just below and above it. They are as follows: Lowest Occurrence (LO) of *Morozovella crater* (41.55 m), LO *Sphenolithus consipicuus* (41.78 m), Lowest Rare Occurrence (LRO) of *Calcidiscus protoannulus* (41.93 m), LO of *Morozovella aragonensis* (42.47 m), LRO of *Ericsonia formosa* (42.63 m), LO of *Ericsonia formosa* (44.07 m), LO of *Girgisia gammation* (44.07 m), Lowest Common Occurrence (LCO) of *Morozovella aragonensis* (45.40 m), LO of *Discoaster lodoensis* 45.85, Highest Rare Occurrence (HRO) of *Discoaster multiradiatus* (47.10 m), and LCO of *Discoaster lodoensis* (50.00 m). The LO of *M. aragonensis* defines the bases of planktonic foraminiferal Zone P7 and E5 of Berggren et al. (1995) and Wade et al. (2011), respectively. The LO of *D. lodoensis* marks the bases of calcareous nannofossil Zones NP12 and CP10 of Martini (1971) and Okada and Bukry (1980), respectively. Therefore, the studied segment spans from the uppermost part of planktonic foraminiferal Zone P6b to the Zone P7 of Berggren et al. (1995) and from the uppermost part of planktonic foraminiferal Zone E4 to the middle part of Zone E5 of Wade et al. (2011) and from the lower-middle part of calcareous nannofossil Zones NP11 and CP9b to the Zones NP12 and CP10 of Martini (1971) and Okada and Bukry (1980), respectively.

4.5.2 *$CaCO_3$ content, bulk, $\delta^{13}C$ and $\delta 1^{8}O$ isotopes, and paleomagnetic records*

The calcium carbonate content record has an average value of ~83.2% (minimum ~49.5% and maximum ~98% at 45.84 m and 46.7 m, respectively) (Fig. 4.4). The χ varies from 0.01 to 5.79 x 10^{-6} SI/g, with an average value of 1.25 x 10^{-6} SI/g (Fig. 4.4). Magnetic susceptibility and calcium carbonate records show a significant negative correlation (r=−0.65). Several discrete intervals containing lower carbonate contents and higher values of χ mostly linked to the marly beds are recognized (Fig. 4.4). The most evident of these are: 41.50–41.80 m, 42.35-42.50 m, 43.85-44.10 m, 45.65-45.95 m and 48.40-48.60 m (Fig. 4.4). Relatively high values of χ are related to low values of $CaCO_3$ and correspond to peaks in abundance of paramagnetic (e.g., increased amount of clay minerals) and ferromagnetic minerals in the sediments. In order to document the variation of magnetic mineralogy (composition) and its properties (concentration, and dimension of magnetic grains), a range of rock magnetic parameters was used. In particular, these parameters exhibit marked changes throughout the studied segment (Fig. 4.4). The ARM shows an average value of 2.69 x 10^{-7} Am^2/kg (minimum of 4.56 x 10^{-8} and maximum of 3.05 x 10^{-6} Am^2/kg). The IRM ranges from 1.26 x 10^{-6} to 7.86 x 10^{-4} Am^2/kg with an arithmetic mean of 3.36 x 10^{-5} Am^2/kg. The HIRM ranges from 2.88 x 10^{-7} to 5.98 × 10^{-4} Am^2/kg with an arithmetic mean of 3.87 × 10^{-5} Am^2/kg (Fig. 4.4). The S-$ratio_{300}$ varies from 0.07, at 46.09 m to 1.00 at 42.47 m, with an arithmetic mean of 0.35. Higher values of these parameters are associated with marly beds and their surroundings. The bulk carbonate $\delta^{13}C$ record displays background values of 0.06‰–1.48‰ (average ~0.74‰) along the studied interval that is characterized by two short, distinct CIEs at 41.50–41.80 m and 45.65–45.95 m, respectively (Fig. 4.4). Although according to Corfield et al. (1991), the Paleogene Scaglia–type sediments near Gubbio might be affected by diagenesis and the oxygen isotope values might be diagenetically altered, several $\delta^{18}O$ are evidenced. In particular, we highlighted negative spikes in correspondence of most marly beds, where the most prominent are represented by 43.85-44.10 m, 45.65-45.95 m and 48.40-48.60 m.

4.5.3 *Biotic changes*

4.5.3.1 *Calcareous nannofossils*

Calcareous nannofossils assemblages have low species richness and exhibit, generally, moderate to poor diversification. The assemblages are characterized by large abundances of *Sphenolithus* spp. (mostly *S. radians*), *Discoaster* spp., *Toweius* spp., and *Zygrablithus bijugatus*, with subordinate numbers of *Ericsonia* spp., *Coccolithus* spp., and *Tribrachiatus orthostylus* (Fig. 4.5). Although populations are dominated by warm-water and oligo-mesotrophic taxa, significant changes towards warmer and more oligotrophic conditions are evidenced in correspondence of the marly layer at 45.65–45.95 m (Fig. 4.5).

4.5.3.2 *Planktonic foraminifera*

Planktonic foraminifera are abundant, generally well-diversified. Evidences of poor to moderate preservation are only found within the 45.82–45.88 m. The assemblages are, generally, dominated

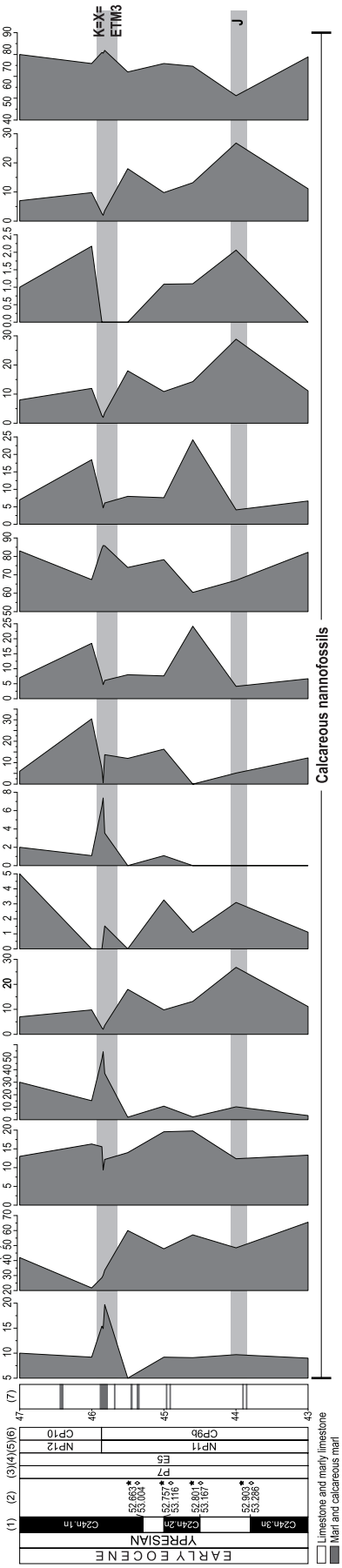

Figure 4.5 – Changes in selected calcareous nannofossil genera, species, and ecological groups across the studied segment at Contessa Road. Magnetobiochronostratigraphy as in Figure 4.4. The gray shaded areas mark the recognized hyperthermal events.

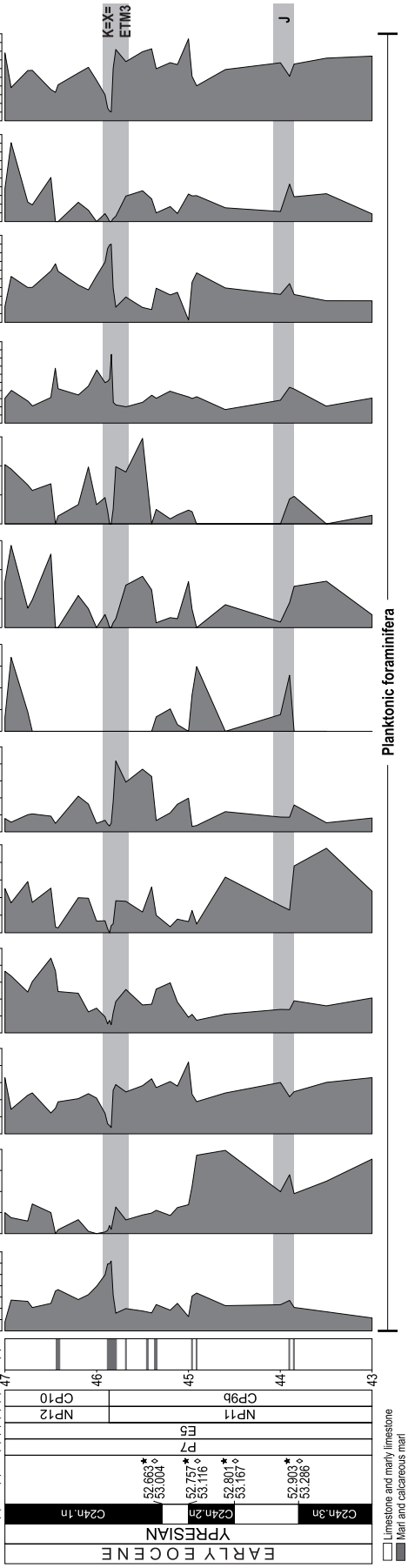

Figure 4.6 – Changes in selected planktonic foraminiferal genera, species, and ecological group across the studied segment at Contessa Road. Magnetobiochronostratigraphy as in Figure 4.4. The gray shaded areas mark the recognized hyperthermal events.

by *Acarinina* spp. and subbotinids (*Subbotina* and *Parasubbotina*), with subordinate numbers of *Morozovella* spp., *Igorina* spp., *Globanomalina* spp. and *Globorotaloides* spp. (Fig. 4.6). Significant reductions of subbotinids, *Igorina* spp., *Globanomalina* spp., and *Pseudohastigerina* have been documented across the two marly intervals at 43.85–44.10 m and 45.65–45.95 m. In the latter, a marked reduction of *Acarinina* spp. is also evidenced. On the contrary, higher values of *Morozovella* spp. are found in these two marly intervals. The FI displays higher percentages in correspondence of the two marly layers at 43.85–44.10 m and 45.65–45.95 m, the highest value is found at 45.84 m. The assemblages are dominated by warm-water taxa. A marked increase of warm-water taxa accompanied by a significant decrease of cool-water taxa is found in the marly interval at 45.65–45.95 m (Fig. 4.6).

4.5.3.3 *Benthic foraminifera*

The P/(P+B) ratio shows only minor fluctuations throughout the studied segment with decreasing values normally associated with marly intervals (Fig. 4.6). The mean value of P/(P+B) is 99.4%, typical for lower-middle bathyal section, the lowest one is found at 45.86 m. The fluctuations of the P/(P+B) ratio are well mirrored by the coarse fraction (Fig. 4.6). Assemblages are generally well-diversified and moderately to good preserved throughout the segment, except within the marly layer at 45.65–45.95 m where a poor preservation has been found (Fig. 4.6). Although the populations are dominated by calcareous-hyaline forms (ca. 77%, in mean), significant increase of agglutinans are found in the marly layers at, from bottom to top, 43.90 m, 45.45 m, and 45.68–45.88 m. Similar fluctuations are shown in the percentages of tubular agglutinated forms, FD and *Glomospira* spp. (Fig. 4.6). Infaunal and epifaunal taxa occur in different proportions within the assemblages, but the infaunal taxa prevail in most of the samples (Fig. 4.6). Epifaunal taxa tend to increase in correspondence of the marly layer at 45.45 m and 45.82–45.91 msl (Fig. 4.6).

4.6 Discussion

4.6.1 *Early Eocene carbon isotope excursions*

High resolution stable carbon isotope global records through the middle Paleocene-lower Eocene interval reveal numerous short-term negative excursions (i.e., Cramer et al., 2003; Zachos et al., 2010). These short–lived negative CIEs accompanied with elevated surface temperature, deep-see carbonate dissolution, biotic turnover, accelerated weathering and hydrologic cycles provide evidence of alterations of carbon cycling are termed “hyperthermals” (e.g., Kennett and Stott, 1991; Zachos et al., 2001; Bralower et al., 2002; Cramer et al., 2003; Nicolo et al., 2007; Quillévéré et al. 2008; Westerhold et al., 2008; Leon-Rodriguez and Dickens, 2010, and references therein). Although among these the PETM represents the most acute and studied event (i.e., Kennett and Stott, 1991; Zachos et al., 2010), other major and minor events have been documented including the

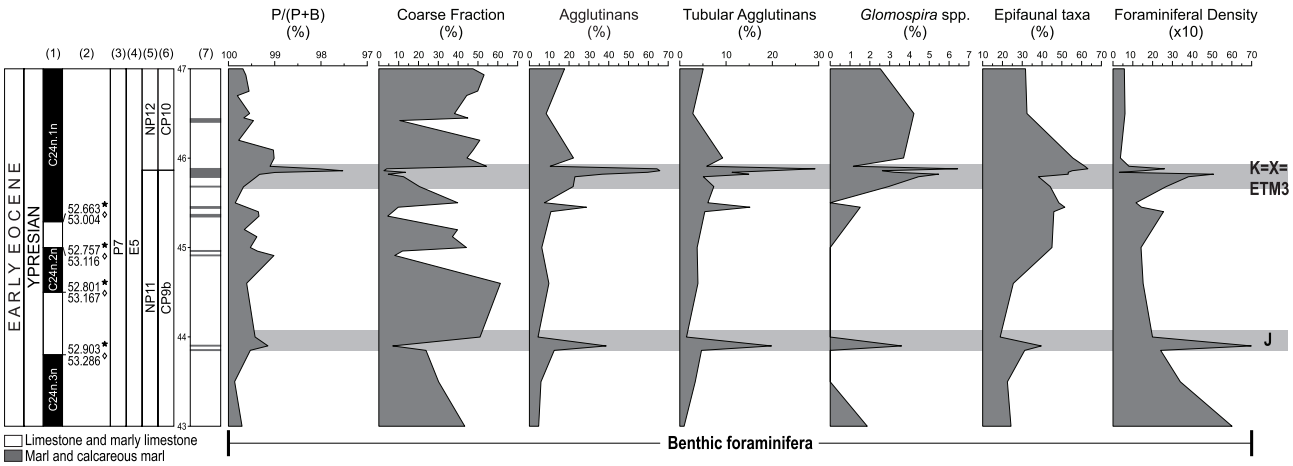

Figure 4.7 – Changes in coarse fraction and selected benthic foraminiferal parameters [P/(P+B) ratio, foraminiferal density (FD), agglutinans vs. calcareous ratio, and infauna vs. epifauna ratio] and the relative abundances of tubular agglutinans and *Glomospira* spp. across the studied segment at Contessa Road. Magnetobiochronostratigraphy as in Figure 4.4. The gray shaded areas mark the recognized hyperthermal events.

ETM2 or ELMO or H1 (Lourens et al., 2005; Sluijs et al., 2009; Stap et al., 2009, 2010), the ETM3 or X or K (Cramer et al., 2003; Röhl et al., 2005, Agnini et al., 2009), I1, I2 and J (Cramer et al., 2003; Nicolo et al., 2007, Agnini et al., 2009; Zachos et al., 2010). The Contessa Road section, with its complete, continuous and well−preserved record, represents a sedimentary sequence of the subtropical–tropical western Tethys Ocean where the hyperthermals can be constrained and studied (Coccioni et al., 2006; Giusberti et al., 2009; Galeotti et al., 2010). On the basis of calcium carbonate and isotopic analyses coupled with cyclostratigraphy, Galeotti et al. (2010) provide compelling evidence and constrain most of these hyperthermals for the early Eocene interval. Here we provide higher resolution, integrated stratigraphic analyses for the C24n.3n–C23r.2r interval to better constrain the hyperthermals at Contessa Road and to correlate these events with those already recognized in deep-sea cores and land-based sections (Figs. 4.2 and 4.4). In particular, the ~0.55‰ CIE occurring at 41.50–41.80 m and within Chron C24n.3n, planktonic foraminiferal Zones P6b of Berggren et al. (1995) and E4 of Wade et al. (2011), and calcareous nannofossil Zones NP11 of Martini (1971) and CP9b of Okada and Bukry (1980) can be confidently correlated with DSDP Sites 550 and 577, and ODP Sites 1262 and 1215. This marly layer at Contessa Road is the sedimentary expression of I1 event of Cramer et al. (2003) (Figs. 4.2 and 4.4). Immediately above at 42.35–42.50 m, we identified a marly layer characterized by marked reduction of calcium carbonate content, major increase in χ and environmental magnetism and a complex shift of $\delta^{13}C$ (Fig. 4.4). This layer according to the magnetobiostratigraphical constrain can be correlated with I2 event of Cramer et al. (2003) and already identified at DSDP Sites 550 and 577 and ODP Site 1262 (Figs. 4.2 and 4.4). A ~0.3‰ CIEs is recognized at 43.85–44.10 m that falls within Chron C24r.2r, planktonic foraminiferal Zones P7 of Berggren et al. (1995) and E5 of Wade et al. (2011), and calcareous nannofossil Zones NP11 of Martini (1971) and CP9b of Okada and Bukry (1980) and is the sedimentary expression of J event of Cramer et al. (2003). The J event has been also recognized at DSDP Sites 550 and 577, ODP Site 1262 and at Farra section (Fig. 4.4). An additional CIE is found at the marly layer at 45.65–45.95 m and is constrained within Chron C24n.1n, planktonic foraminiferal Zones P7 of Berggren et al. (1995) and E5 of Wade et al. (2011), and between calcareous nannofossil Zones NP11/NP12 of Martini (1971) and CP9b/CP10 of Okada and Bukry (1980). This marly layer can be confidently correlated with ETM3 (K or X) event as also documented at DSDP Sites 550 and 577, ODP Sites 1262, 1215, 1258, at Possagno and Farra Section and at Galala succession (i.e., Cramer et al., 2003; Agnini et al., 2006, 2009; Westerhold and Röhl, 2009; Leon-Rodriguez and Dickens, 2010) (Fig. 4.4). The uppermost CIE corresponding at marly layer (48.40–48.60 m) and characterized by major reduction of calcium carbonate and spikes in χ and environmental magnetisms can be well correlated with the L event of Cramer et al. (2003) and identified at DSDP Site 550.

4.6.2 *Comparison of proxy to other ETM3 records*

The ETM3 represents along with PETM and ETM2 one of the most acute hyperthermal event ever recognized (Cramer et al., 2003; Thomas et al., 2011). At Contessa Road, the ETM3 is characterized by a marked ~0.7‰ CIE, ~0.5‰ oxygen isotope excursion, lower calcium carbonate content, increase χ and environmental magnetisms (Fig. 4.4). The CIE is slightly greater than that found at Possagno section (~0.4‰) (Agnini et al., 2009), lower than that documented at ODP Site 1215 (~1.0‰) or Galala succession (~1.5‰) (Leon-Rodriguez and Dickens, 2010; Höntzsch et al., 2011) but can be well compared with the excursion found ~0.5‰ at DSDP Site 577, ~0.7‰ at DSDP Site 550, ~0.6‰ at Farra section, ~0.8‰ at Walvis Ridge 1262 (Cramer et al., 2003; Röhl et al., 2004, 2005; Thomas et al., 2006; Agnini et al., 2009). At Farra section that represents Tethyan analogue of the lower–bathyal Contessa Road section but deposited at upper-middle bathyal depth, a 45% reduction of calcium carbonate across the ETM3 is documented by Agnini et al. (2009), whereas this change is ~30% at Contessa Road section. This difference is certainly due to the shallower nature of the Farra section and its near-continental, hemipelagic setting. The increase in χ as recognized at Contessa Road section has also be found at ODP Sites 1215 (Honolulu, Hawaii), 1258 (Demerara Rise, central Atlantic), 1262 (Walvis Ridge, southern Atlantic) (Westerhold and Röhl, 2009; Leon-Rodriguez and Dickens, 2010; Zachos et al., 2010). Relatively high values of χ correspond to peak in abundance of paramagnetic (e.g., increased amount of clay minerals) and ferromagnetic minerals in the

sediments. The χ peaks correspond to ETM3 clay-rich horizon that represents increased in terrigenous sedimentation, likely due to global accelerated hydrological and weathering cycles (e.g. Lourens et al., 2005; Stap et al., 2009). The enhanced weathering, normally encountered during hyperthermal, increase the terrigenous component transported to the pelagic environments and consequently alter the composition of sediment. The changes of χ and calcium carbonate are well mirrored by variations of rock magnetic properties (ARM, IRM, HIRM and S-ratio$_{300}$) (Fig. 4.4). These parameters are widely used for studies of sedimentary environments, mainly in deep-sea cores and land-based sections (Verosub and Roberts, 1995) and their variations, in many cases, are climatically modulated (e.g. Jovane et al., 2007; 2009; Venuti et al., 2007; 2011). Across the ETM3 at Contessa Road section, higher values of IRM and ARM confirm an enrichment of the entire magnetic component (concentration) and high concentration of finer magnetic grains, respectively. Useful insight about the magnetic coercitivity of the magnetic carriers is provided by HIRM. The presence of low coercivity magnetic mineral (i.e., magnetite) is indicated by the value of S-ratio$_{300}$ close to unity. In contrast, low S-ratio$_{300}$ values and high values of HIRM indicate the presence of high–coercivity magnetic minerals (i.e., hematite). High values (>0.6) of S–ratio$_{300}$ during the ETM3 at 45.82 m indicate that the magnetic mineral assemblage is dominated by low-coercivity magnetic mineral (e.g. magnetite and titanomagnetite). The coercivity parameters indicate that the magnetic fraction is dominated by a complex mixture that include titano-magnetite and the oxidized phase of magnetite (maghemite), and hematite.

4.6.3 *Biotic changes across the ETM3 event and inferred environmental effects*

Changes in geochemical, magnetic, and isotopic parameters are well-reflected by remarkable changes in the relative abundances, preservation and taxonomical composition of calcareous nannofossil and foraminiferal assemblages recognized across the ETM3 at Contessa Road (Figs. 4.5–4.7). These changes reveal that the ETM3 represents an abrupt environmental perturbation influencing the biota living in photic zone and at the seafloor. In particular, a marked shift towards warmer and more oligotrophic conditions is inferred by calcareous nannofossil analyses. In the more shallow, near-continental, and hemipelagic Farra section, Agnini et al. (2009), documented an increase of warm-eutrophic calcareous nannofossil taxa suggesting a transient enrichment in dissolved nutrients. Warmer water conditions during the ETM3 are also supported by the planktonic foraminiferal assemblages, where marked increases of the warm-water *Acarinina* are accompanied by an evident reduction of the cool-water subbotinids. These planktonic foraminiferal changes are consistent with the finding of Agnini et al. (2009) at Farra section. The clear divergence in productivity responses between the two Tethyan sections across the ETM3 seems, at first sight, at odd. However, according to Gibbs et al. (2006), during the PETM an increase in productivity can be inferred in shelf environments whereas prevailing oligotrophic conditions occur at more open-ocean bathyal settings. The lowering in nutrient availability may have resulted from a widespread increase in stratification and less efficient biological pumping (Gibbs et al., 2006). Previous nannofossil analyses (e.g., Kelly et al., 1998; Bralower, 2002; Tremolada and Bralower, 2004; Gibbs et al., 2006) at open–ocean sites in the Atlantic, Indian, and Pacific Oceans have supported the idea of decreased productivity concomitant with the early stage of the PETM. On the basis of benthic foraminiferal accumulation rate and relative abundance of species, Thomas et al. (2011) documented a lowering in the food supply to the seafloor at Walvis Ridge during the three major hyperthermals (PETM, ETM2 and ETM3). Moreover, Röhl et al. (2005) documented during the ETM3 at Walvis Ridge, benthic foraminiferal assemblages dominated by small individuals of *Nuttallides truemphy*, a possible low-food indicator (Thomas, 1998) and abyssaminids, thin–walled species that might indicate oligotrophy (Thomas, 2007). No reduction in the oxygen availability in the water column can be inferred by low occurrences of low–oxygen tolerant taxa (i.e., *Chiloguembelina*) at Contessa Road section. This is also supported by Thomas et al. (2011), who found, across the ETM3 at Walvis Ridge, no evidence in the benthic foraminiferal assemblages that OMZs expanded to the depth transect. A slight decrease followed immediately by an increase of epifaunal taxa is documented at Contessa Road suggesting a change in the nutrient supply to the seafloor. No marked changes in the percentages of epifaunal taxa was found at Farra across the ETM3 (Agnini et al., 2009), whereas a clear increase of epifaunal taxa has been

documented across the first marly layer of PETM at Contessa Road (Giusberti et al., 2009). The increase abundance of *Glomospira* spp. is documented across the ETM3, this taxon is considered as characteristic in stressed environments and resistant to carbonate dissolution and able to live in environments with low carbonate supplies (Boersma, 1986; Ortiz, 1995; Kaminski and Gradstein, 2005). Higher FI and percentages of agglutinans accompanied by lower P/(P+B) ratio and coarse fraction values during the ETM3 strongly support the effect of enhanced carbonate dissolution, most likely induced by a shallowing of the lysocline caused by acidification of the oceans. These data are also supported by lower calcium carbonate content and higher values of χ. At Contessa Road, remarkably, it was shown that low calcium carbonate content is associated with increase insolation and warmer conditions (Galeotti et al., 2010). The CIEs might have been triggered by the injection of a range of isotopically depleted carbon that which once absorbed by the ocean lead to perturbation of the carbonate saturation state and dissolution as well as global warming (Zachos et al., 2010). The effect of ocean acidification has been largely documented during all major hyperthermals (i.e., Leon-Rodriguez and Dickens, 2010). The condensed intervals across the ETM2 and ETM3 at Contessa road testify that the reduction in carbonate content is triggered by carbonate dissolution (Galeotti et al., 2010). As predicted by carbon cycle models for the PETM (Kelly et al., 2005, 2010), the lysocline would have deepened as an enhanced silicate weathering mechanism on land neutralizes ocean acidification with increased preservation of carbonate in the ocean as is revealed by the increase in coarse fraction, carbonate content and fragmentation index. In the late Paleocene and early Eocene (Zachos et al., 2010) negative CIEs are in phase with maxima in eccentricity and both events corresponds to insolation maxima (Galeotti et al., 2010), this swing in carbon cycle may have been orbitally paced (Lourens et al., 2005).

4.7 Conclusion

Detailed analyses of calcareous nannofossils and foraminiferal assemblages, and high-resolution geochemical, isotopic and magnetic records across the middle Ypresian at Contessa Road (Gubbio, Italy) allow us to better constrained a major (ETM3) and four minor (I1, I2, J, L) hyperthermals. The ETM3 is characterized by prominent and short–live negative excursions in both $\delta^{13}C$ and $\delta^{18}O$ of ~0.7‰ and ~0.5‰, respectively. These excursions are associated by major changes in the rock magnetic properties and marked environmental changes. Although, the magnitude and effect of ETM3 appear less intense then the well-known PETM and ETM2, remarkable environmental disruptions in both the photic zone and the seafloor took place across the ETM3. In particular, changes in the calcareous nannofossils and foraminiferal assemblages provide compelling evidences of a shift towards warmer and more oligotrophic conditions during the event. The ETM3 involves change in productivity conditions and enhanced dissolution of carbonates and suggests unstable conditions in the marine ecosystem than can be readily compared to those reported in other major early Eocene hyperthermal events (PETM and ETM2). The massive injection of 13C-depleted carbon to the ocean and atmosphere may have altered the deep-sea pH, triggering a rapid and transient shoaling of the lysocline and contributing to a greenhouse warming. As for other early Paleogene hyperthermal events, the cause of the ETM3 event is likely to be found in changes, in the distribution of carbon within surface biosphere reservoirs, likely controlled by orbital cycles.

CHAPTER 5

New insights into the pattern, timing, and duration of the evolutionary origin of the foraminiferal genus *Hantkenina*

5.1 Introduction

The Earth's climate and the ocean circulation patterns changed dramatically during the Eocene Epoch (Zachos et al. 1994; Zachos et al., 2001, Zachos et al., 2010; Dickens, 2011). The greenhouse world that had prevailed through the Cretaceous to early Eocene gradually yielded to cooler conditions that led finally to polar glaciations and to an icehouse world. A series of pronounced high−latitude cooling events took place in the early middle Eocene and near the middle−late Eocene boundary. Moreover, the opening of high−latitude and closing of low−latitude tectonic gateways changed progressively the surface−ocean circulation patterns. In particular, deep waters cooled, and a reorganization of the vertical thermal structure of the water column took place. All these changing conditions led to severe biological productivity alterations in many places around the world (Keller, 1983; Boersma et al., 1987; Premoli Silva and Boersma, 1988; Zachos et al., 1994; Diester−Haas and Zahn, 1996). These alterations were also associated with some evolutionary turnover in many biological groups in the oceans and even on the continents (Prothero, 1994). At low−latitudes, planktonic foraminifera that had peaked in diversity and morphological disparity in the warm early middle Eocene, underwent significant extinctions toward the end of the middle Eocene. The early Paleogene dominant surface dwellers like the "muricate" forms (*Morozovella*, *Acarinina*, and *Igorina*), were eliminated by the end of the middle Eocene (Berggren and Pearson, 2005; Luciani et al., 2010). Probably their extinction was linked to the generally global cooling (Keller, 1983; Boersma and Premoli Silva, 1991; Keller et al., 1992; Pearson, 1996). At the same time, cold−tolerant deeper dwelling species increased in abundance and some new genera appeared on the scene (Keller et al., 1992). In this scenario, the most distinctive, and enigmatic evolutionary bioevent was the origin of the planktonic foraminiferal genus *Hantkenina*. The genus *Hantkenina* is characterized by planispiral coiling and nonporous hollow chamber extensions called "tubulospines". It evolved gradually during the middle Eocene from the genus *Clavigerinella*, which shows radial elongate, clavate, or digitate chambers, but no tubulospines of (e.g., Banner and Lowry, 1985; Pearson, 1993; Coxall et al., 2003; Rögl and Egger, 2010, 2011). This evolutionary trend, firstly restricted to the deep water of Tethyan region and subsequently followed by the exchange and emigration of *Hantkenina* into the rest of the world ocean (Coxall et al., 2003). As a consequence, the hantkeninids had a worldwide distribution at low and mid latitudes, and their extinction at 33.9 Ma denotes the Eocene/Oligocene boundary (Coccioni et al., 1988; Berggren et al., 1995).

Over the last decades, transitional clavate−tubulospinose morphologies have been occasionally reported (Premoli Silva and Spezzaferri, 1990; Pearson, 1993; Coxall et al., 2000, 2003; Rogl and Egger 2010, 2011), suggesting that the evolution of *Hantkenina* probably involved gradual morphological transition. This interpretation is difficult to corroborate due to the rarity of the *Hantkenina* near its first occurrence interval and a lack of suitable stratigraphic record of correlative age. Moreover, the early middle Eocene Zone P9–P10 transition (Berggen et al., 1995), which would be expected to contain clues to the origin of *Hantkenina*, occurs in a stratigraphic interval that is

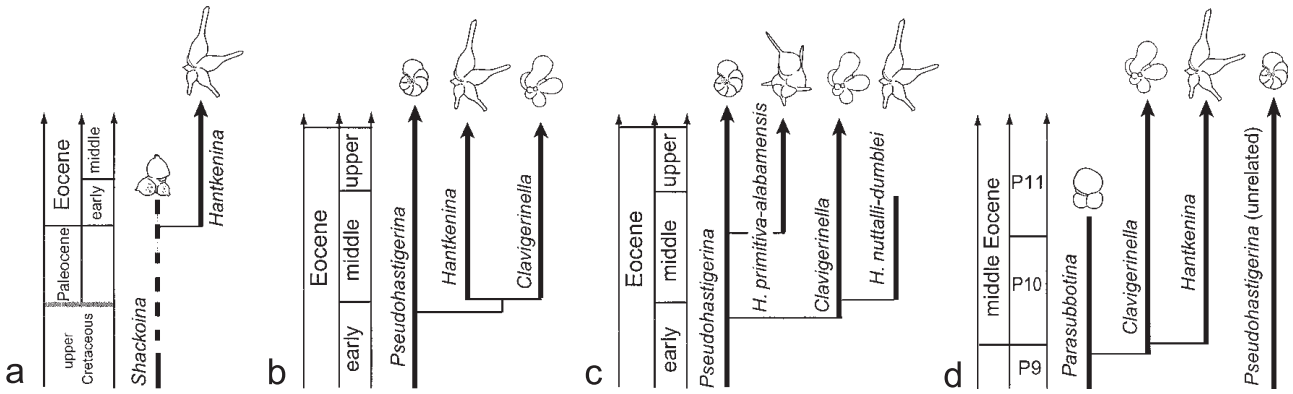

Figure 5.1 – The various hypotheses on *Hantkenina* phylogeny from Coxall et al. (2003). See text for explanation.

often poorly represented in the deep−sea sediment record (e.g., Premoli Silva and Boersma, 1986; McGowran, 1986; Olsson and Wise, 1987; Aubry, 1995). This interval is affected by a hiatus in most sections worldwide. For example, this hiatus is very common in the Atlantic Ocean and in northern Europe (Aubry, 1995; Payros et al., 2009). This phenomenon has been linked with a major sea−level fall (Haq et al., 1987; Vail and Hardenbol, 1979; Aubry, 1991, 1995) and contemporaneous widespread occurrence of siliceous biofacies, suggesting increased levels of ocean productivity at that time (McGowran, 1989). However, in recent years new material has become available that has helped fill at least some of the gaps (Coxall et al., 2003, Rögl and Egger 2010, 2011). The most complete and suitable sites where the first hantkeninids were found are Contessa Highway (Gubbio, Italy) (Lowrie et al., 1982; Cresta et al., 1989), Ocean Drilling Program Site 865 (mid Pacific), Deep Sea Drilling Program sites 94 (Gulf of Mexico) and 549 (northeast Atlantic) (Coxall et al., 2000, 2003), Kilwa drill sites in Tanzania (Coxall et al., 2003, Coxall and Pearson 2006) and Holzhäusl section (Salzburg, Austria) (Coxall et al., 2003; Rögl and Egger 2010, 2011).

Many hypotheses have been formulated to clarify Hantkenina earliest phylogeny. At first, some authors supposed that *Hantkenina* is a monophyletic taxon and evolved from the Cretaceous tubulospinose genus *Shackoina* in the early middle Eocene (e.g. Cushman and Wickenden, 1930; Cushman, 1933; Thalmann, 1932, 1942; Rey, 1939; Brönnimann, 1950; Bolli et al., 1957) (Fig. 5.1a). On the contrary, others stated that *Hantkenina* is polyphyletic and middle and late Eocene groups evolved independently from different pseudohastigerinid ancestors (Blow and Banner, 1962; and Blow, 1979; Berggren et al., 1967) (Fig. 5.1b). In this context, stellate early middle Eocene forms are linked to the proposed ancestor *Pseudohastigerina* via intermediate morphotype *Clavigerinella*, which is considered sister taxon to *Hantkenina*. Another supposition is that *Hantkenina* is monophyletic but evolved directly from genus Pseudohastigerina at the base of the middle Eocene (intermediates unknown), and *Clavigerinella* is sister taxon to Hantkenina (Dieni and Proto Decima 1964; Steineck 1971; Banner and Lowry 1985, Pearson, 1993) (Fig. 5.1c). Others suggested that Hantkenina is monophyletic, evolved from *Clavigerinella* and is unrelated to *Pseudohastigerina* (Shockina, 1937; Benjamini and Reiss, 1979) (Fig. 5.1d).

More recently, Coxall et al. (2003), using comparative morphologic observations, ontogenetic and morphometric analyses, documented rare transitional hantkeninid material from Holzhäusl section (Salzburg, Austria). Multiple lines of evidence disclosed that *Hantkenina* and *Clavigerinella* have many shared features. In particular, at Holzhäusl, some specimens of *Clavigerinella* exhibit slightly constricted or pointed ends on some of the chambers. This feature was interpreted as representing, an extremely rare transitional stage between clavate chambers and tubolospines, strongly indicate that *Clavigerinella* is the real ancestor of *Hantkenina* (Coxall et al., 2003). In addition, some morphological intermediate forms between *Parasubbotina* and *Clavigerinella* were discovered, supporting the view that *Clavigerinella* and thus the hantkeninids were descended from a cancellate spinose trochospiral group and not, from the smooth−walled, planispiral *Pseudohastigerina*, as many workers in the past believed. After Coxall et al. (2003) this evolutionary trend and the transition from *Clavigerinella* to *Hantkenina* were also reported at the Kilwa drill sites

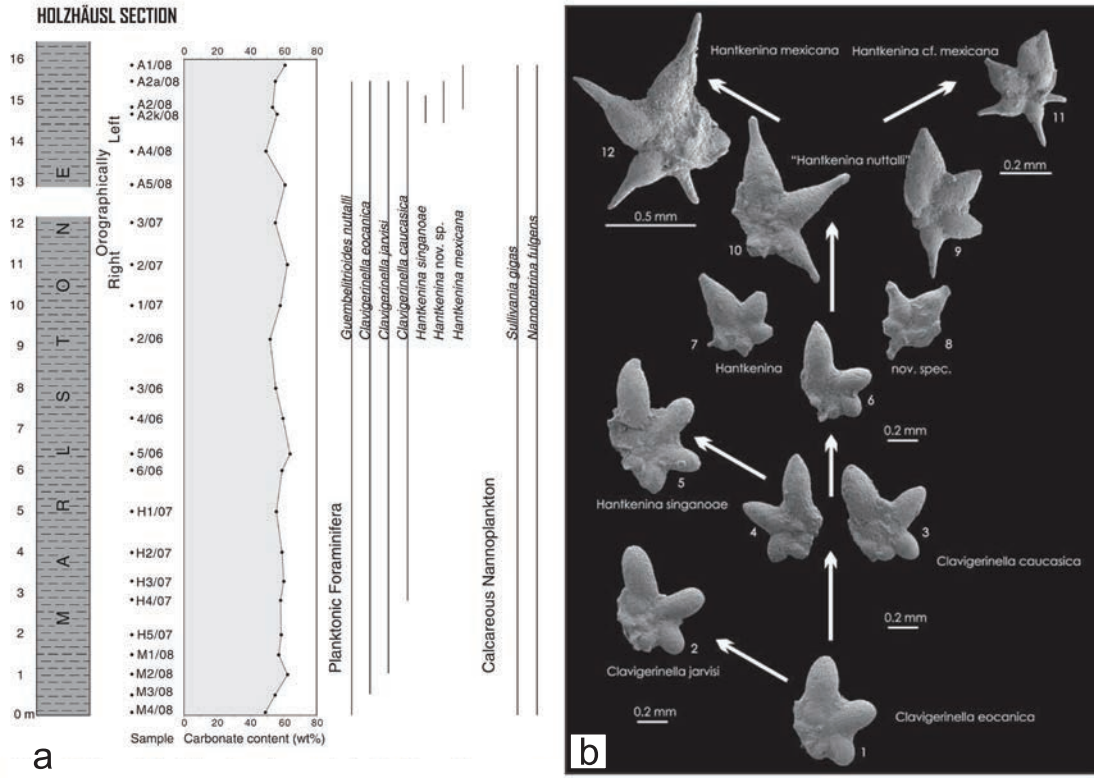

Figure 5.2 – From Rögl and Egger (2010): (a) Log of Holzhäusl section, distribution of important planktonic specie; and (b) evolutionary lineage from *Clavigerinella* to *Hantkenina*. 1. *Clavigerinella eocanica* (Nuttall). 2. *Clavigerinella jarvisi* (Cushman). 3, 4. *C. caucasica* (Subbotina). 5. *Hantkenina singanoae* Coxall and Pearson, later chambers ending in hood–like nub. 6–8. *Hantkenina nov.* sp. (=*Hantkenina gohrbandti* in Rögl and Egger, 2011) later chambers with pointed non–perforated chamber end (6), primary chamber of final whorl with distinct tubulospine, second chamber with pointed end, later chamber probably with tubulospines (broken off) (7), chambers ending in proto–tubulospines with short thickened tips (8). 9, 10. "*Hantkenina nuttalli*" variation of *Hantkenina mexicana*, with broad strongly appressed chambers ending in a distal tubulospine (9), with slender chambers ending in tubulospines that show perforations nearly up to short non–perforated ends, similar to those of 8. 11. *Hantkenina* cf. *mexicana* Cushman. chambers. 12. *Hantkenina mexicana* Cushman. Typical development with slender chambers and long tubulospines.

in Tanzania by Pearson et al. (2004) and Coxall and Pearson (2006). At this locality, Coxall and Pearson (2006) discovered a newly species, named *Hantkenina singanoae* that possesses proto−tubulospines and/or terminal nubs, and was considered to be the missing link between the two genera. This new species was erected to include a range of diverse morphologies that appear transitional between the less evolved *Clavigerinella caucasica* and the more evolved *Hantkenina Mexicana*. More in details, H*antkenina singanoae* differs from *Clavigerinella caucasica* by possessing rudimentary terminal constrictions and/or cylindrical extensions to the chamber ends, and it differs from *Hantkenina mexicana* in lacking true non−porous tubulospines (Coxall and Pearson, 2006). The *Clavigerinella caucasica−Hantkenina singanoae* and *Hantkenina singanoae−Hantkenina mexicana* interfaces are not clear−cut since the transition between them is gradual (Coxall and Pearson, 2006). For the first time, the discovery of the new species *Hantkenina singanoae* has undoubtedly shed light on the gradual nature of the enigmatic *Clavigerinella−Hantkenina* transition. However, this finding has opened further questions concerning the modalities of the evolution from the clavate chambers of *Clavigerinella caucasica* to the true tubulospines of *Hantkenina Mexicana*. It still appears unclear how, and unlikely that, straight tubulospines of the younger *Hantkenina* species could evolve from the proto−tubolospines of *Hantkenina singanoae*. To fill this gap, Rögl and Egger (2010, 2011) carried out a high−resolution study at the northwestern Tethyan deep–water section of Holzhäusl (Salzburg, Austria) that allowed to reconstruct a more complex pattern of the gradual evolutionary origin of the genus *Hantkenina* from *Clavigerinella* than previously shown (Fig. 5.2). At the Holzhäusl section, these authors reported on the finding of a newly discovered *Hantkenina* species

for which the new name *Hantkenina gohrbandti* was introduced. The new species *Hantkenina gohrbandti* shows initially rounded chambers in the juvenile stage, followed by ovate−elongate chambers, and finally chambers with a pointed tip, ending commonly in a hollow nub (Pl. 4, Fig. 5 in Rögl and Egger, 2011) (Fig. 5.2). The nub appears as a rounded, hollow and perforated structure and some rare juvenile specimens show the first occurrences of real tubulospines. In some instances a true tubulospine is already developed in juvenile chambers and the following chambers are pointed or with a thickened nub (for comparison see Pl. 4, Fig. 4 in Rögl and Egger, 2011). These range of diverse morphologies, might suggest that *Hantkenina gohrbandti* would include different morphotypes displaying the same stratigraphic distribution Rögl and Egger (2011). The new species *Hantkenina gohrbandti* is distinguished from *Clavigerinella*, especially *Clavigerinella caucasica* Subbotina by the development of pointed chamber ends with a nub in the youngest chambers, forming a proto−tubulospine in sense of Coxall and Pearson (2006). In contrast to *Hantkenina singanoae* Pearson and Coxall (in Coxall and Pearson, 2006), the straight and pointed chamber ends differ clearly from the cylindrical, commonly hood−like chamber ends in *Hantkenina singanoae* (for comparison see Pl. 3, Fig. 13 of the holotype of *Hantkenina singanoae* in Rögl and Egger, 2011). In *Hantkenina mexicana* true tubulospines are constantly developed in the later chambers of the final whorl (Coxall et al., 2006). Rögl and Egger (2010, 2011) also found and described some intermittent forms between *Hantkenina gohrbandti* and *Hantkenina mexicana* (forma *Hantkenina nuttalli* Toumarkine) show blunt, somewhat irregular tubulospines (Pl. 2, Figs. 7−8 in Rögl and Egger, 2011). The transition between both species is also visible in the small grooves along proto−tubulospines and real tubulospines (Pl. 3, Figs. 3, 11−12 in Rögl and Egger, 2011), which may correspond to protoplasmatic structures.

Noteworthy, at the Holzhäusl section, the first occurrence of *Hantkenina gohrbandti* is slightly below the first occurence of *Hantkenina singanoae*, and the stratigraphic ranges of both species overlap (Rögl and Egger, 2011). On the basis of this stratigraphic distribution and its peculiar morphologic characters, Rögl and Egger (2010, 2011) stated that *Hantkenina gohrbandti* is the real ancestor of the genus *Hantkenina*. Interestingly, Coxall et al. (2003) already described similar primitive tubulospines on some specimens collected at the Holzhäusl section, but later, the same specimens were placed in the new species *Hantkenina singanoae* (Coxall and Pearson 2006, Pl. 8.13, Figs. 16−17).

5.2 Objectives

This study aims to document a well–constrained and more complete pattern of the gradual evolutionary origin of the foraminiferal genus Hantkenina from Clavigerinella than hitherto shown, at Tethyan Contessa Highway reference section (Gubbio, Italy). A high–resolution study has produced a detailed nine–stage pattern for this evolutionary lineage. Moreover, the related time frame and duration are assessed using the available astronomical calibration of the Contessa Highway record.

5.3 Location and stratigraphic setting

The Contessa Highway section (lat. 43°22′51″N; long. 12°33′44″E), located a few kilometers northwest of Gubbio (central Italy) (Fig. 5.3), is probably one of the best studied Tethyan Cenozoic successions. This reference section, which has been proposed by Jovane et al. (2010) as the Global Stratotype Section and Point for the Lutetian/Bartonian boundary, outcrops along Highway SS452 and is characterized by a complete and undisturbed record of many crucial aspects of the Earth's history from the Cretaceous−Paleogene (K/Pg) boundary to the upper Oligocene (e.g., Lowrie et al., 1982; Montanari et al., 1985; Cresta et al., 1989; Jovane et al., 2007, 2010; Coccioni et al., 2010; cum references therein). Owing to the continuous deposition in a pelagic setting, a rather modest tectonic overprint, and the availability of excellent age control through magneto–, bio–, chemo– and tephrostratigraphy, and direct radioisotopic dates from interbedded volcaniclastic layers, the Contessa Highway section have played a prominent role in the establishment of standard Paleogene time scales. The base of this section is placed 95 m above the K/Pg boundary and a normal fault interrupts the section at its top (Jovane et al., 2007, 2010). The middle Eocene portion of the Contessa Highway section, represented by the Scaglia Variegata Formation, is composed of alternations of gray, green and reddish brown well–bedded coccolith−foraminiferal marly limestones, calcareous marls and marls deposited at an average sedimentation rate of ~0.69 cm/kyr in middle to lower bathyal depths (800−1500 m) and at ~30°N paleolatitude (Jovane et al., 2007, 2010). It

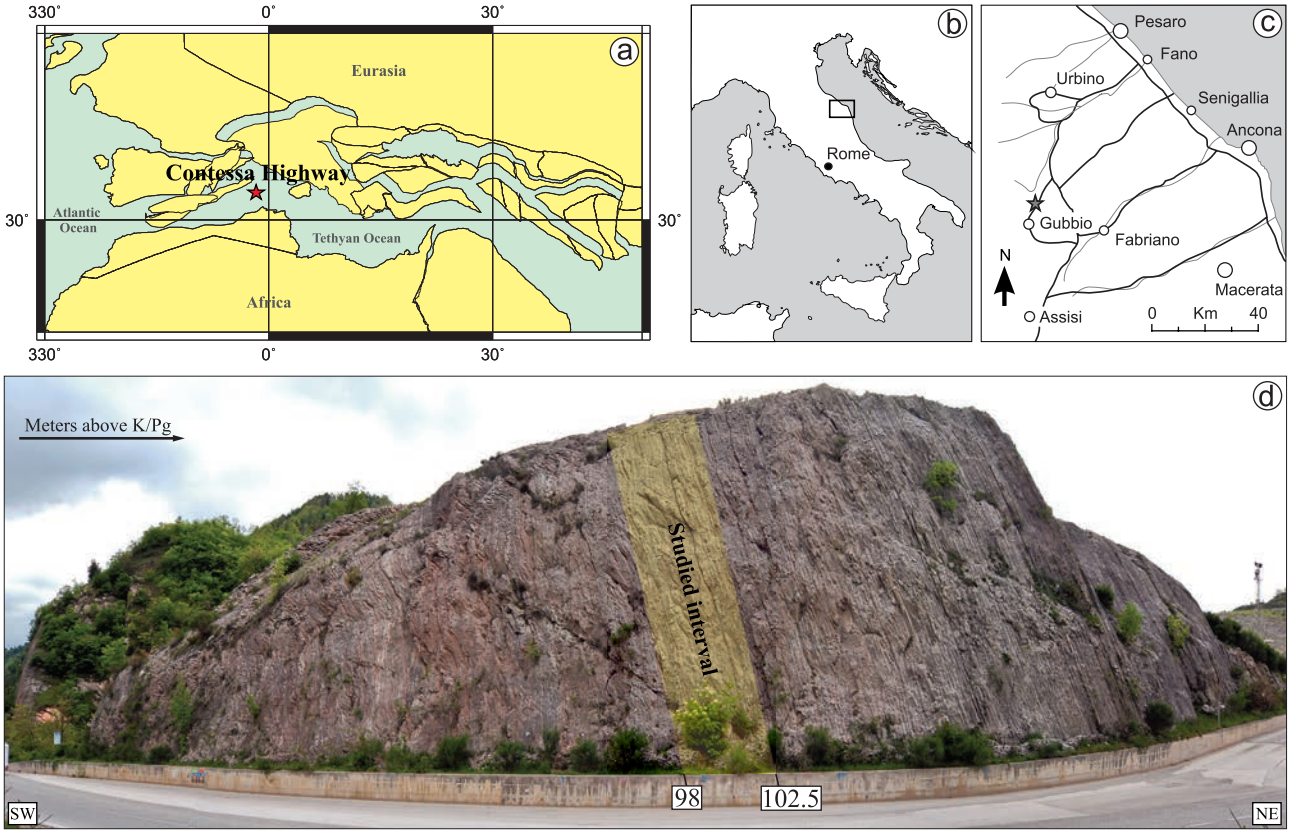

Figure 5.3 – (a) Paleogeographic reconstruction of the Tethys at the time of the first occurrence of hantkeninids and paleo–location of Contessa Highway Section. Reconstruction made using the Web–based software at http://www.odsn.de/odsn/index.html (Hay et al., 1999). (b-c) Location of the Contessa Highway Section near Gubbio (Italy). (d) Contessa Highway outcrop and studied interval from meter 98.0 to 102.50 m.

shows clear cyclicity with bundles of limestone−marl couplets deposited under orbital control (Jovane et al., 2010).

This study focuses on a 4.5 m−thick, continuous and undisturbed stratigraphic interval located from 98 to 102.5 m above the K/Pg boundary (Fig. 5.4). Following Jovane et al. (2010), it falls within the lower part of magnetic polarity Chron C20r, the middle of the calcareous nannofossil Subzone NP15b of Aubry (1991) and the middle–lower part of the calcareous nannofossil Subzone CP13b of Okada and Bukry (1980), and spans the uppermost part of the planktonic foraminiferal Zone P9 to the lowermost part of Zone P10 of Berggren et al. (1995) and the uppermost part of the planktonic foraminiferal Zone E8 to the lowermost part of Zone E9 of Wade et al. (2011). According to astronomical calibration ages of Jovane et al. (2010), the studied segment spans from 46.135 to 45.261 Ma (874 kyr) and was deposited at an average sedimentation rate of ~0.51 cm/kyr (Fig. 2).

5.4 Materials and methods

A total of one hundred and sixteen bulk rock samples was collected throughout the studied segment (Fig. 5.4) at an average spacing of ~4 cm corresponding to ~5.6 kyr. Due to the overall scarcity of *Clavigerinella* and *Hantkenina* near their appearance levels, a large amount (~2 kg) of each sample had to be processed by sieving through a 63 μm mesh and drying at 50 °C following the cold acetolyse technique for lithified sediments of Lirer (2000). The washed residues were studied with a binocular microscope and ~5,000 specimens of *Clavigerinella* and *Hantkenina* were identified following the taxonomic criteria of Coxall and Pearson (2006) and Rögl and Egger (2010, 2011). Scanning electron micrographs were taken of the most representative specimens. All the material studied is housed in the laboratory of the Dipartimento di Scienze della Terra, della Vita e dell'Ambiente at the Università di Urbino, Italy.

5.5 Pattern, timing, and duration of the evolutionary transition from *Clavigerinella* to *Hantkenina* at Contessa Highway Section

The planktonic foraminiferal assemblages of the studied segment are abundant, moderately to well preserved and diversified. They are characterized by *Acarinina praetopilensis*, *Catapsydrax unicavus*, *Guembelitrioides nuttalli*, *Igorina broedermanni*, *Morozovella aragonensis*, *Parasubbotina eoclava*, *Pseudohastigerina wilcoxensis*, *Subbotina linaperta*, *S. eocaena*, *Turborotalia frontosa* and, from 98.5 m to 100.75 m, by *Clavigerinella* and *Hantkenina*, respectively. On the whole, clavigerinellids and earliest hantkeninids represent a very minor component (<1%) of the assemblages, consistent with small populations of possibly long−lived individuals such as those inhabiting the mesopelagic zone (200−2000 m).

According to the range of the main evolutionary events, our data support a well–constrained nine–stage pattern for the gradual evolutionary transition from *Clavigerinella* to *Hantkenina*. Based on the astronomical calibrated ages of Jovane et al. (2010), these stages have different durations.

Stage 1 (98–98.5 m; 46.135–46.028 Ma)
Only rare transitional forms of *Parasubbotina eoclava–Clavigerinella eocanica* are present.

Stage 2 (98.5–99.2 m; 46.028–45.897 Ma)
The lowest occurrence (LO) of *C. eocanica* (Plate 1, Figs. 2–4), which evolved from *P. eoclava* (Pl. 1, Fig. 1), is recognizable at the base of this stage (Fig. 5.4).

Stage 3 (99.2 100.85 m; 45.897– 45.564 Ma)
Clavigerinella caucasica (Plate 1, Fig. 5–8) first appears at the base of this stage (Fig. 5.4). Interestingly, a temporary but significant relative increase in abundance of clavigerinellids is found at the base of this stage. Above 99.97 m there are overall increasing numbers of clavigerinellids and, later on, hantkeninids. According to the astronomically calibrated ages of Jovane et al. (2010), the evolution from *C. eocanica* to *C. caucasica* occurred in 131 kyr (Fig. 5.5).

Stage 4 (100.85–100.9 m; 45.564–45.556 Ma)
Following Rögl and Egger (2011), the newly discovered species *Hantkenina gohrbandti* is distinguished by pointed chamber ends extending up to a thickened nub (proto−tubulospine) and in some cases by the first tubulospines. Hence, *H. gohrbandti* would include different morphotypes displaying the same stratigraphic distribution. However, our high–resolution study showed a discrete stratigraphic distribution for each of the three recognized morphotypes. The LO of *H. gohrbandti* morphotype 1 (Plate 1, Figs. 9–16; Plate 3, Figs. 1–7) is recognized at the base of this stage (Fig. 5.4). Based on the astronomically calibrated ages of Jovane et al. (2010), the evolution from *C. caucasica* to *H. gohrbdandti* morphotype 1 occurred in 333 kyr (Fig. 5.5).

Stage 5 (100.9–101 m; 45.556–45.542 Ma)
The initial appearance of *H. gohrbandti* morphotype 2 (Plate 2, Fig. 1; Plate 3, Fig. 8) occurs at the base of this stage (Fig. 5.4). According to the astronomically calibrated ages of Jovane et al. (2010), the evolution from *H. gohrbandti* morphotype 1 to *H. gohrbandti* morphotype 2 occurred in 8 kyr (Fig. 3).

Stage 6 (101–101.2 m; 45.542–45.508 Ma)
Hantkenina gohrbandti morphotype 3 (Plate 2, Figs. 2–6; Pl. 3, Figs. 9–13) first appears at the base of this stage (Fig. 5.4). Interestingly, the initial entry of *Hantkenina singanoae* (Pl. 2, fig 7; Pl. 3, fig. 14), which was erected by Pearson and Coxall (in Coxall and Pearson, 2006) to include a range of diverse morphologies that appear transitional between *C. caucasica* and *Hantkenina mexicana* and according to Coxall and Pearson (2006) is considered to be the missing link between the genera *Clavigerinella* and *Hantkenina*, is recognized at the base of this stage (Fig. 2). Similarly to that observed by Rögl and Egger (2011) at Holzhäusl, at Contessa Highway section *H. singanoae* occurs in very small numbers. Transitional forms between *H. gohrbandti* morphotype 3 and *Hantkenina cf. mexicana* "forma *H. nuttalli* Toumarkine" (Plate 2, Figs. 8–12; Plate 3, Fig. 15) are found throughout this stage. Remarkably, a major peak in the relative abundance of clavigerinellids and earliest hantkeninids is observed. According to the astronomical calibrated ages of Jovane et al. (2010), the evolution from *H. gohrbandti* morphotype 2 to *H. gohrbandti* morphotype 3 occurred in 34 kyr (Fig. 5.5).

Stage 7 (101.2–101.25 m; 45.508–45.502 Ma)
The LO of *Hantkenina* cf. *mexicana* "forma *Hantkenina nuttalli* Toumarkine" is recognized at the base of this stage (Fig. 2). Based on the astronomical

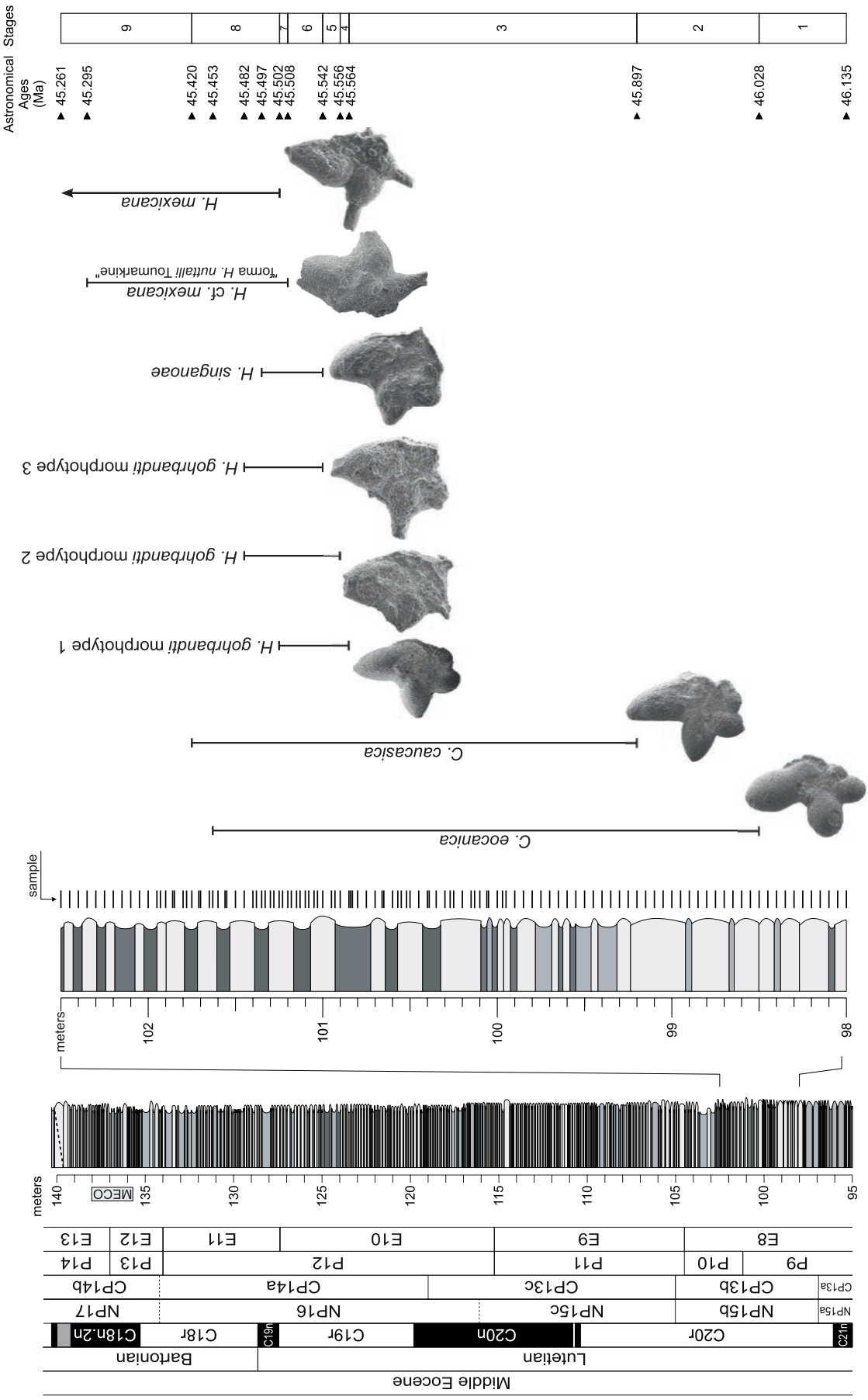

Figure 5.4 – Integrated stratigraphy of the Contessa Highway section (Jovane et al., 2010) and distribution of *Clavigerinella* and *Hantkenina* throughout the studied segment. A nine–stage pattern is recognized for the evolutionary transition from *Clavigerinella* to *Hantkenina*. Calcareous nannofossil Zones and Subzones NP and CP are, respectively, from Martini (1971) and Aubry (1991), and from Okada and Bukry (1980). Planktonic foraminiferal Zones P and E are from Berggren et al. (1995) and Wade et al. (2011), respectively. Chronostratigraphy is after Molina et al. (2011). Astronomically calibrated ages are from Jovane et al. (2010).

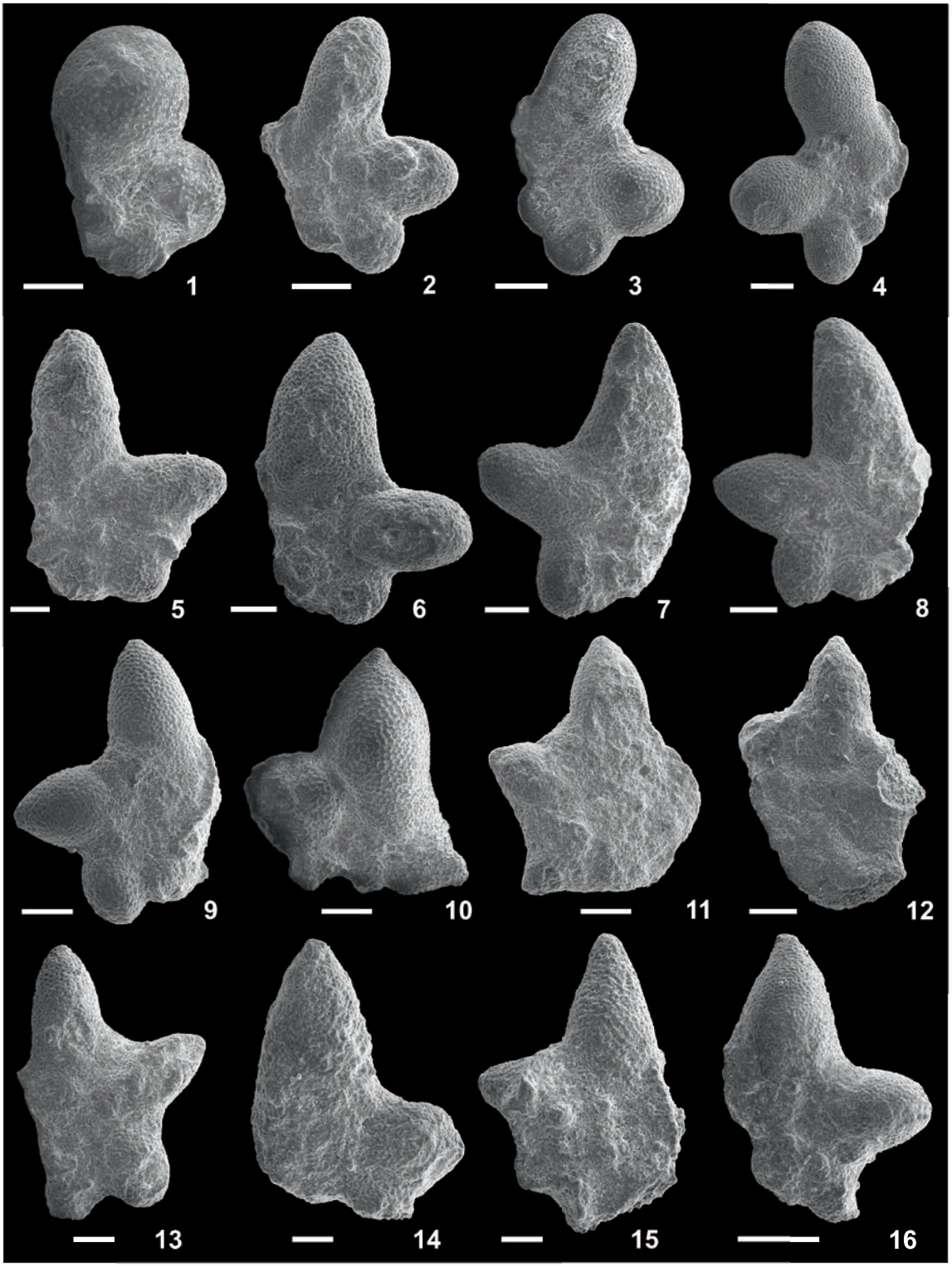

Plate 5.1 – Fig 1. *Parasubbotina eoclava* Coxall, Huber and Pearson (sample m 100). Fig. 2. *Clavigerinella eocanica* (Nuttal) (m 101.2). Fig 3. *Clavigerinella eocanica* (Nuttal) (m 101.2). Fig. 4. *Clavigerinella eocanica* (Nuttal) (m 101.2). Fig. 5. *Clavigerinella caucasica* (Subbotina) (m 101.8). Fig. 6. *Clavigerinella caucasica* (Subbotina) (m 101.18). Fig. 7. *Clavigerinella caucasica* (Subbotina) (m 101.8). Fig. 8. *Clavigerinella caucasica* (Subbotina) (m 101.2). Fig. 9. *Hantkenina gohrbandti* Rögl and Egger morphotype 1 (m 101.2). Fig. 10. *Hantkenina gohrbandti* Rögl and Egger morphotype 1 (m 101.2). Fig. 11. *Hantkenina gohrbandti* Rögl and Egger morphotype 1 (m 101.2). Fig. 12. *Hantkenina gohrbandti* Rögl and Egger morphotype 1 (m 101). Fig 13. *Hantkenina gohrbandti* Rögl and Egger morphotype 1 (m 101.08). Fig. 14. *Hantkenina gohrbandti* Rögl and Egger morphotype 1 (m 101). Fig. 15. *Hantkenina gohrbandti* Rögl and Egger morphotype 1 (m 101.1). Fig. 16. *Hantkenina gohrbandti* Rögl and Egger morphotype 1 (m 100.9). Scale bar for all figures: 100 μm.

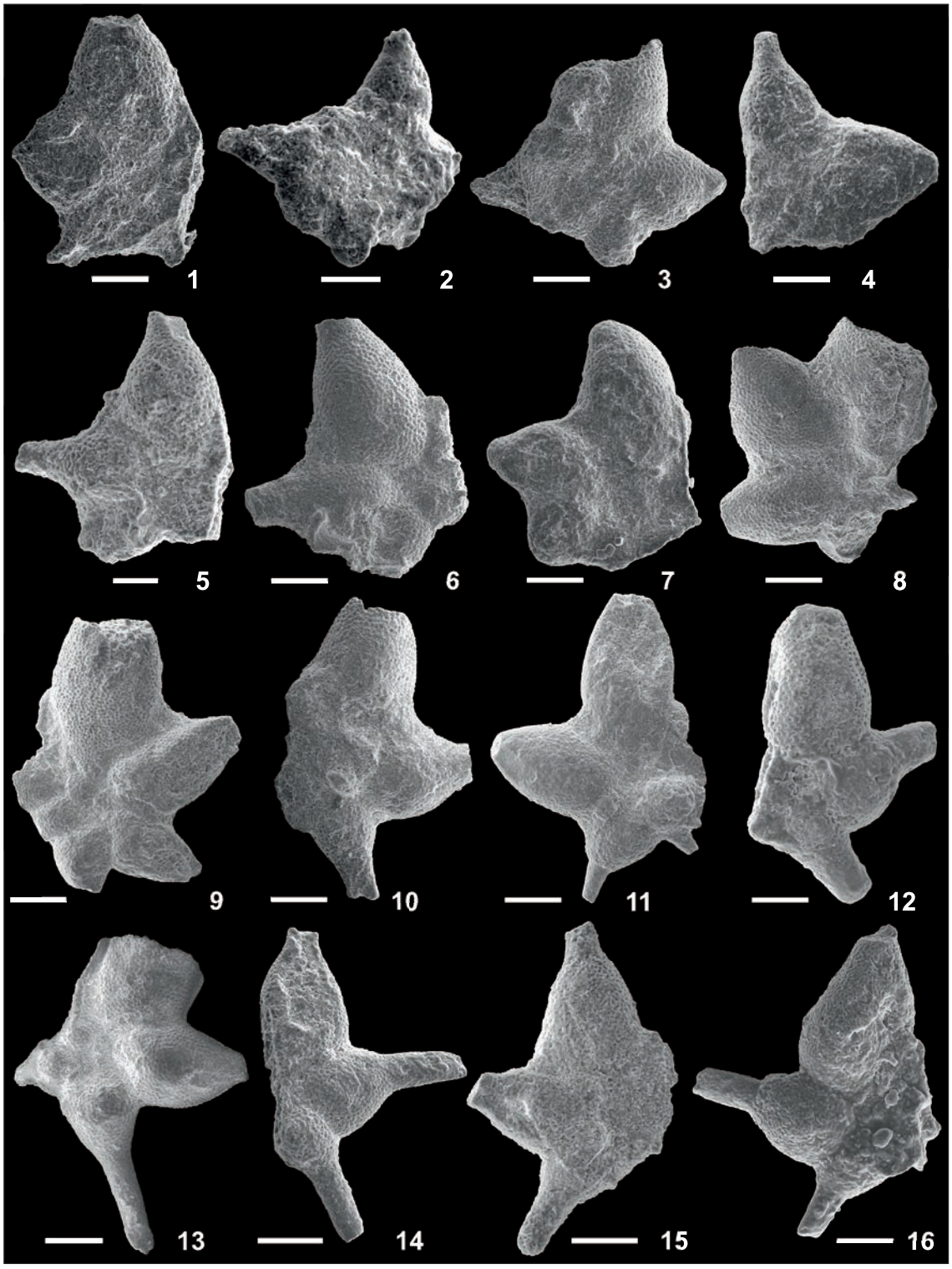

Plate 5.2 – Fig 1. *Hantkenina gohrbandti* Rögl and Egger morphotype 2 (m 101.25). Fig. 2. *Hantkenina gohrbandti* Rögl and Egger morphotype 3 (m 101.2). Fig 3. *Hantkenina gohrbandti* Rögl and Egger morphotype 3 (m 101.08). Fig. 4. *Hantkenina gohrbandti* Rögl and Egger morphotype 3 (m 101.2). Fig. 5. *Hantkenina gohrbandti* Rögl and Egger morphotype 3 (m 101.18). Fig. 6. *Hantkenina gohrbandti* Rögl and Egger morphotype 3 (m 101.3). Fig. 7. *Hantkenina singanoae* Pearson and Coxall (m 101.05). Fig. 8. *Hantkenina* cf. mexicana "forma *H. nuttalli* Toumarkine" (metro 101.8). Fig. 9. *Hantkenina* cf. *mexicana* "forma *H. nuttalli* Toumarkine" (m 101.93). Fig. 10. *Hantkenina* cf. mexicana "forma *H. nuttalli* Toumarkine" (m 101.85). Fig. 11. *Hantkenina* cf. *mexicana* "forma *H. nuttalli* Toumarkine" (m 101.8). Fig. 12. *Hantkenina* cf. *mexicana* Cushman "forma *H. nuttalli* Toumarkine" (m 101.85). Fig 13. *Hantkenina mexicana* Cushman (m 101.25). Fig. 14. *Hantkenina mexicana* Cushman (m 101.95). Fig. 15. *Hantkenina mexicana* Cushman (m 101.3). Fig. 16. *Hantkenina mexicana* Cushman (m 101.95). Scale bar for all figures: 100 μm.

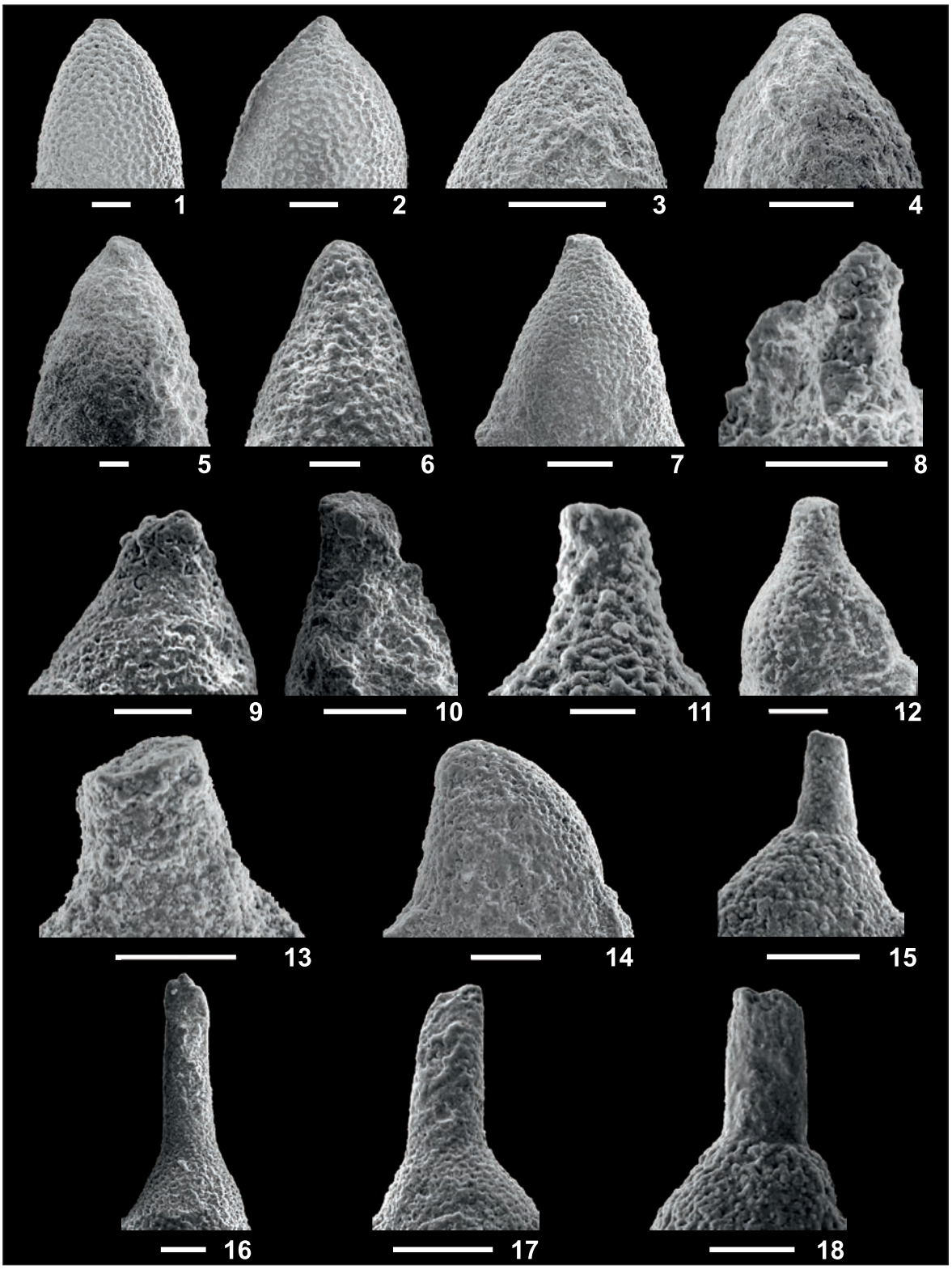

Plate 5.3 – **Fig 1.** *Hantkenina gohrbandti* Rögl and Egger morphotype 1, final chamber of specimen in Pl. 1, Fig. 9 ends with a terminal nub. **Fig. 2.** *Hantkenina gohrbandti* Rögl and Egger morphotype 1, terminal nub at the end of the final chamber of specimen in Pl. 1, Fig. 10. **Fig. 3.** *Hantkenina gohrbandti* Rögl and Egger morphotype 1, final chamber of specimen in Pl. 1, Fig. 11 ends with a terminal nub. **Fig. 4.** *Hantkenina gohrbandti* Rögl and Egger morphotype 1, terminal nub at the end of the final chamber of specimen in Pl. 1, Fig. 12. **Fig. 5.** *Hantkenina gohrbandti* Rögl and Egger morphotype 1, final chamber of specimen in Pl. 1, fig. 14 ends with a terminal nub. **Fig. 6.** *Hantkenina gohrbandti* Rögl and Egger morphotype 1, terminal nub at the end of the final chamber of specimen in Pl. 1, Fig. 15. **Fig. 7.** *Hantkenina gohrbandti* Rögl and Egger morphotype 1, final chamber of specimen in Pl. 1, fig. 16 ends with a terminal

nub. **Fig. 8.** *Hantkenina gohrbandti* Rögl and Egger morphotype 2, short tubulospine of the primary chamber of specimen in Pl. 2, Fig. 1. **Fig. 9.** *Hantkenina gohrbandti* Rögl and Egger morphotype 3 (m 101.2), thickened conical knob at the end of the final chamber of specimen in Pl. 2, Fig. 2. **Fig. 10.** *Hantkenina gohrbandti* Rögl and Egger morphotype 3 (m 101.2), tubulospine of the prelast chamber of specimen in Pl. 2, Fig. 2. **Fig. 11.** *Hantkenina gohrbandti* Rögl and Egger morphotype 3 (m 101.18), tubulospine of the prelast chamber of specimen in Pl. 2, fig. 5. **Fig. 12.** *Hantkenina gohrbandti* Rögl and Egger morphotype 3 (m 101.2), tubulospine of the final chamber of specimen in Pl. 2, Fig. 4 ends with a blunt tubulospine. **Fig. 13.** *Hantkenina gohrbandti* Rögl and Egger morphotype 3 (m 101.3), tubulospine of the prelast chamber of specimen in Pl. 2, fig. 6. **Fig. 14.** *Hantkenina singanoae* Pearson and Coxall (m 101.05), final chamber of specimen in Pl. 2, Fig. 7 ends with a distal hood (proto–tubulospine). **Fig. 15.** *Hantkenina* cf. *mexicana* "forma *H. nuttalli* Toumarkine" (m 101.8), tubulospine of the third–last chamber of specimen in Pl. 2, Fig. 11. **Fig. 16.** *Hantkenina mexicana* Cushman (m 101.25), tubulospine of the third–last chamber of specimen in Pl. 2, Fig. 13. **Fig. 17.** *Hantkenina mexicana* Cushman (m 101.95), tubulospine of the second–last chamber of specimen in Pl. 2, fig. 14. **Fig. 18.** *Hantkenina mexicana* Cushman (m 101.95), tubulospine of the second–last chamber of specimen in Pl. 2, Fig. 16. Scale bar for all figures: 50 µm

calibrated ages of Jovane et al. (2010), the evolution from *H. gohrbandti* morphotype 1 to *H.* cf. *mexicana* "forma *H. nuttalli* Toumarkine" occurred in 56 kyr (Fig. 5.4).

Stage 8 (101.25–101.75 m; 45.502–45.420 Ma)

At the base of this stage, *H. mexicana* (Plate 2, Figs. 13–16; Plate 3, Figs. 16–18) finally appears (Fig. 5.4). *Hantkenina singanoae*, *H. gohrbandti* and *C. eocanica* gradually disappear at 45.497 Ma, 45.482 Ma and 45.453 Ma, respectively (Fig. 5.4). However, the disappearance of *C. eocanica* appears to only be temporary since this species has been observed ranging into the uppermost Eocene of the western Atlantic Ocean (Pearson and Chaisson, 1997). Interestingly, from 100.13 m (middle part of Stage 3) up to 101.3 m (lower part of Stage 8), the adult chambers of *C. eocanica* and *C. caucasica* are generally longer and to some extent more slender than those of the same species in the underlying stratigraphic levels. Based on these morphological features, these forms might resemble *Clavigerinella jarvisi*; however, typical specimens of this species were never found at the Contessa Highway section. According to the astronomically calibrated ages of Jovane et al. (2010), the evolution from *C. eocanica* to *H. mexicana* occurred in 526 kyr (Fig. 5.5).

Stage 9 (101.75–102.5 m; 45.420–45.261 Ma)

The base of this stage is marked by the highest occurrence of *C. caucasica* (Fig. 5.4). *Hantkenina* cf. *mexicana* "forma *H. nuttalli* Toumarkine" occurs up to higher stratigraphic levels above which only *H. mexicana* survives (Fig. 5.4). Stage 9 represents the first step towards hantkeninid development. Later, in fact, hantkeninids gradually diversify and become a consistent component of the planktonic foraminiferal assemblages up to the Eocene–Oligocene boundary (Coxall et al., 2003; Coxall and Pearson, 2006).

5.6 Paleoecological and paleoceanographic insights

Chamber elongation is a recurring morphological feature of Cretaceous and Cenozoic planktonic foraminiferal evolution, with the fossil record beginning 130 million years ago (Coccioni et al.,

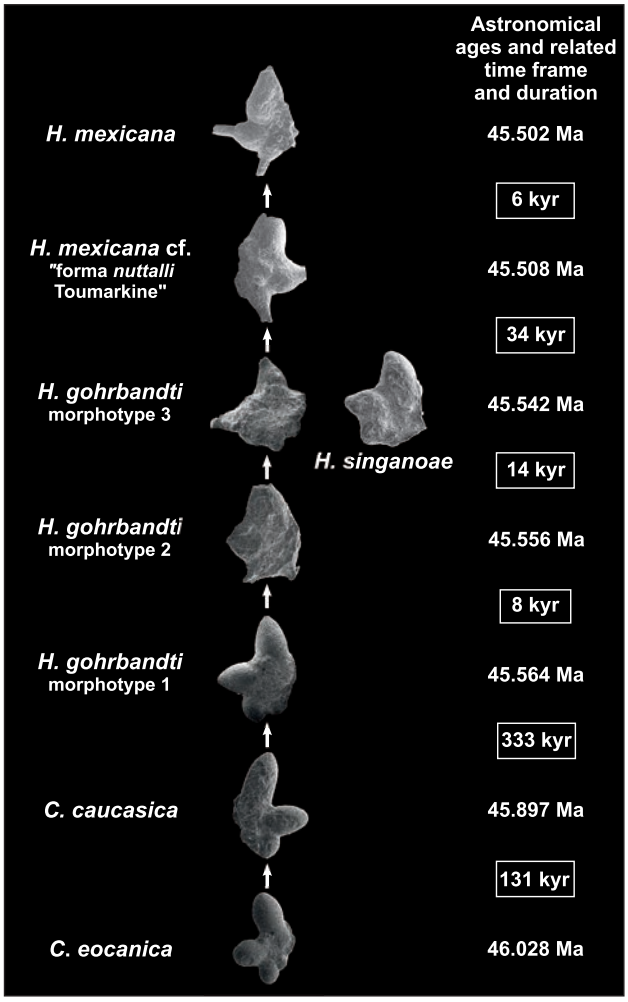

Fig. 5.5 – Synoptic scheme of pattern, timing, and duration of the evolutionary origin of the foraminiferal genus Hantkenina at Contessa Highway section. Astronomically calibrated ages are from Jovane et al. (2010).

2006). Stable isotope studies indicate that most fossil digitate species lived in deep–water habitats below the thermocline and are hypothesized to have lived near or in oxygen minimum zones (Coxall et al., 2007). Chamber elongation is commonly interpreted as an adaptation to poorly oxygenated and/or eutrophic environments, although additional physico−chemical and biological controls on their distribution, such as temperature, salinity, nutrients, food type, and trace elements, could be not disregarded (Coccioni et al., 2006; Coxall et al., 2007; Luciani et al., 2010).

Our findings show that during the middle Eocene from 46 to 45.5 Ma (Fig. 5.4), primarily as a result of poorly oxygenated and usually food–poor waters, deep–mesopelagic planktonic foraminifera, probably living close to the redoxcline where oxygen levels begin to increase, may have developed different life strategies by adopting morphological modifications to tolerate temporary exceptionally stressful environmental conditions unfavorable to other planktonic species. As a striking element in their deep–water ecologic opportunism, this allowed for an increased effective shell size and food gathering efficiency and would have enabled the "digitate" clavigerinellids and earliest hantkeninids (i.e., *H. gohrbandti* morphotypes 1 to 3 and *H. singanoae*) to radiate. Subsequently, the skeletal adaptations (tubulospines) acquired by *Hantkenina* would have enabled these morphotypes to utilize a wider range of food sources and thus diversify into broader oceanic realms than clavigerinellids and earliest hantkeninids (see Coxall et al., 2003).

If the relative abundance of digitate planktonic foraminifera is proportional to the strength of the environmental perturbation as suggested for Cretaceous digitates by Coccioni et al. (2006), and if these forms can be used as a proxy for intervals of oxygen minimum zone (OMZ) expansion as proposed by Coxall et al. (2007), then our findings imply that sustained and expanded OMZ conditions and possibly enhanced eutrophication might have occurred during the middle Eocene from 46 to 45.5 Ma. Interestingly, several marker events such as a peak in abundance of the benthic foraminifera *Aragonia aragonensis* and the co–occurrence of warm–water calcareous nannofossils at the Spanish Agost section (Larrasoaña et al., 2008; Ortiz et al., 2008), may be evidence of a transient warm or hyperthermal event possibly leading to reduced water–column stratification and increased eutrophication just before the evolutionary appearance of hantkeninids.

5.7 Summary and conclusions

This high–resolution study of the Contessa Highway reference section reveals a detailed, well–constrained and more complete view of the gradual evolutionary transition from *Clavigerinella* to *Hantkenina* than hitherto shown. Based on the range of the main evolutionary events, nine–stage pattern are recognized for this evolutionary lineage, and the related time frame and duration are assessed using the astronomical calibrated ages available for the Contessa Highway record. The gradual evolution from *C. caucasica* to *H. gohrbandti*, which more specifically as *H. gohrbandti* morphotype 1 may be considered the real ancestor of *Hantkenina*, occurred in 333 kyr with the *H. gohrbandti* first appearance date at 45.564 Ma. Our new findings show that during the middle Eocene, from 46 to 45.4 Ma and with a major pulse centered at 45.521 Ma, deep–mesopelagic planktonic foraminifera, probably living close to the redoxcline, may have developed morphological modifications, principally resulting from poorly oxygenated and usually food–poor waters, to tolerate temporary exceptionally stressful environmental conditions unfavorable to other planktonic species. This suggests that sustained and expanded OMZ conditions and associated enhanced eutrophication might have existed in the western Tethyan area during that time. Our well–constrained findings may help in building an expanded database of the stratigraphic and biogeographic distribution and the paleoecology of digitate species over time as well as providing a major advance in biochronologic resolution and a template for future progress of the Cenozoic time scale.

5.8 Taxonomic notes

Order Foraminiferida Eichwald, 1830
Suborder Rotaliina Delage and Hérouard, 1896
Superfamily Globigerinaceae Carpenter, Parker and Jones, 1862
Family Globigerinidae Carpenter, Parker and Jones, 1862

Genus *Parasubbotina* Olsson, Hemleben, Berggren and Lin, 1992
Parasubbotina eoclava Coxall, Huber and Pearson, 2003
(Plate 1, Figure 1)
Parasubbotina eoclava Coxall, Huber and Pearson

2003: 256, pl. 8, figs. 1–15.
Parasubbotina eoclava Olsson, Pearson and Huber 2006: 99–100, pl. 5.9, figs. 1–16.

This species is distinguished by lateral compression of the test, very low trochospiral coiling, slight elongation of the final chambers and a prominent apertural lip.

Genus *Clavigerinella* Bolli, Loeblich and Tappan, 1957

Clavigerinella eocanica (Nuttall, 1928)
(Plate 1, Figures 2–4)
Hastigerinella eocanica Nuttall, 1928: 376, pl. 50, figs. 9–11.
Clavigerinella eocanica Coxall, Huber and Pearson, 2003: pl. 1, figs. 9–14; pl. 6, figs. 1–4.
Clavigerinella eocanica Coxall and Pearson, 2006: 222–224, pl. 8, figs. 10–19.
Clavigerinella jarvisi Larrasoaña et al. 2008: fig. 4F.
Clavigerinella eocanica Rögl and Egger, 2010: fig. 3.1.
Clavigerinella jarvisi Rögl and Egger, 2010: fig. 3.2.

This species evolved from *P. eoclava* by radial elongation of the chambers and lowering of the coil height to form a planispiral. It is distinguished from all other clavigerinellids by having unmodified, smoothly rounded clavate chambers.

Clavigerinella caucasica (Subbotina, 1958)
(Plate 1, Figure 5–8)
Hastigerinella caucasica Subbotina, 1958: 58, pl. II, Figs. 8a–b.
Clavigerinella–Hantkenina transitions Coxall, Huber and Pearson, 2003: pl. 6, figs. 5–8.
Clavigerinella caucasica Pearson et al., 2004: pl. 2, figs. 16–17.
Clavigerinella caucasica Coxall and Pearson, 2006: 218–221, pl. 8.1, figs. 10–19.
Clavigerinella jarvisi Rögl and Egger, 2010: fig. 3.2.
Clavigerinella caucasica Rögl and Egger, 2010: figs. 3.3, 3.4.
Clavigerinella caucasica Rögl and Egger, 2011: pl. 4, fig. 1.

This species, which evolved from *C. eocanica* by slightly tapering into an acute or pointed tip of the adult chambers, represents the first stage in the gradual morphological transition to *Hantkenina* (Coxall and Pearson, 2003, 2006; Rögl and Egger, 2010, 2011).

Family Hantkeninidae Cushman, 1927

Genus *Hantkenina* Cushman, 1924

Hantkenina gohrbandti Rögl and Egger, 2011 – morphotype 1
(Plate 1, Figures 9–16; Plate 3, Figures. 1–7)
Hantkenina nov. spec. Rögl and Egger 2010: figs. 3.6, 4.2.
Rögl and Egger 2011: 5–6, pl. 1, figs. 1–8; pl. 2, figs. 1–3; pl. 3, figs. 1–8; pl. 4, fig. 5.

Hantkenina gohrbandti morphotype 1 evolved from *C. caucasica* by the development of pointed chamber ends with a nub that appears as a rounded, hollow and perforate structure in the youngest chambers, and forming a proto–tubulospine in sense of Coxall and Pearson (2006). This morphotype represents the real ancestor of the genus *Hantkenina.*

Hantkenina gohrbandti Rögl and Egger, 2011 – morphotype 2
(Plate 2, Figure 1; Plate 3, Figure 8)
Hantkenina singanoae Coxall and Pearson, 2006: 252–253, pl. 8.13, figs. 16–17.
Hantkenina nov. spec. Rögl and Egger 2010: 24, fig. 3.7; 25, fig. 4.3.
Hantkenina gohrbandti Rögl and Egger 2011: 5–6, pl. 2, fig. 4; pl. 3, fig. 10; pl. 4, fig. 4.

Hantkenina gohrbandti morphotype 2 evolved from *H. gohrbandti* morphotype 1 by the development of a short, real tubulospine in the primary chambers of final whorl. After developing a tubulospine in the inner whorl, the following chambers are pointed or with an acute nub.

Hantkenina gohrbandti Rögl and Egger, 2011 – morphotype 3
(Plate 2, Figures 2–6; Plate 3, Figures 9–13)
"Primitive" *H. nuttalli* Coxall, Huber and Pearson, 2003: pl. 6, figs. 9, 16.
Hantkenina singanoae Coxall and Pearson, 2006: 252–253, pl. 8.13, figs. 16–17.
Hantkenina nov. sp. Rögl and Egger, 2010: figs. 3.8, 4.4.
Hantkenina gohrbandti Rögl and Egger, 2011: pl. 2, figs. 5, 6, 9; pl. 3, fig. 11.

Hantkenina gohrbandti morphotype 3 evolved from *H. gohrbandti* morphotype 2 by the development of blunt tubulospines in different chambers of the the final whorl. Other chambers of the final whorl with pointed ends or thickened conical knobs.

Hantkenina singanoae Pearson and Coxall, 2006
(Plate 2, Figure 7; Plate 3, Figure 14)

Transitional *Hantkenina* sp. Pearson et al., 2004: pl. 2, 18–21.
Hantkenina singanoae Coxall and Pearson, 2006: 251–253, pl. 8.13, figs. 1–15.
Hantkenina singanoae Rögl and Egger, 2010: figs. 3.5, 4.1.
Hantkenina singanoae Rögl and Egger, 2011: pl. 1, fig. 9; pl. 3: figs. 9,13.

Hantkenina singanoae, which according to Coxall and Pearson (2006) should bridge the gap between digitate and tubulospinose morphologies, also evolved from *C. caucasica* by constriction of the terminal chamber ends. This species is characterized by later chambers ending in a terminal, hood–like nub or cylindrical projection (proto–tubulospines). Proto–tubulospines are smooth and distinctly porous in contrast to the true tubulospines of *H. mexicana* and subsequent hantkeninids, which are usually imperforate (Coxall and Pearson, 2006). Distal chamber ends can be inclined in an anterior, posterior or dorso–ventral direction and proto–tubulospines are commonly bent (Pearson and Coxall in Coxall and Pearson, 2006). At Contessa Highway section, the stratigraphic range of *H. singanoae* overlaps with that of *H. gohrbandti* morphotype 3 (Fig. 2). In addition, this species occurs in very small numbers, the characteristic hood is rudimentary developed (Pl. 3, fig. 14), and no specimens with cylindrical projections were found. Accordingly, in contrast to Pearson et al. (2006) and in agreement with Rögl and Egger (2010, 2011), *H. singanoae* is considered to be an evolutionary side branch of the *Clavigerinella–Hantkenina* transition, since it is unlikely that the bent chamber ends of this species developed into straight tubulospines. Interestingly, specimens of *H. singanoae* having long terminal nubs like those recognized in the Kilwa drill sites of Tanzania (Pearson et al., 2004; Coxall and Pearson, 2006) do not occur at Contessa Highway (western–central Tethys) and Holzhäusl (northwestern Tethys) sections. This would suggest that the elongation of the terminal nub could represent an ecological adaptation and is, therefore, of paleoenvironmental significance.

Hantkenina cf. *mexicana* "forma *H. nuttalli* Toumarkine" (Toumarkine, 1981)
(Plate 2, Figures 8–12; Plate 3, Figure 15)

Hantkenina mexicana var. *aragonensis* Nuttall, 1930: 284, pl. 24, figs. 2–3; fig. 3 = holotype *H. nuttalli* Toumarkine by subsequent designation.
Hantkenina nuttalli Toumarkine, 1981: 112, pl. 1, fig. 4
Hantkenina nuttalli Toumarkine and Lutherbacher, 1985: 121, pl. 23, figs. 3–5.
Hantkenina nuttalli Coxall et al., 2003: 245, pl. 3, figs. 1,5.
Hantkenina mexicana Coxall and Pearson, 2006: pl. 8.10: figs. 2–5.
Hantkenina mexicana Larrasoaña et al. 2008: fig. 4H.
"*Hantkenina nuttalli*" Rögl and Egger, 2010: figs. 3.9, 3.10.
Hantkenina cf. *mexicana* "forma *H. nuttalli* Toumarkine" Rögl and Egger, 2011: pl. 2, figs. 7, 8; pl. 3, fig. 14.

Various authors have used Toumarkine's (1981) concept of *H. nuttalli* to represent "primitive–looking" early hantkeninids with digitate chambers and stout, broad based tubulospines. Coxall and Pearson (2006) regard *H. nuttalli* Toumarkine 1981 as a junior synonym of *H. mexicana* Cushman 1924 and following Blow (1979) adopt a broad sense of *H. mexicana* to include the spectrum of early stellate hantkeninid morphologies from their origin in the middle Eocene. Howewer, both at Holzhäusl (Rögl and Egger, 2010, 2011) and Contessa Highway, forms of *H. mexicana* with broad strongly appressed chambers and stout, broad based tubulospines, here named *Hantkenina* cf. *mexicana* "forma *H. nuttalli* Toumarkine" in agreement with Rögl and Egger (2011), first appear slightly before the LO of typical specimens of *H. mexicana* and occurs within a discrete stratigraphic range. *Hantkenina* cf. *mexicana* "forma *H. nuttalli* Toumarkine" evolved from *H. gohrbandti* morphotype 3 by lengthening of the tubulospines and their empacement on each chambers of the final whorl.

Hantkenina mexicana Cushman, 1924
(Plate 2, Figures 13–16; Plate 3, Figures 16–18)

Hantkenina mexicana Cushman, 1924: 3, pl. 2: fig. 2
Hantkenina mexicana Coxall and Pearson, 2006: pl.

8.10: figs. 1, 6–21.
Hantkenina cf. *mexicana* Rögl and Egger, 2010: fig. 3.11.
Hantkenina mexicana Rögl and Egger, 2011: pl. 3, figs. 12, 15; pl. 4, figs. 2–3.

Hantkenina mexicana evolved from *Hantkenina* cf. *mexicana* "forma *H. nuttalli* Toumarkine" by the separation of the final whorl chambers that gives rise to a peripheral outline distinctly stellate and the emplacement of the tubulospines of each chambers in central position with respect to the radial chamber axis.

CHAPTER 6

Conclusions

In the previous chapters, it was presented and discussed an investigation of the main environmental perturbations of the Paleogene pelagic succession in the Umbria–Marche Basin. To reach this objective, several integrated analyses at high–resolution were performed on some critical intervals to constrain where these environmental perturbations are expected to occur. A multiproxy approach was applied in these studies, in order to avoid misinterpretations and to extract a robust paleoenvironmental signal along the water column. This integrating approach has required a pool of abiotic (carbonate content, $d^{13}C$ and $d^{18}O$ stable isotopes, magnetic susceptibility, environmental magnetism) and biotic parameters (quantitative analysis on calcareous nannofossils, planktonic and benthic foraminifera). In particular sea–surface (calcareous nannofossils, and planktonic foraminifera) and sea–floor assemblages (benthic foraminifera) were combined to reveal the complex biotic responses to environmental changes along the water column.

To follow, a summary of the scientific contributions of this Thesis is given:

1. In the lower Danian, new high–resolution biochronostratigraphic and magnetic susceptibility data and geochemical records from the Contessa Highway section (Gubbio, Italy) provide the first direct evidence of the early Danian Dan–C2 hyperthermal event beyond the Atlantic Ocean. This suggests a supra–regional, possibly global, nature of this transient warming event with a carbon cycle perturbation. For the first time for this event, biotic responses to environmental changes were investigated and documented. Several dramatic changes in calcareous nannoplankton and foraminifera assemblages are interpreted as a consequence of significant environmental instability. In addition, first evidence of a further short–lived hyperthermal event, termed the "Lower C29n" event, not known up to now are provided. As for other early Paleogene hyperthermal events, the cause of the Dan–C2 event is likely to be found in changes, in the distribution of carbon within surface biosphere reservoirs, possibly controlled by orbital cycles. However, the third and last phase of Deccan volcanism, with its huge release of greenhouse gases into the atmosphere during the Dan–C2 event would be also taken into account.

2. Detailed analyses of calcareous nannofossils and foraminiferal assemblages, and high–resolution geochemical, isotopic and magnetic records across the Selandian–Thanetian transition at Contessa Road Section have allowed to recognize and accurately document a 250 kyr–lasting interval of environmental perturbations, named the Selandian–Thanetian Transition Event (STTE). The remarkable changes in the relative abundances, preservation and composition of calcareous nannofossils and foraminiferal assemblages show that during the STTE an abrupt environmental perturbation took place and reached its climax during the ELPE equivalent, where these changes appear to be more prominent. The environmental instability is not confined within the photic zone but extends to the seafloor resulting in little more trophic conditions of the sea surface waters with an enhanced, but of short measure, nutrient availability on the seafloor under almost unchanged warm–water conditions and marked rise of lysocline. These changes clearly outline a complex paleoenvironmental evolution in the western central Tethys across the Selandian–Thanetian stages The Contessa Road represents the first land–based section where the STTE is recognized and its effects documented.

3. Detailed analyses of calcareous nannofossils and foraminiferal assemblages, and high–resolution geochemical, isotopic and magnetic records across the middle Ypresian at Contessa Road Section have allowed to better constrained the Eocene Thermal Maximum 3 (K or X) and four minor (I1, I2, J, L) suspected hyperthermals. The ETM3 testifies stressed ecological responses among calcareous nannoplankton and foraminifera, which highlight marked environmental perturbation affecting the geobiosphere and resulting in warmer and more oligotrophic sea surface waters and carbonate dissolution. Although, the magnitude and effect of ETM3 appear less intense then the well–known PETM and ETM2, the input of a large mass of isotopically depleted carbon into the ocean and atmosphere may have altered the deep–sea pH, triggering a rapid and transient shoaling of the lysocline and contributing to a greenhouse warming.

4. Linked to the middle Eocene climatic transition, it is presented and discussed a high–resolution study of the Tethyan Contessa Highway reference section (Gubbio, Italy), that has produced a detailed, well–constrained and more complete pattern of the gradual evolutionary origin of the foraminiferal genus *Hantkenina* from *Clavigerinella* than hitherto shown. A nine–stage pattern is presented for this evolutionary lineage. For the first time, since Cushmann introduced the genus *Hantkenina* in 1924, evolutionary time−frame and duration of this origin are assessed using the astronomical calibration of the Contessa Highway record. The evolution of *Clavigerinella caucasica* to *Hantkenina gohrbandti,* the real ancestor of *Hantkenina,* occurred in 333 kyr with the *H. gohrbandti* first appearance dated at 45.564 Ma. These findings show that during the middle Eocene, from 46 to 45.5 Ma and with a major pulse centered at 45.521 Ma deep−mesopelagic planktonic foraminifera may have developed different morphological modifications, principally related to poorly oxygenated and usually food−poor waters, to tolerate temporary exceptionally stressful environmental conditions. This suggests that sustained and expanded oxygen minimum zone conditions and associated enhanced eutrophication might have occurred during that time.

References

Abdul–Aziz, H., Di Stefano, A., Foresi, L.M., Hilgen, F.J., Iaccarino, S.M., Kuiper, K.F., Lirer, F., Salvatorini, G., Turco, E., 2008. Astronomical climate control on paleosol stacking patterns in the upper Paleocene–lower Eocene Willwood formation, Bighorn Basin, Wyoming. Geology 36, 531–534.

Agnini, C., Fornaciari, E., Giusberti, L., Grandesso, P., Lanci, L., Luciani, V., Muttoni, G., Pälike, H., Rio, D., Spofforth, D.J.A., Stefani, C., 2011. Integrated biomagnetostratigraphy of the Alano section (NE Italy). A proposal for defining the middle–late Eocene boundary. Geological Society America Bulletin 123, 841–872.

Agnini, C., Fornaciari, E., Raffi, I., Rio, D., Rohl, and U., Westerhold, T. 2007. High–resolution nannofossil biochronology of middle Paleocene to early Eocene at ODP Site 1262: implications for calcareous nannoplankton evolution. Marine Micropaleontolology 64, 215–248.

Agnini, C., Macrì, P., Backman, J., Brinkhuis, H., Fornaciari, E., Giusberti, L., Luciani, V., Rio, D., Sluijs, A., Speranza, F., 2009. An early Eocene carbon cycle perturbation at ~52.5 Ma in the Southern Alps: Chronology and biotic response. Paleoceanography 24, PA2209.

Agnini, C., Muttoni, G., Kent, D.V., Rio, D., 2006. Eocene biostratigraphy and magnetic stratigraphy from Possagno, Italy: The calcareous nannofossil response to climate variability. Earth and Planetary Science Letters 241, 815–830.

Alegret, L., Molina, E., Thomas, E., 2003. Benthic foraminiferal turnover across the Cretaceous/Paleogene boundary at Agost (southeastern Spain). Paleoenvironmental inferences. Marine Micropaleontology 48, 251–279.

Alegret, L., Thomas, E., 2001. Upper Cretaceous and lower Paleogene benthic foraminifera from northeastern Mexico. Micropaleontology 47, 269–316.

Alvarez, W., Arthur, M.A., Fischer, A.G., Lowrie, W., Napoleone, G., Premoli Silva, I., Roggenthen, W.M., 1977. Upper Cretaceous–Paleocene magnetic stratigraphy at Gubbio, Italy V. Type section for the Late Cretaceous–Paleocene geomagnetic reversal time scale. Geological Society American Bulletin 88, 383–389.

Arenillas, I., Molina, E., Ortiz, S., Schmitz, B., 2008. Foraminiferal and $\delta^{13}C$ isotopic event–stratigraphy across the Danian–Selandian transition at Zumaya (northern Spain): Chronostratigraphic implications. Terra Nova 20, 38–44.

Arthur, M.A., Hinga, K.R., Pilson, M.E.Q., Whitaker, E., Allard, D., 1991. Estimates of pCO_2 for the last 120 My based on 6°C of marine phytoplankton organic matter. EOS 72,166.

Aubry, M.–P., 1991. Sequence stratigraphy: eustasy or tectonic imprint? Journal of Geophysical Research 96, 6641–6679.

Aubry, M.–P. 1992. Late Paleogene calcareous nannoplankton evolution: A tale of climatic deterioration. In: Prothero, D.R., and Berggren, W.A. (eds) Eocene–Oligocene climatic and biotic evolution. Princeton University Press, Princeton, New Jersey, 272–309.

Aubry, M.–P., 1995. From chronology to stratigraphy: Interpreting the lower and middle Eocene stratigraphic record in the Atlantic Ocean, in Berggren, W.A., Kent, D.V., Hardebol, J., (eds.), Geochronology, Time Scales and global stratigraphic correlation: A unified Temporal Framework for an Historical Geology. Society of Economic Paleontologists and Mineralogists, Special Publication 54, 213–274.

Backman, J., Shackleton, N.J., 1983. Quantitative biochronology of Pliocene and early Pleistocene calcareous nannofossils from the Atlantic, Indian and Pacific oceans. Marine Micropaleontolology 8, 141–170.

Banner, F.T., Lowry, F.M., 1985. The stratigraphical record of planktonic foraminifera and its evolutionary implications. Special Papers in Palaeontology 33, 117–130.

Barke, J., Abels, H.A., Sangiorgi, F., Greenwood, D.R., Sweet, A.R., Donders, T., Reichart, G.R., Lotter, A.F., Brinkhuis, H., 2011. Orbitally forced Azolla blooms and Middle Eocene Arctic hydrology: Clues from palynology. Geology 39, 427–430.

Barker, P.F., Filippelli, G.M., Florindo, F., Martin, E.E., Scher, H.D., 2007. Onset and role of the Antarctic Circumpolar Current. Deep–Sea Research, Part II–Topical Studies in Oceanography 54, 2388–2398.

Barrera, E., Huber, B.T., 1993. Eocene to Oligocene oceanography and temperatures in the Antarctic Indian Ocean. American Geophysical Union, Washington, D.C., 60, 49–65.

Barron, E.J., 1985. Explanations for the Tertiary global cooling trend. Palaeogeography, Palaeoclimatology, Palaeoecology 50, 729–739.

Barron, E.J., Hay, W.W., Thompson, S., 1989. The hydrologic cycle: a major variable during earth history: Palaeogeography, Palaeoclimatology, Palaeoecology 75, 157–174.

Bartol, M., Pavšič, J., Dobnikar, M., Bernasconi, S.M., 2008. Unusual *Braarudosphaera bigelowii* and *Micrantholithus vesper* enrichment in the Early Miocene sediments from the Slovenian Corridor, a seaway linking the Central Paratethys and the Mediterranean. Palaeogeography, Palaeoclimatology, Palaeoecology 267, 77–88.

Bellagamba, M., Coccioni, R., 1990. Deep–water agglutinated foraminifera from the Massignano section (Ancona, Italy): a proposed stratotype for the Eocene–Oligocene boundary, in Hemleben, C.H., Kaminski, M.A., Khunt, W., Scott, D., (eds) Paleoecology, biostratigraphy, paleoceanography and taxonomy of agglutinated foraminifera. Dordrecht, Netherlands, Kluwer, Nato asi series 327, 883–921.

Benjamini, C., Reiss, Z., 1979. Wall–hispidity and perforation in Eocene planktonic foraminifera. Micropaleontology 25, 141–150.

Berggren, W.A., Hollister, C.D., 1977. Plate tectonics and paleocirculation–commotion in the ocean. Tectonophysics 11, 11–48.

Berggren, W.A., Kent, D.V., Swisher, C.C., and Aubry, M.P. 1995. A revised Cenozoic geochronology and chronostratigraphy. In: Berggren, W.A., Kent, D.V., Aubry, M.P., and Hardenbol, J. (eds) Geochronology, Time Scales and Global Stratigraphic Correlation. Society for Sedimentary Geology, Special Publication, 54, 129– 212.

Berggren, W.A., Olsson, R.K., Reyment, R.A., 1967. Origin and development of the foraminiferal genus Pseudohastigerina. Micropaleontology 13, 265–288.

Berggren, W.A., Pearson, P.N., 2005. A revised tropical to subtropical Paleogene planktonic foraminiferal zonation. Journal of Foraminiferal Research 35, 279–298.

Berggren, W.A., Pearson, P.N., 2006. Tropical to subtropical planktonic foraminiferal zonation of the eocene and oligocene. in: Pearson, P.N., Olsson, R.K., Huber, B.T. Hemleben, CH., Berggren, W.A. (eds) Atlas of Eocene planktonic foraminifera. Cushman Foundation Special Publication 41, 29–40.

Bernaola, G., Baceta, J.I., Orue–Extebarria, X., Alegret, L., Martin–Rubio, M., Arostegui, J., Dinarès–Turell, J., 2007. Evidence of an abrupt environmental disruption during the mid–Paleocene biotic event (Zumaia section, western Pyrenees). Geological Society of American Bulletin 119, 785–795.

Bernaola, G., Monechi, S., 2007. Calcareous nannofossil extinction and survivorship across the Cretaceous–Paleogene boundary at Walvis Ridge (ODP HOLE 1262C, South Atlantic Ocean). Palaeogeography, Palaeoclimatology, Palaeoecology 255, 132–156.

Bijl, P.K., Houben, A.J.P., Schouten, S., Bohaty, S.M., Sluijs, A., Reichart, G–J., Damsté, J.S.S., Brinckhuis, H., 2010. Transient middle Eocene atmospheric CO_2 and temperature variations. Science 330, 819–821.

Billups, K., Pälike, H., Channell, J.E.T., Zachos, J.C., Shackleton, N.J., 2004. Astronomic calibration of the late Oligocene through early Miocene geomagnetic polarity time scale. Earth and Planetary Science Letters 224, 33–44.

Blow, W.H., 1979. The Cainozoic Globigerinida. A study of the morphology, taxonomy, evolutionary relationships and the stratigraphical distribution of some of the Globigerinida (mainly Globigerinacae). Leiden, E. J. Brill, 3, 1413.

Blow, W.H., Banner, F.T., 1962. The mid–Tertiary (upper Eocene to Aquitanian) Globigerinacae, in Eames, F.T., and others, (eds.), Fundamentals of mid–Tertiary stratigraphical correlation. London, Cambridge University Press, 61–151.

Bodiselitsch, B., Montanari, A., Koeberl, C., Coccioni, R., 2004. Delayed climate cooling in the late Eocene caused by multiple impacts: High resolution geochemical studies at Massignano, Italy. Earth and Planetary Science Letters 223, 283–302.

Boersma, A., Premoli Silva, I., 1991. Distribution of Palaeogene planktonic foraminifera: Analogies with the recent?: Palaeogeography, Palaeoclimatology, Palaeoecology 83, 29–48.

Boersma, A., Premoli Silva, I., Shackleton, N.J.,

1987. Atlantic Eocene planktonic foraminiferal paleohydrographic indicators and stable isotope Paleoceanography. Paleoceanography 2, 287–331.

Bohaty, S.M., Zachos, J.C., 2003. Significant Southern Ocean warming event in the late middle Eocene. Geology 31, 1017–1020.

Bohaty S.M., Zachos J.C., Florindo F., Delaney, M.L., 2009. Coupled greenhouse warming and deep–sea acidifications in the middle Eocene. Paleoceanography 24, PA2207.

Bolli, H.M., Beckmann, J.–P., Saunders, J.B., 1994. Benthic foraminiferal biostratigraphy of the south Caribbean region. Cambridge University Press, UK.

Bolli, H.M, Loeblich, A.R., Jr., Tappan, H., 1957. Planktonic foraminiferal families Hnatkeninidae, Orbulinidae, Globorotaliidae, and Globotruncanidae. In: Loeblich, A.R., Jr., Tappan, H., Beckmann, J.P., Bolli, H.M., Montanari Gallitelli, E., Troelsen, J.C. (Eds.), Studies in Foraminifera. United States National Museum Bulletin 215, 3–50.

Bornemann, A., Schulte, P., Sprong, J., Steurbaut, E., Youssef, M., Speijer, R.P., 2009. Latest Danian carbon isotope anomaly and associated environmental change in the Southern Tethys (Nile Basin, Egypt). Journal of the Geological Society166, 135–1142.

Boscolo Galazzo, F., Giusberti, L., Luciani, L., 2011. Perturbation at the sea floor across the middle Eocene climatic optimum as recorded by benthic foraminifera in the Alano di Piave Section (bl, north–eastern Italy VIII Forum Italiano di Scienze della Terra, Sessione M1 "Micro– e meioorganismi come indicatori ambientali e paleoambientali", 21–23 Settembre, Torino, Epitome, 4, pag. 229.

Bosellini, A,. 1989. dynamics of tethyan carbonate platforms. in: Crevello, P., Wilson, J.L., Sarg, R., Reed, R., (eds) controls of carbonate platform and basin development. Society for Sedimentary Seology, Special Publication 44, 3–14.

Bowen, G.J., Beerling, D.J., Koch, P.L., Zachos, J.C., Quattlebaum, T., 2004. A humid climate state during the Palaeocene/Eocene thermal maximum. Nature 432, 495–499.

Bralower, T.J., 2002. Evidence of surface water oligotrophy during the Paleocene–Eocene thermal maximum: Nannofossil assemblage data from Ocean Drilling Program Site 690, Maud Rise: Weddell Sea. Paleoceanography 17, 1023.

Bralower, T.J., Mutterlose, J., 1995. Calcareous nannofossil biostratigraphy of Site 865, Allison Guyot, Central Pacific Ocean: a tropical Paleogene reference section, in Winterer, E.L., Sager, W.W., Firth, J.V., Sinton, J.M. (eds.), Proceeding of Ocean Drilling Project, Scientific Results 143, College Station, TX (Ocean Drilling Program), 31–74.

Bralower, T.J., Premoli Silva, I., and Malone, M.J. 2002. New evidence for abrupt climate change in the Cretaceous and Paleogene. An Ocean Drilling Program expedition to Shatsky Rise, northwest Pacific. Geological Society of America Today, 12, 4–10.

Bralower, T.J., Premoli Silva, I., Malone, M.J., 2006. Leg 198 synthesis: A remarkable 120–m.y. record of climate and oceanography from Shatsky Rise, northwest Pacific Ocean. In: Bralower, T.J., Premoli Silva, I., and Malone, M.J. (Eds.), Proceeding of Ocean Drilling Project, Scientific Results 198, 1–47.

Bralower, T.J., Röhl, U., Petrizzo, M.R., Zachos, J., Premoli–Silva, I., and Thomas, D., 2003, Constraining the controls on carbonate accumulation in deep sea sequences: A global dissolution event in the early late Paleocene: Geological Society of America, Abstracts with Programs 35, 205.

Brinkhuis, H., Biffi, U., 1993. Dinoflagellate cyst stratigraphy of the Eocene/Oligocene transition in central Italy. Marine Micropaleontology 22, 131–183.

Broecker, W.S., and Clark, E. 1999. $CaCO_3$ size distribution: a paleocarbonate ion proxy? Paleoceanography 14, 596–604.

Broecker, W.S., and Clark, E. 2001. Re–evaluation of the CaCO3 size index paleocarbonate ion proxy. Paleoceanography 16, 669–671.

Brönnimann, P., 1950. The genus Hantkenina Cushman in Trinidad and Barbados, B.W.I. Journal of Paleontology 24, 397–420.

Brown, R.E., Koeberl, C., Montanari, A., Bice D.M., 2009. Evidence for a change in Milankovitch forcing caused by extraterrestrial events at Massignano, Italy, Eocene–Oligocene boundary GSSP, in: Koeberl, C., Montanari, A. (eds) the late Eocene earth–hothouse, icehouse, and impacts. Geological Society of America Special Paper 452, 1–19.

Caldeira, K., Rampino, M.R., 1990. Carbon dioxide emissions from Deccan volcanism and K/T boundary greenhouse effect. Geophysical Research Letters 17, 1299–1302.

Carpenter, W.B., Parker, W.K., Jones, T.R., 1862. Introduction to the study of foraminifera. Ray Society, London, 319.

Centamore, E., Chiocchini, M., Jacobacci, A., Manfredini, M., Manganelli, P., 1980. The evolution

of the umbrian–marchean basin in the Apennine section of the alpine orogenic belt (central Italy), in: Cogne, J., Slansky, M., (eds) Memoire du bureau de recherches geologiques et minieres 108, 289–305.

Channell, J.E.T., D'argenio, B.,. Horwath, F., 1979. Adria, the african promontory, in mesozoic mediterranean palaeogeography. Earth Science Review 15, 213–292.

Chenet, A.L., Courtillot, V., Fluteau, F., Gérard, M., Quidelleur, X., Khadri, S.F.R., Subbarao, K.V., Thordarson, T., 2009. Determination of rapid Deccan eruptions across the Cretaceous–Tertiary boundary using paleomagnetic secular variation: 2. Constraints from analysis of eight new sections and synthesis for a 3500–m–thick composite section. Journal of Geophysical Research 114, 1–38.

Chenet, A.L., Quidelleur, X., Fluteau, F., Courtillot, V., Bajpai, S., 2007. ^{40}K–^{40}Ar dating of the Main Deccan large igneous province: Further evidence of KTB age and short duration. Earth and Planetary Science Letters 263, 1–15.

Coccioni R. 1996. The Cretaceous of the Umbria–Marche Apennines (Central Italy), in: Wiedmann J., (ed) Symposium "Cretaceous Stratigraphy, Paleobiology and Paleobiogeography", Tübingen, 7–10 March, 129–136.

Coccioni, R., Galeotti, S., 2003. Deep–water benthic foraminiferal events from the Massignano Eocene/Oligocene boundary stratotype section and point (central Italy): biostratigraphic, paleoecologic, and paleoceanographic implications, in: Prothero, D.R., Ivant, I.C., Nesbitt, E., (eds) From greenhouse to icehouse: the marine Eocene–Oligocene transition. New York, Columbia University press, 438–452.

Coccioni, R., Luciani, V., 2004. Planktonic foraminifera and environmental changes across the Bonarelli Event (OAE2, latest Cenomanian) in its type area: a high–resolution study from the Tethyan reference Bottaccione section (Gubbio, central Italy). Journal of Foraminiferal Research 34, 109–129.

Coccioni, R., Angori, E., Catanzariti, R., Giusberti, L., Guasti, E., Luciani, V., Marsili, A., Monechi, S., Sprovieri, M., Tateo, F., 2006. The Early Paleogene hyperthermal events (EPHEs): new insights from the classical Tethyan Contessa road section (Gubbio, Italy). In: Caballero, F., Apellaniz, E., Baceta, J.I., Bernaola, G., Orue–Etxebarria, X., Payros, A., Pujalte, V. (Eds.), Climate and Biota of the Early Paleogene 2006, Bilbao, Volume of Abstracts 27.

Coccioni, R., Bancalà, G., Catanzariti, R., Fornaciari, E., Frontalini, F., Giusberti, L., Jovane, L., Luciani, V., Sideri, M., (submitted). Reassessment of the Paleogene integrated stratigraphy and chronology of the Umbria–Marche Basin (central Italy): paleoenvironmental, paleoceanographic and paleoclimatic implications. In: Jovane L. (ed) Special Publication of Geological Society of London "Magnetostratigraphy: Not only a dating tool".

Coccioni, R., Di Leo, R., Galeotti, S., Monechi, S., 1994. Integrated biostratigraphy and benthic foraminiferal faunal turnover across the Paleocene–Eocene boundary at Trabakua Pass section, Northern Spain. Paleopelagos 4, 87–100.

Coccioni, R., Franchi, R., Nesci, O., Wezel, F.C., Battistini, F., and Pallecchi, P., 1989. Stratigraphy and mineralogy of the Selli Level (Early Aptian) at the base of the Marne a Fucoidi in the Umbro–Marchean Apennines, Italy. In: Wiedmann J. (ed) Cretaceous of the Western Tethys. Proceedings 3rd International Cretaceous Symposium, Tübingen 1987,. E. Schweizerbart'sche Verlagsbuchhandlung, Stuttgart, 563–584.

Coccioni, R., Frontalini, F., Bancalà, G., Fornaciari, E., Jovane, L., Sprovieri, M., 2010. The Dan–C2 hyperthermal event at Gubbio (Italy): Global implications, environmental effects, and cause(s). Earth and Planetary Science Letters 297, 298–305.

Coccioni, R., Frontalini, F., Spezzaferri, S., 2009. Late Eocene impact–induced climate and hydrological changes: evidence from the Massignano global stratotype section and point (central Italy). Geological Society of America Special Paper 452, 97–118.

Coccioni, R., Galeotti, S., Gravili, M. 1995. Latest Albian–early Turonian deep–water agglutinated foraminifera in the Bottaccione section (Gubbio, Italy)–Biostratigraphic and palaeoecology implications. Revista Espanola de Paleontologia, Numero Homenaje Al Dr. Guillermo Colom 1, 135–152.

Coccioni, R., Luciani, V., Marsili, A., 2006. Cretaceous oceanic anoxic events and radially elongated chambered planktonic foraminifera: Paleoecological and paleoceanographic implications. Palaeogeograhy, Palaeoclimatology, Palaeoecology 235, 66−92.

Coccioni, R., Marsili, A., Montanari, A., Bellanca, A., Neri, R., Bice, D.M., Brinkhuis, H., Church, N., Macalady, A., McDaniel, A., Deino, A., Lirer, F., Sprovieri, M., Maiorano, P., Monechi, S., Nini, C., Nocchi, M., Pross, J., Rochette, P., Sagnotti,

L., Tateo, F., Touchard, Y., Van Simaeys, S., Williams, G.L., 2008. Integrated stratigraphy of the Oligocene pelagic sequence in the Umbria–Marche basin (northeastern Apennines, Italy): a potential Global Stratotype Section and Point (GSSP) for the Rupelian/Chattian boundary. Geological Society of American Bulletin 120, 487–511.

Coccioni, R., Monaco, P., Monechi, S., Nocchi, M., Parisi, G., 1986. the Eocene/Oligocene boundary at Massignano (Ancona, Italy): biostratigraphy based on calcareous nannofossils and planktonic foraminifera. bulletin of liaison and information, international geological correlation program project 196, 6, 37–44.

Coccioni, R., Monaco, P., Monechi, S., Nocchi, M., Parisi, G., 1988. biostratigraphy of the eocene/oligocene boundary at massignano (ancona, italy). in: Premoli Silva, I., Coccioni, R., Montanari, A., (eds) the eocene–oligocene boundary in the marche–umbria basin (italy). international subcommission on paleogene stratigraphy Special Publication, industrie grafiche fratelli Aniballi, Ancona, 59–80.

Colosimo, A.B., Bralower, T.J., and Zachos, J.C., 2006. Evidence of lysocline shoaling at the Paleocene/Eocene Thermal Maximum on Shatsky Rise, northwest Pacific. In: Bralower, T.J., et al. (eds) Proceedings of the Ocean Drilling Program, Scientific Results, 198, College Station, Texas, 1–36.

Corfield, R.M., Cartlidge, J.E., Premoli–Silva, I., and Housley, R.A., 1991. Oxygen and carbon isotope stratigraphy of the Palaeogene and Cretaceous limestones on the Bottaccione Gorge and the Contessa Highway sections, Umbria, Italy. Terra Nova 3, 414–422.

Corliss, B.H., 1985. Microhabitats of benthic foraminifera within deep–sea sediments. Nature 314, 435–438.

Coxall, H.K., D'Hondt, S., Zachos, J.C., 2006. Pelagic evolution and environmental recovery after the Cretaceous–Paleogene mass extinction. Geology 34, 297–300.

Coxall, H.K., Huber, B.T., Pearson, P.N., 2003. Origin and morphology of the Eocene planktonic foraminifer *Hantkenina*. Journal of Foraminiferal Research 33, 237−261.

Coxall, H.K., Pearson, P.N., 2006. Taxonomy, biostratigraphy, and phylogeny of the Hantkeninidae (Clavigerinella, Hantkenina, and Cribrohantkenina). In: Pearson, P.N., Olsson, R.K., Huber, B.T., and Hemleben, Ch., (Eds.), Atlas of Eocene planktonic foraminifera. Cushman Foundation Special Publication 41, 213–256.

Coxall, H.K., Wilson, P.A., Pälike, H., Lear, C.H., and Backman, J., 2005, Rapid stepwise onset of Antarctic glaciation and deeper calcite compensation in the Pacific Ocean. Nature 433, 53–57.

Coxall, H.K., Wilson, P.A., Pearson, P.N., Sexton, P.F., 2007. Iterative evolution of digitate planktonic foraminifera. Paleobiology 33, 495−516.

Cramer, B.S., Wright, J.D., Kent, D.V., Aubry, M.−P., 2003, Orbital climate forcing of δ13C excursions in the late Paleocene–early Eocene (chrons C24n−C25n). Paleoceanography 18, PA1097.

Cresta, S., Monechi, S., Parisi, G., 1989. Mesozoic−Cenozoic stratigraphy in the Umbria−Marche area: Geological field trips in the Umbria−Marche Apennines (Italy). Memorie Descrittive della Carta Geologica d'Italia 39, 1–185.

Crouch, E.M., Heilmann–Clausen, C., Brinkhuis, H., Hugh E.G., Morgans, H.E.G., Rogers, K.M., Hans Egger, H., Schmitz, B., 2001. Global dinoflagellate event associated with the late Paleocene thermal maximum. Geology 29, 315–318.

Crowley, T.J., Kim, K.Y., Mengel, J.G., Short, D.A., 1992. Modeling 100,000–year climate fluctuations in pre–pleistocene time series. Science 255, 705–707.

Cushman, J.A., 1924. A new genus of Eocene Foraminifera. Proceedings of the United States National Museum 66, 1–4.

Cushman, J.A., 1933. Foraminifera, their classification and economic use. Special Publications of the Cushman Laboratory of Foraminiferal Research 2nd edition.

Cushman, J.A., Wickenden, R.T., 1930. The development of Hantkenina in the Cretaceous with a description of a new species. Contributions from the Cushman Laboratory of Foraminiferal Research 6, 39–43.

Delage, Y., Hérouard, E., 1896. Traité de Zoologie Concrète 1, La Cellule et les Protozoaires. Paris: Schleicher Frères.

D'Hondt, S., Keller, G., 1991. Some patterns of planktic foraminiferal assemblage turnover at the Cretaceous–Tertiary boundary. Marine Micropaleontology 17, 77–118.

D'Hondt, S., King, J., Gibson, C., 1996. Oscillarity marine response to the Cretaceous–Tertiary impact. Geology 24, 611–614.

Dickens, G.R., 2000. Methane oxidation during the Late Palaeocene Thermal Maximum. Bulletin de la

Société Géologique de France 171, 37–49.
Dickens, G.R., 2001. The potential volume of oceanic methane hydrates with variable external conditions. Organic Geochemistry 32, 1179–1193.
Dickens, G.R., 2003. Rethinking the global carbon cycle with a large, dynamicand microbially mediated gas hydrate capacitor. Earth and Planetary Science Letters 213, 169–183.
Dickens, G.R., 2011. Methane release from gas hydrate systems during the Paleocene–Eocene thermal maximum and other past hyperthermal events: Setting appropriate parameters for discussion. Climate of the Past Discussions 7, 1139–1174.
Dickens, G.R., Castillo, M.M., Walker, J.C.G., 1997. A blast of gas in the latest Paleocene: simulating first–order effects of massive dissociation of oceanic methane hydrate. Geology 25, 259–262.
Dickens, G.R., O'Neil, J.R., Rea, D.K., Owen, R.M., 1995. Dissociation of oceanic methane hydrate as a cause of the carbon isotope excursion at the end of the Paleocene. Paleoceanography 10, 965–971.
Dickens, G.R., O'Neill, J.R., Rea, D.K., Owen, R.M., 2005. Dissociation of oceanic methane hydrate as a cause of the carbon isotope excursion at the end of the Paleocene. Paleoceanography 10, 965–971.
Dieni, I., Proto Decima, F.P., 1964. Cribrohantkenina ed atri Hantkeninidae nell'Eocene superiore di Castelnuovo (Colli Euganei). Rivista Italiana di Paleontologia e Stratigrafia 70, 555–592.
Diester–Haass, L., Zahn, R., 1996. Eocene–Oligocene transition in the Southern Ocean: History of water mass circulation and biological productivity. Geology 24, 263–266.
Dinarès–Turell, J., Baceta, J.I., Bernaola, G., Orue–Etxebarria, X., Pujalte, V., 2007. Closing the Mid–Palaeocene gap: toward a complete astronomically tuned Palaeocene Epoch and Selandian and Thanetian GSSPs at Zumaia (Basque Basin, W Pyrenees). Earth and Planetary Science Letters 262, 450–467.
Dinarès–Turell, J., Baceta, J.I., Pujalte,V., Orue–Extebarria, X., Bernaola, G., Lorito, S., 2003. Untangling the Palaeocene climatic rhythm: an astronomically calibrated Early Palaeocene magnetostratigraphy and biostratigraphy at Zumaia (Basque basin, northern Spain). Earth and Planetary Science Letters 216, 483–500.
Dinarès–Turell, J., Stoykova, K. Baceta, J.I., Ivanov, M., Pujalte, V., 2010. High–resolution intra– and interbasinal correlation of the Danian–Selandian transition (Early Paleocene): The Bjala section (Bulgaria) and the Selandian GSSP at Zumaia (Spain). Palaeogeography, Palaeoclimatology, Palaeoecology 297, 511–533.
Duff, P.M.D., 1987. Mesozoic and Tertiary coals: A major world energy resource. Modern Geology 11, 29–50, 1987.
Duncan, R.A., Backmann, J., Peterson, L.C., and others (eds.), Proceedings of the Ocean Drilling P roject, Scientific Results 115, College Station TX, (Ocean Drilling Program), 227–314.
Dupont–Nivet, G., Krijgsman, W., Langereis, C.G., Abels, H.A., Dai, S., Fang, X., 2007. Tibetan Plateau aridification linked to global cooling at the Eocene–Oligocene transition. Nature 445, 635–638.
Edgar, K.M., Wilson, P.A., Sexton, P.F. & Suganuma, Y., 2007. No extreme bipolar glaciation during the main Eocene calcite compensation shift. Nature 448, 908–911.
Eichwald, E. Von., 1830. Zooologica Specialis 2, Vilna, 323.
Ellis, M.S., Gunther, G.L., Ochs, A.M., Roberts, S.B., Wilde, E.M., Schuenemeyer, J.H., Power, H.C., Stricker, G.D., Blake, D., 1999. Coal resources, Powder River basin, U.S. Geological Survey Professional Paper 1625–A, 32.
Erwin, D.H., 2001. Lessons from the past: biotic recoveries from mass extinctions. Proceeding of the National Academy Sciences of the United States of America 98, 5399–5403.
Fischer, A., Arthur, M.A, 1977. Secular variations in the pelagic realm, in Cook, H.E., Enos, P., (eds), Deep water carbonate environments. Society for Sedimentary Geology Special Publication 25, 19–50.
Fornaciari, E., Giusberti, L., Luciani, V., Tateo, F., Agnini, C., Backman, J., Oddone, M., Rio, D., 2007. An expanded Cretaceous–Tertiary transition in a pelagic setting of the Southern Alps (central–western Tethys). Palaeogeography, Palaeoclimatology, Palaeoecology 255, 98–131.
Frakes, L.A, Kemp, E.M, 1972. Influence of continental positions on early Tertiary climates. Nature 240, 97–100.
France–Lanord C., Derry L.A., 1997. Organic carbon burial forcing of the carbon cycle from Himalayan erosion. Nature 390, 65–75.
Galbrun, B., Gardin, S., 2004. New chronostratigraphy of the Cretaceous–Paleogene boundary interval at Bidart (France). Earth and Planetary Science Letters 224, 19–32.
Galeotti, S., Angori, E., Coccioni, R., Ferrari, G.,

Galbrun, B., Monechi, S., Premoli Silva, I., Speijer, R., Turi, B., 2000. Integrated stratigraphy across the Paleocene/Eocene boundary in the Contessa Road section, Gubbio (central Italy). Bulletin de la Société Géologique de France 171, 355–365.

Galeotti, S., Kaminski, M.A., Coccioni, R., Speijer, R., 2004. High resolution deep water agglutinated foraminiferal record across the Paleocene/Eocene transition in the Contessa Road Section (central Italy). In: Bubik, M., Kaminski, M.A. (Eds.), Proceedings of the Sixth International Workshop on Agglutinated Foraminifera. Grzybowski Foundation Special Publication, 8, 83–103.

Galeotti, S., Krishnan, S., Pagani, M., Lanci, L., Gaudio, A., Zachos, J.C., Monechi, S., Morelli, G., Lourens, L., 2010. Orbital Chronology of Early Eocene hyperthermals from the Contessa Road section, central Italy. Earth and Planetary Science Letters. 290, 192–200.

Gardin, S., Monechi, S., 1998. Palaeoecological change in middle to low latitude calcareous nannoplankton at the Cretaceous/Tertiary Bulletin de la Société Géologique de France 169, 709–723.

Gibbs, S.J., Bralower, T.J., Bown, P.R., Zachos, J.C., and Bybell, L. 2006. Shelf–open ocean calcareous phytoplankton assemblages across the Paleocene–Eocene Thermal Maximum: implications for global productivity gradients. Geology, 34, 233–236.

Gibbs, S.J., Stoll, H.M., Bown, P.R., Bralower, T.J., 2010. Ocean acidification and surface water carbonate production across the Paleocene–Eocene thermal maximum. Earth and Planetary Science Letters 295, 583–592.

Giusberti, L., Coccioni, R., Sprovieri, M., Tateo, F., 2009. Perturbation at the sea floor during the Paleocene–Eocene Thermal Maximum: Evidence from benthic foraminifera at Contessa Road, Italy. Marine Micropaleontology 70, 102–119.

Giusberti, L., Rio, D., Agnini, C., Backman, J., Fornaciari, E., Tateo, E., Oddone, M., 2007. Mode and tempo of the Paleocene–Eocene thermal maximum in an expanded section from the Venetian pre–Alps. Geological Society of American Bulletin 119, 391–412.

Gradstein, F.M., Ogg, J.G., Smith, A.G., 2004. A Geologic Time Scale 2004. Cambridge University Press, UK.

Hambrey, M.J., Ehrmann, W.U., Larsen, B., 1991. Cenozoic glacial record of the Prydz Bay continental shelf, East Antarctica. In Barron, J., Larsen, B., et al., Proceeding Ocean Drilling Project, Scientific Results 119, College Station, TX (Ocean Drilling Program), 77–132.

Hancock, H.J.L., and Dickens, G.R., 2005. Carbonate dissolution episodes in Paleocene and Eocene sediment, Shatsky Rise, West–Central Pacific. Proceedings of the Ocean Drilling Program, Scientific Results, College Station, Texas, 198, 1–58.

Handley, L., Crouch E.M., Pancost, R.D., 2011. A New Zealand record of sea level rise and environmental change during the Paleocene–Eocene Thermal Maximum. Palaeogeography, Palaeoclimatology, Palaeoecology 305, 185–200.

Haq, B.U., Hardenbol, J., Veil, P.U., 1987. Chronology of fluctuating sea levels since the Triassic. Science 235, 1156–1166.

Haq, B.U., Lohmann, G.P., 1976. Early Cenozoic calcareous nannoplankton biogeography of the Atlantic Ocean. Marine Micropaleontology 1, 119–194.

Harding, I.C., Charles, A.J., Marshall, J.E.A., Pälike, H., Roberts, A.P., Wilson, P.A., Jarvis, E. Thorne, R., Morris, E., Moremon, R., Pearce, R. B., Akbari, S., 2011. Sea–level and salinity fluctuations during the Paleocene–Eocene thermal maximum in Arctic Spitsbergen. Earth and Planetary Science Letters 303, 97–107.

Hay, W.W., DeConto, R., Wold, C.N., Wilson, K.M., Voigt, S., Schulz, M., Wold–Rossby, A., Dullo, W.–C., Ronov, A.B., Balukhovsky, A.N., Soeding E., 1999. Alternative global cretaceous paleogeography, in Barrera, E., Johnson, C., (eds.), The Evolution of Cretaceous Ocean/Climate Systems. Geological Society of America Special Paper 332, 1–47.

Herguera, J.C., Berger, W.H., 1991. Paleoproductivity from benthic foraminifera abundance: glacial to postglacial change in the west–equatorial Pacific. Geology 19, 1173–1176.

Higgins, J.A., Schrag, D.P., 2006. Beyond methane: Towards a theory for Paleocene–Eocene Thermal Maximum. Earth and Planetary Science Letters 245, 523–537.

Hilgen, F.J., Kuiper, K.F., Lourens, L.J., 2010. Evaluation of the astronomical time scale for the Paleocene and earliest Eocene. Earth Planet. Sci. Lett. 300, 139–151.

Hodell D.A., Kamenov, G.D., Hathorne, E.C., Zachos, J.C., Röhl, U., Westerhold, T., 2007. Variations in the strontium isotope composition of seawater during the Paleocene and early Eocene from ODP Leg 208 (Walvis Ridge). Geochemistry,

Geophysics, Geosystems 8, Q09001.

Hollis, C.J., Dickens, G.R., Field, B.D., Jones, C–M., Strong, C.P., 2005. The Paleocene–Eocene transition at Mead Stream, New Zealand: A southern Pacific record of early Cenozoic global change. Palaeogeography, Palaeoclimatology, Palaeoecology 215, 313–343.

Höntzsch, S., Scheibner , C., Guasti, E., Kuss , J., Marzouk , A.M., Rasser, M.V. 2011. Increasing restriction of the Egyptian shelf during the Early Eocene? — New insights from a southern Tethyan carbonate platform. Palaeogeography, Palaeoclimatology, Palaeoecology, 302, 349–366.

Huber, B.T., MacLeod, K.G., Norris, R.D., 2002. Abrupt extinction and subsequent reworking of Cretaceous–Tertiary boundary: evidence from the subtropical North Atlantic. In: Koeberl, C., MacLeod, K.G. (Eds.), Catastrophic Events and Mass extinctions: Impacts and Beyond. Geological Society of America Special Paper 356, 277–289. Boulder, Colorado.

Huber, M., Sloan, L.C., 2001. Heat transport, deep waters, and thermal gradients: Coupled simulation of an Eocene greenhouse climate. Geophysical Research Letters 28, 3481–3484.

Hyland, E., Murphy, B., Varela, P., Marks, K., Colwell, L., Tori, F., Monechi, S., Cleaveland, L., Brinkhuis, H., Van Mourik, C.A., Coccioni, R., Bice, D., Montanari, A., 2009. Integrated stratigraphy and astrochronologic calibration of the Eocene–Oligocene transition in the Monte Cagnero section (northeastern Apennines, Italy): a potential parastratotype for the MassignanoGSSP, in: Koeberl, C., Montanari, A., (eds) The late Eocene earth–hothouse, icehouse and impacts. Geological Society of America, Special Paper 452, 303–322.

Ingram, B.L., Coccioni, R., Montanari, A., Richter, F.M., 1994. Strontium Isotopic Composition of Mid–Cretaceous Seawater. Science, 264, 546–550.

Jahren, A.H., 2007. The Arctic forest of the middle Eocene. Annual Review of Earth and Planetary Sciences 35, 509–540.

Jorissen, F.J., De Stigter, H.C., and Widmark, J.G.V., 1995, A conceptual model explaining benthic foraminiferal microhabitats. Marine Micropaleontology 26, 3–15.

Jovane, L., Coccioni, R., Marsili, A., Florindo, F., Acton, G., Sprovieri, M., 2009. The late Eocene greenhouse–icehouse transition: observations from the Massignano global stratotype section and point (GSSP), in Koeberl, C., Montanari, A., (eds) The late Eocene earth–hot house, ice house, and impacts. Geological Society of America, Special Paper 452, 149–168.

Jovane, L., Florindo, F., Coccioni, R., Dinarès–Turell. J., Marsili, A., Monechi, S., Roberts, A.P., Sprovieri, M. 2007a. The Middle Eocene climatic optimum event in the Contessa section, Umbria Apennines, Italy. Geological Society of American Bulletin, 119, 413–427.

Jovane, L., Florindo, F., Dinares–Turell, J., 2004. Environmental magnetic record of paleoclimate change from the Eocene–Oligocene stratotype section, Massignano, Italy. Geophysical Research Letters 31, L15601.

Jovane, L., Florindo, F., Sprovieri, M., Pälike, H., 2006. Astronomic calibration of the late Eocene/early Oligocene Massignano section (central Italy). Geochemistry, Geophysics, Geosystems 7, Q07012.

Jovane, L., Sprovieri, M., Coccioni, R., Florindo, F., Marsili, A., Laskar, J., 2010. Astronomical calibration of the middle Eocene Contessa Highway section (Gubbio, Italy). Earth and Planetary Science Letters 298, 77–88.

Jovane, L., Sprovieri, M., Florindo, F., Acton, G., Coccioni, R., Dall'antonia, B., Dinarès–turrell, J., 2007b. Eocene–Oligocene paleoceanographic changes in the stratotype section, Massignano, Italy: clues from rock magnetism and stable isotopes. Journal of Geophysical Research 112, b11101.

Kaminski, M.A., Gradstein, F.M., 2005. An Atlas of Paleogene Cosmopolitan Deep–Water Agglutinated Foraminifera. Grzybowski Foundation, Special Publication 10.

Keller, G., 1983, Palaeoclimatic analysis of middle Eocene through Oligocene planktic foraminiferal faunas. Palaeogeography, Palaeoclimatology, Palaeoecology 59, 882–903.

Keller, G., 1989. Extended Cretaceous/Tertiary boundary extinctions and delayed population change in planktonic foraminifera from Brazos River, Texas. Paleoceanography 4, 287–332.

Keller, G., Adatte, T., Gardin, S., Bartolini, A., Bajpai, S., 2008. Main Deccan volcanism phase ends near the K–T boundary: Evidence from the Krishna–Godavari Basin, SE India. Earth and Planetary Science Letters 268, 293–311.

Keller, G., Macleod, N., Barrera, E., 1992. Eocene–Oligocene faunal turnover in planktic foraminifera, and Antarctic glaciation, in Prothero, D.R., and Berggren, W.A., (eds), Eocene and Oligocene climatic and biotic evolution. Princeton, New

Jersey, Princeton University Press, 218–244.

Kelly, D.C., Bralower, T.J., Zachos, J.C., 1998. Evolutionary consequences of the latest Paleocene thermal maximum for tropical planktonic foraminifera. Palaeogeography, Palaeoclimatology, Palaeoecology 141, 139–161.

Kelly, D.C., Nielsen, T.M.J., McCarren, H.K., Zachos, J.C., and Röhl, U., 2010, Spatiotemporal patterns of carbonate sedimentation in the South Atlantic: Implications for carbon cycling during the Paleocene–Eocene thermal maximum: Palaeogeography, Palaeoclimatology, Palaeoecology 293, p. 30–40.

Kelly, D.C., Bralower, T.J., Zachos, J.C., Silva, I.P., Thomas, E., 1996. Rapid diversification of planktonic foraminifers in the tropical Pacific (ODP Site 865) during the Late Paleocene Thermal Maximum. Geology 24, 423–426.

Kelly, D.C., Zachos, J.C., Bralower, T.J., Schellenberg, S.A., 2005. Enhanced terrestrial weathering/runoff and surface ocean carbonate production during the recovery stages of the Paleocene–Eocene thermal maximum. Paleoceanography 20, 4023.

Kennett, J.P., 1977. Cenozoic evolution of Antarctic glaciations, the circum–Antarctic Ocean, and their impact on global Paleoceanography. Journal of Geophysical Resesearch 82, 3843–3860.

Kennett, J.P., and Stott, L.D., 1991, Abrupt deep−sea warming, palaeoceanographic changes and benthic extinctions at the end of the Palaeocene. Nature 353, 225–229.

Killops, S.D., Hollis, C.J., Morgans, H.E.G., Sutherland, R., Field, B.D., Leckie, D.A., 2000. Paleoceanographic significance of Late Paleocene dysaerobia at the shelf/slope break around New Zealand. Palaeogeography, Palaeoclimatology, Palaeoecology 156, 51–70.

Kirsty, M., Edgar, S.M., Bohaty, S.J., Gibbs, Wilson, P.A., 2011. Transient symbiont bleaching of planktonic foraminifera during the Middle Eocene Climatic Optimum. Berichte Geol. B.–A., 85 (ISSN 1017–8880)–CBEP 2011, Salzburg, June 5th – 8th, 69.

Kroon, D., Zachos, J.C., and Leg 208 Scientific Party, 2007. Leg 208 synthesis: Cenozoic climate cycles and excursions. Proceeding of Ocean Drilling Project, Scientific Results 208. College Station, TX, 1–55.

Kuhnt, W., 1990. Agglutinated foraminifera of western Mediterranean Upper Cretaceous pelagic limestones (Umbrian Apennines, Italy and Betic Cordillera, Southern Spain). Micropaleontology 36, 297–330.

Kuhnt, W., Kaminski, M.A., 1996. The response of benthic foraminifera to the K/T boundary Event: a review, in: Jardine, S., De Klasz, I., Debenay, J.P., (Eds.), Geologie de l'Afrique et de l'Atlantique Sud – Compte–rendu des colloques de geologie d'Angiers. Bulletin Du Centre De Recherches Elf Exploration Production Aquitaine, Memoir 16, 433–442.

Kurtz, A., Kump, L., Arthur, M., Zachos, J.C., Paytan, A., 2004. Early Cenozoic decoupling of the global carbon and sulfur cycles. Paleoceanography 18, 1090.

Kvenvolden, K.A. 1993. Gas hydrates: geological perspective and global change. Reviews of Geophysics 31, 173–187.

Larrasoaña, J.C., Gonzalvo, C., Molina, E., Monechi, S., Ortiz, S., Tori, F., Tosquella, J., 2008. Integrated magnetobiochronology of the Early/Middle Eocene transition at Agost (Spain): Implications for defining the Ypresian/Lutetian boundary stratotype. Lethaia 41, 395–415.

Lasaga, A.C., Berner, R.A., Ganels, R.M., 1985. An improved geochemical model of atmospheric CO_2 fluctuations over the past 100 million years, in Sundquist, E.T., Broecker, W.S., (eds), Natural variations in carbon dioxide and the carbon cycle. American Geophysical Union 32, 397–411.

Lawver, L.A., Gahagan, L.M., 2003. Evolution of Cenozoic seaways in the circum–Antarctic region. Palaeogeography, Palaeoclimatology, Palaeoecology 198, 11–37.

Lear, C.H., Bailey, T.R., Pearson, P.N., Coxall, H.K., Rosenthal, Y., 2008. Cooling and ice growth across the Eocene–Oligocene transition. Geology 36, 251–254.

Lear, C.H., Elderfield, H., Wilson, P.A., 2000. Cenozoic deep sea temperatures and global ice volumes from Mg/Ca in benthic foraminiferal calcite. Science 287, 269–272.

Leon–Rodriguez, L., Dickens, G.R. 2010. Constraints on ocean acidification associated with rapid and massive carbon injections: The early Paleogene record at ocean drilling program site 1215, equatorial Pacific Ocean. Palaeogeography, Palaeoclimatology, Palaeoecology 298, 409–420.

Lirer, F., 2000, A new technique for retrieving calcareous microfossils from lithified lime deposits. Micropaleontolog 46, 365–369.

Livermore, R., Hillenbrand, C.–D., Meredith, M.,

Eagles, G., 2007. Drake Passage and Cenozoic climate: An open and shut case? Geochemistry, Geophysics, Geosystems 8, Q01005.

Lourens, J.L., Sluijs, A., Kroon, D., Zachos, J.C., Thomas, E., Röhl, U., Bowles, J., and Raffi , I., 2005, Astronomical pacing of late Paleocene to early Eocene global warming events. Nature 435, 1083–1087.

Lowrie, W., Lanci, L., 1994. Magnetostratigraphy of Eocene–Oligocene boundary sections in Italy: no evidence for short subchrons within chrons 12r and 13r. Earth and Planetary Science Letters 126, 247–258.

Lowrie, W., Alvarez, W., Napoleone, G., Perch–Nielsen, K., Premoli Silva, I., Toumarkine, M. 1982. Paleogene magnetic stratigraphy in Umbrian pelagic carbonate rocks: The Contessa sections, Gubbio. Geological Society of American Bulletin, 93, 414–432.

Luciani, V., 2011. The record of muricate symbiont–bearing planktonic foraminifera from the subtropical odp site 1051 a (atlantic ocean) across the early eocene climatic optimum (EECO). VIII Forum Italiano di Scienze della Terra, Sessione M1 "Micro– e meioorganismi come indicatori ambientali e paleoambientali", 21–23 Settembre, Torino, Epitome 4, 230.

Luciani, V., Giusberti, L., Agnini C., Backman J., Fornaciari, E., Rio, D., 2007. The Paleocene–Eocene Thermal Maximum as recorded by Tethyan planktonic foraminifera in the Forada section (northern Italy). Marine Micropaleontology 64, 189–214.

Luciani, V., Giusberti, L., Agnini, C., Fornaciari, E., Rio, D., Spofforth, D.J., Pälike, H., 2010. Ecological and evolutionary response of Tethyan planktonic foraminifera to the middle Eocene climatic optimum (MECO) from the Alano section (NE Italy). Palaeogeography, Palaeoclimatolology, Palaeoecolology 292, 82–95.

Lunt, D.J. Ridgwell, A., Sluijs, A., Zachos, J., Hunter, S., Haywood, A., 2011. A model for orbital pacing of methane hydrate destabilization during the Palaeogene. Nature Geoscience 4,775–778.

Luterbacher, H.P., Premoli–Silva, I., 1964. Biostratigrafia del limite Cretaceo–Terziario nell'Appennino centrale. Rivista Italiana di Paleontologia e Stratigrafia 70, 67–128.

Martini, E. 1971, Standard Tertiary and Quaternary calcareous nannoplankton zonation In: Farinacci, A., (ed) Proceedings of the Second Planktonic Conference, Rome 1970, Rome, Tecnoscienza, 2, 739–785.

Mattias, P., Crocetti, G., Barrese, E., Montanari, A., Coccioni, R., Farabollini, B., Parisi, E., 1992. Caratteristiche mineralogiche e litostratigrafiche della sezione eo–oligocenica di Massignano (Ancona, Italia) comprendente il limite scaglia variegata–scaglia cinerea. Studi geologici Camerti 12, 93–103.

Mcgowran, B., 1986. Cainozoic oceanic and climatic events: the Indo–pacific foraminifera biostratigraphic record: Palaeoceanography, Palaeoclimatology, Palaeoecology 55, 247–256.

McGowran, B., 1989. Silica burp in the Eocene ocean. Geology 17, 857–860.

McGowran, B., 1990. Fifty million years ago: American Scientist 78, 30–39.

McInherney, F.A., Wing, S., 2011. A perturbation of carbon cycle, climate, and biosphere with implications for the future, Annual Review of Earth and Planetary Sciences 39, 489–516.

Meehl, G.A., Stocker, T.F., Collins, W.D., Friedlingstein, P., Gaye, A.T., Gregory, J.M., Kitoh, A., Knutti, R., Murphy, J.M., Noda, A., Raper, S.C.B., Watterson, I.G., Weaver, A.J., Zhao, Z.–C., 2007. Global Climate Projections. In Solomon, S., Qin, D., Manning, M., Chen, Z., Marquis, M., Averyt, K.B., Tignor, M., Miller, H.L., (Ees.), Climate Change 2007: The Physical Science Basis. Contribution of Working Group I to the Fourth Assessment Report of the Intergovernmental Panel on Climate Change. Cambridge University Press, Cambridge.

Milkov, A.V., 2005. Molecular and stable isotope compositions of natural gas hydrates: a revised global dataset and basic interpretations in the context of geological settings, Organic Geochemistry 36, 681–702.

Miller, K.G., Kominz, M.A., Browning, J.V., Wright, J.D., Mountain, G.S., Katz, M.E., Sugarman, P.J., Cramer, B.S., Christie–Blick, N., Pekar, S.F., 2005. The Phanerozoic record of global sea–level change. Science 310, 1293–1298.

Miller, K.G., Wright, J.D., Fairbanks, R.G., 1991. Unlocking the ice house: Oligocene–Miocene oxygen isotopes, eustasy, and margin erosion. Journal of Geophysical Research 96, 6829–6848.

Molina, E., Alegret, L., Apellaniz, E., Bernaola, G., Caballero, F., Dinarès–Turell, J., Hardenbol, J., Heilmann–Clausen, C., Larrasoaña, J.C., Luterbacher, H.P., Monechi, S., Ortiz, S., Orue–

Extebarria, X., Pairos, A., Pujalte, V., Rodríguez–Tovar, F.J., Tori, F., Tosquella, J., Uchman, A., 2011, The Global Stratotype Section and Point (GSSP) for the base of the Lutetian Stage at the Gorrondatxe section, Spain. Episodes 34, 86–108.

Molina, E., Arenillas, J., Arz, J.A., 1996. The Cretaceous/Tertiary boundary mass extinction in planktic Foraminifera at Agost, Spain. Revue de Micropaléontologie 39, 225–243.

Monaco, P., Nocchi, M. Parisi, G., 1987. Analisi stratigrafica e sedimentologica di alcune sequenze pelagiche dell'Umbria sud–orientale dall'Eocene inferiore all'Oligocene inferiore. Bollettino della Società Geologica italiana 106, 71–91.

Montanari, A., Carey, S., Coccioni, R., Deino, A., 1994. Early Miocene tephra in the Apennine pelagic sequence: an inferred sardinian provenance and implications for western mediterranean tectonics. Tectonics 13, 1120–1134.

Montanari, A., Drake, R., Bice, D.M., Alvarez, W., Curtis, G.H., Turrin, B.T., DePaolo, D.J., 1985. Radiometric time scale for the upper Eocene and Oligocene based on K–Ar and Rb–Sr dating of volcanic biotites from the pelagic sequence of Gubbio, Italy. Geology 13, 596–599.

Montanari, A., Koeberl, C., 2000. Impact Stratigraphy: The Italian Record (Lecture notes in Earth Science, 93). Berlin, Springer.

Montanari, A., Odin, G.S., Coccioni, R., (eds) 1997. Miocene Stratigraphy–An Integrated Approach. Developments in Palaeontology and Stratigraphy, Elsevier Science, 15, 694.

Moran, K., Backman, J., Brinkhuis, H., Clemens, S.C., Cronin, T., Dickens, G.R., Eynaud, F., Gattacceca, J., Jakobsson, M., Jordan, R.W., Kaminski, M., King, J., Koc, N., Krylov, A., Martinez, N., Matthiessen, J., McInroy, D., Moore, T. C., Onodera, J., O'Regan, M., Pälike, H., Rea, B., Rio, D., Sakamoto, T., Smith, D. C., Stein, R., St. John, K., Suto, I., Suzuki, N., Takahashi, K., Watanabe, M., Yamamoto, M., Farrell, J., Frank, M., Kubik, P., Jokat, W., Kristoffersen, Y., 2006. The Cenozoic palaeoenvironment of the Arctic Ocean. Nature 441, 601–605.

Morrill, C., Small, E.E., Sloan, L.C., 2001. Modeling orbital forcing of lake level change: Lake Gosiute (Eocene), North America. Global and Planetary Change 29, 57–76.

Musavu–Moussavou, B., Danielan, T., Baudin, F., Coccioni, R., Fröhlich, F. 2007. The Radiolarian biotic response during OAE2. A high–resolution study across the Bonarelli level at Bottaccione (Gubbio, Italy). Reveu de micropaléontologie, 50, 253–287.

Nagy, J., 2005. Delta–influenced foraminiferal facies and sequence stratigraphy of Paleocene deposits in Spitsbergen. Palaeogeograpy, Palaeoclimatology, Palaeoecology 222, 161–179.

Nicolo, M.J., Dickens, G.R., Hollis, C.J., Zachos, J.C. 2007. Multiple early Eocene hyperthermals: Their sedimentary expression on the New Zealand continental margin and in the deep sea. Geology, 35, 699–702.

Nordt, L., Atchley, S., Dworkin, S., 2003. Terrestrial Evidence for Two Greenhouse Events in the Latest Cretaceous. Geological Society of America Today 13, 4–9.

Norris, R.D., Huber, B.T., Self–Trail, J., 1999. Synchroneity of the K–T oceanic mass extinction and meteorite impact: Black Nose, western North Atlantic. Geology 27, 419–422.

Norris, R.D., Kroon, D., Huber, B.T., Erbacher, J., 2001. Cretaceous–Palaeogene ocean and climate in the subtropical North Atlantic. In: Kroon, D., Norris, R.D., Klaus, A. (Eds.), Western North Atlantic Palaeogene and Cretaceous Palaeoceanography. Geological Society of London Special Publication 183, 1–22.

Norris, R.D., Kroon, D., Klaus, A., and others, 1998. Site 1049 Shipboard Scientific Party. Proc. ODP, Initial Rep., 171B, College Station, TX, 47–91

Nuttall, W.L.F., 1928. Notes on the Tertiary Foraminifera of southern Mexico. Journal of Paleontology 2, 372–376.

Ogg, J.G., Bardot, L., 2001. Aptian through Eocene magnetostratigraphic correlation of the Blake Nose transect (Leg 171B), Florida continental margin. Proceeding Ocean Drilling Program, Scientific Results 171B, 1–58.

Ogg, J., Lugowski, A., 2009. TSCreator visualization of enhanced Geologic Time Scale 2004 database (Version 4.2; 2009) http://www.tscreator.org.

Ogg, J.G., Ogg, G., Gradstein, F.M., 2008. The Concise Geologic Time Scale. Cambridge University Press, UK.

Ogg, J.G., Smith, A.G., 2004. The geomagnetic polarity time scale, in A Geological Timescale 2004, F., Ogg, J., Smith, A., (eds), Cambridge Univ. Press, Cambridge, U.K., 63–86.

Okada, H., Bukry, D., 1980, Supplementary modification and introduction of code numbers to the low−latitude coccolith biostratigraphy zonation

(Bukry, 1973; 1975). Marine Micropaleontology 5, 321–325.

Olsson, R.K., Hemleben, Ch., Berggren, W.A., Liu, C., 1992. Atlas of Paleogene Planktonic Foraminifera. Smithsonian Contributions to Paleobiology 85, 252 p.

Olsson, R.K., Pearson, P.N., Huber, B.T., 2006. Taxonomy, biostratigraphy, and phylogeny of Eocene *Catapsydrax*, *Globorotaloides*, *Guembelitrioides*, *Paragloboralia*, *Parasubbotina*, *and Pseudoglobigerinella* n. gen, in: Pearson, P.N., Olsson, R.K., Huber, B.T., Hemleben, Ch., (Eds.), Atlas of Eocene planktonic foraminifera. Cushman Foundation Special Publication 41, 67–110.

Olsson, R.K., Wise, S.W., 1987,. Upper Paleocene to middle Eocene depositional sequences and hiatuses in the New Jersey Atlantic margin, in Ross, C.A. Haman, D., (eds.), Timing and depositional history of eustatic sequences: constraints on seismic stratigraphy, Washington, D.C. Cushman Foundation for Foraminiferal Research 24, 99–112.

Ortiz, S., Gonzalvo, C., Molina, E., Rodríguez–Tovar, F.J., Uchman, A., Vandemberghe, N., Zeelmaekers, E., 2008. Palaeoenvironmental turnover across the Ypresian–Lutetian transition at the Agost section, southeastern Spain: in search of amarker event to define the Stratotype for the base of the Lutetian Stage. Marine Micropaleontology, 69, 297–313.

Ortiz, S., Thomas, E., 2006. Lower–middle Eocene benthic foraminifera from the Fortuna Section (Betic Cordillera, southeastern Spain). Micropaleontology 52, 97–150.

Owen, R.M., Rea, D.K., 1985. Sea floor hydrothermal activity links climate to tectonics: the Eocene Greenhouse. Science 227, 166–169.

Pagani, M., Caldeira, K., Archer, D., Zachos, J.C., 2006b. An ancient carbon mystery. Science 314, 1556–1557.

Pagani, M., Pedentchouk, N., Huber, M., Sluijs, A., Schouten, S., Brinkhuis, H., Sinninghe, J.S., Damsté, Dickens, G.R., and the Expedition 302 Scientists, 2006a. Arctic hydrology during global warming at the Paleocene/Eocene thermal maximum. Nature 442, 671–675.

Pagani, M., Zachos, J., Freeman, K. H., Bohaty, S., Tipple, B., 2005. Marked change in atmospheric carbon dioxide concentrations during the Oligocene. Science 309, 600–603.

Page, S.E., Rieley, J.O., Banks C.J., 2011. Global and regional importance of the tropical peatland carbon pool. Global Change Biology 17, 798–818.

Pälike, H., Norris, R.D., Herrle, J.O., Wilson, P.A., Coxall, H.K., Lear, C.H., Shackleton, N.J., Tripati, A.K., Wade, B.S., 2006. The Heartbeat of the Oligocene Climate System. Science 314, 1894–1898.

Panchuk, K., Ridgwell, A., Kump, L.R., 2008. Sedimentary response to Paleocene–Eocene thermal maximum carbon release: A model–data comparison. Geology 36, 315–318.

Pardo, A., Keller, G., 2008. Biotic effects of environmental catastrophes at the end of the Cretaceous and early Tertiary: *Guembelitria* and *Heterohelix* blooms. Cretaceous Research 29, 1058–1073.

Payros, A., Bernaola, G., Orue–Etxebarria, X., Dinarès–Turell, J., Tosquella, J., Apellaniz, E., 2007. Reassessment of the early–middle Eocene biomagnetochronology based on evidence from the Gorrondatxe section (Basque Country, western Pyrenees). Lethaia 40, 183–195.

Payros, A., Tosquella, J., Bernaola, G., Dinarés–Turell, J., Orue–Etxebarria, X., Pujalte, V., 2009. Filling the North European Early/Middle Eocene (Ypresian/Lutetian) boundary gap: insights from the Pyrenean continental to deep–marine record. Palaeogeography, Palaeoclimatology, Palaeoecology 280, 313–332.

Pearson, P.N., 1993. A lineage phylogeny for the Paleocene planktonic foraminifera: Micropaleontology 39, 193–232.

Pearson, P.N., 1996. Cladogenetic, extinction, and survivorship patterns from a lineage phylogeny: Paleogene planktonic foraminifera: Micropaleontology 42, 179–188.

Pearson, P.N., Palmer, M.R., 2000. Atmospheric carbon dioxide over the past 60 million years. Nature 406, 695–699.

Pearson, P.N., Chaisson, W.P., 1997, Late Paleocene to middle Miocene planktonic foraminifer biostratigraphy In: Miller, C.M., Riegel, R.N., et al. (Eds.), Proceedings of the Ocean Drilling Program, Scientific results 154. College Station, Texas, Ocean Drilling Program, 33–68.

Pearson, P.N., Nicholas, C.J., Singano J.M., Bown P.R., Coxall H.K., Van Dongen, B.E., Huber B.T., Karega A., Lees J.A., Msaky, E., Pancost, R.D., Pearson, M., Roberts, A.P., 2004. Paleogene and Cretaceous sediment cores from the Kilwa and Lindi areas of coastal Tanzania: Tanzania Drilling Project Sites 1–5. Journal of African Earth Sciences 39, 25–62.

Pearson, P.N., Olsson, R.K., Hemleben, C., Huber, B.T., and Berggren, W.A., 2006. Atlas of Eocene Planktonic Foraminifera, Cushman Foundation of Foraminiferal Research Special Publication 41, 514.

Pearson, P.N., Van Dongen, B.E., Nicholas, C.J., Pancost, R.D., Schouten, S., Singano, J.M., Wade, B.S., 2007. Stable warm tropical climate through the Eocene Epoch. Geology 35, 211–214.

Perch–Nielsen, K., 1985. Cenozoic calcareous nannofossils. In: Bolli, H.M., Saunders, J.B., Perch–Nielsen K., (Eds.), Plankton Stratigraphy, Cambridge University Press, UK, 427–554.

Persico, D., and Villa, G. 2004. Eocene–Oligocene calcareous nannofossils from Maud Rise and Kerguelen Plateau (Antarctica): Paleoecological and paleoceanographic implications. Marine Micropaleontology, 52, 153–179.

Petrizzo, M.R. 2005. An early late Paleocene event on Shatsky Rise, northwest Pacific Ocean (ODP Leg 198): evidence from planktonic foraminiferal assemblage. Proceedings of the Ocean Drilling Program, Scientific Results, College Station, Texas, 1–29.

Pirkenseer C., King, C., Steurbaut, E., Speijer, R., 2009. Early Eocene biota (ostracoda, foraminifera) and paleoenvironment of the Blue Marls in the Corbieres Hills (Aude, France): building a framework for the identification of early Eocene hyperthermals in continental margin records. European Geophysical Union, General Assembly, Geophysical Research Abstract 11, 12518.

Pospichal, J.J., 1995. Cretaceous/Tertiary boundary calcareous nannofossils from Agost, Spain. In: Flores, J.A., Sierro, F.J. (Eds.), 5th INA Conference in Salamanca 1993 Proceedings. Universidad de Salamanca, Salamanca, 185–217.

Pospichal, J.J., 1996. Calcareous Nannoplankton Mass Extinction at the Cretaceous/Tertiary Boundary: An Update. In: Ryder, G., Fastovsky, D., Gartner, S. (Eds.), The Cretaceous–Tertiary Event and Other Catastrophes in Earth History, Geological Society of America, Special Paper 307, 335–359.

Preisinger, A., Aslanian, S., Stoykova, K.F., Grass, F., Mauritsch, H.J., Scholger, R., 1993. Cretaceous–Tertiary boundary sections on the coast of the Black Sea near Bjala (Bulgaria). Palaeogeography, Palaeoclimatology, Palaeoecology 104, 219–228.

Premoli–Silva, I., Boersma, A., 1986. Paleogene biofacies of the western North Atlantic, The western North Atlantic region: in Vogt, P.R., Tucholke, B.E., (eds.), The Geology of North America. The Geological Society of America, Boulder, Colorado M, 527–546.

Premoli Silva, I., Boersma, A., 1988. Atlantic Eocene planktonic foraminiferal historical biogeography and palaeohydrographic indices. Palaeogeography, Palaeoclimatology, Palaeoecology 67, 315–356.

Premoli Silva, I., Jenkins, D.G., 1993. Decision on the Eocene–Oligocene boundary stratotype. Episodes 16, 379–382.

Premoli–Silva, I., Spezzaferri, S., 1990. Paleogene planktonic foraminifer biostratigraphy and paleoenvironmental remarks on Paleogene sediments from Indian Ocean sites, Leg 115.

Premoli Silva, I., Coccioni, R., Montanari, A., (eds) 1988. The Eocene–Oligocene Boundary in the Marche–Umbria Basin (Italy). International Subcommission on Paleogene Stratigraphy, Special Publication, Industrie Grafiche Fratelli Aniballi, Ancona, 268.

Pross, J., Houben, A.J.P., Van Simaeys, S., Williams, G.L., Kotthoff, U., Coccioni, R., Wilpshaar, M., Brinkhuis H., 2010. Umbria–Marche revisited: a refined magnetostratigraphic calibration of dinoflagellate cyst events for the Oligocene of the western Tethys. Review of Palaeobotany and Palynology 158, 213–235.

Prothero, D.R., 1994. The Eocene–Oligocene transition: Paradise lost. New York, Columbia University Press, 73–164.

Pujalte, V., Payros, A., Apellaniz, E., 2009. Climate and Biota of the Early Paleogene: recent advances and new perspectives. Geologica Acta 7, 1–9.

Quillévéré, F., Norris, R.D., Kroon, D., Wilson, P.A., 2008. Transient ocean warming and shifts in carbon reservoirs during the early Danian. Earth and Planetary Science Letters 265, 600–615.

Raffi, I., Backman, J., Zachos, J.C., and Sluijs, A. 2009. The response of calcareous nannofossil assemblages to the Paleocene Eocene Thermal Maximum at the Walvis Ridge in the South Atlantic. Marine Micropaleontology, 70, 201–212.

Raymo, M.E. and W.F. Ruddiman, 1992. Tectonic forcing of late Cenozoic climate. Nature 359, 117–122.

Retallack, G.J., 2009. Greenhouse crises of the past 300 million years. Geological Society of American Bulletin 121, 1441–1454.

Rey, M., 1939. Distribution stratrigraphique des Hantkenina dans le Nummulitique du Rharb (Maroc). Bulletin de la Société Géologique de France 5, 321–341 (in French).

Rio, D., Fornaciari, E., and Raffi, I., 1990. Late Oligocene through early Pleistocene calcareous nannofossils from western equatorial Indian Ocean (Leg 115). Proceeding of Ocean Drilling Project, Scientific Results 115, College Station, TX, 175–235.

Robinson, N., Ravizza, G., Coccioni, R., Peucker–Egrenbrink, B., Norris, R. 2009. A high–resolution marine 187Os/188Os record for the late Maastrichtian: distinguishing the chemical fingerprints of Deccan volcanism and the KP impact event. Earth Planetary Science Letters, 281, 159–168

Rögl, F., Egger, H., 2010. The missing link in the evolutionary origin of the foraminiferal genus *Hantkenina* and the problem of the lower–middle Eocene boundary. Geology 38, 23–26.

Rögl, F., Egger, H., 2011. A new planktonic foraminifera species (*Hantkenina gohrbandti* nov. spec.) from the middle Eocene of the northwestern Tethys (Mattsee, Austria). Austrian Journal of Earth Sciences 104, 4–14.

Rögl, F., Perch–Nielsen, K., Preisinger, A., Aslanian, S., Summesberger, H., 1996. Stratigraphy across the Cretaceous/Paleogene Boundary near Bjala, Bulgaria. In: Jardine, S., Klasz, J., Delenay, J.–P. (Eds.), Géologie de l'Afrique e de l'Atlantique sud: Actes Colloques Angers, 1994. Elf Aquitanie Edition, Angers, France, 673–683.

Röhl, U., Norris, R.D., and Ogg, J.G., 2003, Cyclostratigraphy of upper Paleocene and late Eocene sediments at Blake Nose Site 1051 (western North Atlantic), in Wing, S.L., et al., eds., Causes and consequences of globally warm climates in the early Paleogene. Geological Society of America, Special Paper 369, 567–588.

Röhl, U., Westerhold, T., Bralower, T.J., Petrizzo, M.–R., Zachos, J.C., 2004. An Early Late Paleocene Global Dissolution Event and New Constraints for an Astronomically–Tuned Early Paleogene Time Scale, Abstract. 8th International Conference on Paleoceanography, Biarritz, France.

Röhl, U., Westerhold, T., Bralower, T.J., Zachos, J.C., 2007. On the duration of the Paleocene–Eocene thermal maximum (PETM). Geochemistry, Geophysics, Geosystems 8, Q12002.

Röhl, U., Westerhold, T., Monechi, S., Thomas, E., Zachos, J.C., Donner, B., 2005. The third and final EarlyEocene thermal maximum: Characteristics, timing, and mechanisms of the "X" event. Geological Society of America, Abstracts with Programs, 37, 264.

Röhl, U., Westerhold, E., Thomas, E., Monechi, and S., Donner 2009. New focus on the early Eocene Greenhouse World: rates and dates of ancient global warming events or what makes the X event special. European Geophysical Union, General Assembly, Geophysical Research Abstract, 11, 4218.

Romein, A.J.T., 1979. Lineages in early Paleogene calcareous nannoplankton. Utrecht micropaleontological bulletins 22, 231.

Ross, C.A., Ross, J.R.P., 1984. Geology of Coal., John Wiley, Hoboken, N.J., 349.

Roth, P.H., and Thierstein, H., 1972, Calcareous nannoplankton: Leg 14 of the Deep Sea Drilling Project, in Hayes, D.E., et al., Initail Reports, Deep Sea Drilling Project, 14. Washington, D.C., U.S. Government Printing Office, 421–485.

Royer, D.L., 2006. CO_2–forced climate thresholds during the Phanerozoic: Geochimica et Cosmochimica Acta 70, Special Issues 23, 5665–5675.

Scher, H.D., Martin, E.E., 2004. Circulation in the Southern Ocean during the Paleogene inferred from neodymium isotopes. Earth and Planetary Science Letters 228, 391–405.

Schnitker, D., 1980. Global paleoceanography and its deep water linkage to the Antarctic glaciations. Earth Science Reviews 16, 1–20.

Schouten, S., Woltering, M., Rijpstra, W. I. C., Sluijs, A., Brinkhuis,H., Sinninghe Damste´, J. S. 2007. The Paleocene–Eocene carbon isotope excursion in higher plant organic matter: Differential fractionation of angiosperms and conifers in the Arctic. Earth and Planetary Science Letters 258, 581–592.

Schroeder, C.J., Scott, D.B., Medioli, F.S., 1987. Can smaller foraminifera be ignored in paleoenvironmental analyses? Journal of Foraminiferal Research 17, 101–105.

Scopelliti, G., Bellanca, A., Neri, R., Francois, B., Coccioni, R., 2006. Comparative high–resolution chemostratigraphy of the Bonarelli Level from the reference Bottaccione section (Umbria–Marche Apennines) and from an equivalent section in NW Sicily: Consistent and contrasting responses to the OAE2. Chemical Geology 228, 266–285.

Secord, R., Gingerich, P.D., Lohmann, K.C., MacLeod, K.G., 2010. Continental warming preceding the Palaeocene–Eocene thermal maximum. Nature 467, 955–958.

Self, S., Blake, S., Sharma, K., Widdowson, M.,

Sephton, S., 2008. Sulfur and Chlorine in Late Cretaceous Deccan Magmas and Eruptive Gas Release. Science 319, 1654–1657.

Sexton, P.F., Norris, R.D., Wilson, P.A., Pälike, H., Westerhold, T., Röhl, U., Bolton, C.T., Gibbs, S., 2011. Eocene global warming events driven by ventilation of oceanic dissolved organic carbon. Nature 471, 349–352.

Sexton, P.F., Wilson, P.A. and Norris, R.D. 2006. Testing the Cenozoic multisite composite δ18O and δ13C curves: new monospecific Eocene records from a single locality, Demerara Rise (Ocean Drilling ProgramLeg 207). Paleoceanography 21, PA2019.

Shackleton, N.J., 1986. Paleogene stable isotope events, Palaeogeography, Palaeoclimatology, Palaeoecology 57, 91–102.

Shackleton, N.J., Kennett, J.P., 1975. Paleotemperature history of the Cenozoic and the initiation of Antarctic glaciation: Oxygen and carbon isotope analyses, in Kennett, J.P., Houtz, R.E., et al., DSDP Sites 277, 279, and 281: Initial Reports of the Deep Sea Drilling Project, 29, Washington, D.C., Government Printing Office, 743–755.

Shokhina, V.A., 1937. The genus Hantkenina and its stratigraphical distribution in the North Caucasus: Problems of Paleontology. Publication of the Laboratory of Palaeontology, Moscow University 2–3, 425–452.

Short, D.A., Mengel, J.G., Crowley, T.J., Hyde, W.T., North, G.R., 1991. Filtering of Milankovitch cycles by earth's geography, Quaternary Research, N.Y. 35, 157–173.

Sigman, D.M.., De Boer, A.M., Haug, G.H., 2007. Antarctic stratification, atmospheric water vapor, and Heinrich events: A hypothesis for late Pleistocene deglaciations, in Past and Future Changes of the Oceanic Meridional Overturning Circulation: Mechanisms and Impacts, Schmittner, A., Chiang, J.H.C., Hemming, S.R., (eds), American Geophysical Union, Geophysical Monograph 173, 335–350, 2007.

Sinton, C.W., Duncan, R.A., 1998. 40Ar/39Ar ages of lavas from the southeast Greenland margin, ODP Leg 152, and the Rockall Plateau, DSDP Leg 81, Proceeding of Ocean Drilling Program, Scientific Results 152, 387–402.

Slotnick, B.S., Dickens, G.R., Nicolo, M.J., Hollis, C.J., Crampton, J.S., Strong, C.P., Zachos, J.C., Sluijs, A., Lourens, L., Lauretano, V., 2011. Large amplitude variations in carbon cycling and terrestrial weathering during the latest Paleocene and earliest Eocene. Climate Biota of the Early Paleogene, Salzburg, June 5th–8th, Berichte der Geologischen Bundesanstalt 85, 151.

Sluijs, A., Brinkhuis, H., 2009. A dynamic climate and ecosystem state during the Paleocene–Eocene Thermal Maximum—Inferences from dinoflagellate cyst assemblages at the New Jersey Shelf. Biogeosciences 6, 1755–1781.

Sluijs, A., Brinkhuis, H.,Crouch, E.M., John, C.M., Handley, L., Munsterman, D., Bohaty, S.M., Zachos, J.C., Reichart, G.J., Schouten, S., Pancost, R.D., Sinninghe Damsté, J.S., Welters, N.L.D., Lotter, A.F., Dickens, G.R., 2008b. Eustatic variations during the Paleocene–Eocene greenhouse world. Paleoceanography 23, PA4216.

Sluijs, A., Brinkhuis, H., Schouten, S., Zachos, J. C., John, C.M., Bohaty, S., Sinninghe Damsté, J.S., Crouch, E.M., 2007. Environmental precursors to light carbon input at the Paleocene/Eocene boundary. Nature 450, 1218–1221.

Sluijs, A., Röhl, U., Schouten, S., Brumsack, H.–J., Sangiorgi, F., Sinninghe Damsté, J.S., Brinkhuis, H., 2008a. Arctic Late Paleocene–Early Eocene paleoenvironments with special emphasis on the Paleocene–Eocene thermal maximum (Lomonosov Ridge, IODP Expedition 302). Paleoceanography 23, PA1S11.

Sluijs, A., Schouten, S., Donders, T.H., Schoon, P.L., Röhl, U., Reichart, G.–J., Sangiorgi, F., Kim, J.–H., Sinninghe Damste, J.S., Brinkhuis, H., 2009. Warm and wet conditions in the Arctic region during Eocene Thermal Maximum 2. Nature Geoscience 2, 777–780.

Smit, J., 1982. Extinction and evolution of planktonic foraminifera after a major impact at the Cretaceous/Tertiary boundary. In: Silver, L.T., Schultz, P.H. (Eds.), Geological Implications of Impacts of large Asteroids and Comets on the Earth, Geological Society of America, Special Paper 190, 329–352.

Smith, E.M., Carroll, A.R., Mueller, E.R., 2008. Elevated weathering rates in the Rocky Mountains during the Early Eocene Climatic Optimum, Nature Geoscience 1, 370–374.

Speed, C.D., Kroon, D., 2000. Data report: inorganic geochemistry and mineralogy of the Cretaceous/Tertiary boundary section in Hole 1049C. In Kroon, D., Norris, R.D., and Klaus, A. (Eds.), Proceeding of Ocean Drilling Project, Scientific Results 171B, College Station, TX (Ocean Drilling Program),

1–26.

Speijer, R.P., 2000. The late Paleocene event and a potential precursor compared: first results from Egypt. Transactions of the Geological Society in Stockholm 122, 150–151.

Speijer, R.P., 2003. Danian–Selandian sea–level change and biotic excursion on the southern Tethyan margin (Egypt). In: Wings, S.L., Gingerich, P.D., Schmitz, B., Thomas, E., (eds) Causes and Consequences of Globally Warm Climates in the Early Paleogene. Geological Society of America Special Paper 369, 275–290.

Speijer, R.P., Bornemann, A., Kouwenhoven, T.J., Pirkenseer, C., Schulte, P., Stassen, P., Steurbaut, E., 2011. Identification and characterization of early Eocene hyperthermals in shallow marine sequences. Climate Biota of the Early Paleogene, Salzburg, June 5th–8th, Berichte der Geologischen Bundesanstalt 85, 154.

Spezzaferri, S., Basso, D., Coccioni, R., 2002. Late Eocene planktonic foraminiferal response to an extraterrestrial impact at Massignano GSSP (northeastern Apennines, Italy). Journal of Foraminiferal Research 32, 188–199.

Spötl, C., Vennemann, T.W., 2003. Continuous–flow isotope ratio mass spectrometric analysis of carbonate mineral. Rapid Communications in Mass Spectrometry 17, 1004–1006.

Sprong, J., Youssef, M., Bornemann, A., Schulte, P., Steurbaut, E., Stassen, P., Kouwenhoven, T., Speijer, R., 2011 A multi–proxy record of the Latest Danian Event at Gebel Qreiya, Eastern Desert. Egypt Journal of Micropalaeontology 30, 167–182.

Stap, H.L., Lourens, L.J., Thomas, E., Sluijs, A., Bohaty, S., Zachos, J.C., 2010a. High–resolution deep–sea carbon and oxygen isotope records of Eocene Thermal Maximum 2 and H2. Geology 38, 607– 610.

Stap, H.L., Lourens, L.J., Van Dijk, A., Schouten, S., Thomas, E., 2010b. Coherent pattern and timing of the carbon isotope excursion and warming during Eocene Thermal Maximum 2 as recorded in planktic and benthic foraminifera. Geochemistry, Geophysics, Geosystems 11, Q11011.

Stap, L., Sluijs, A., Thomas, E., Lourens, L. 2009. Patterns and magnitude of deep sea carbonate dissolution during Eocene Thermal Maximum 2 and H2, Walvis Ridge, southeastern Atlantic Ocean. Paleoceanography, 24, PA1211.

Steineck, P.L., 1971. Phylogenetic reclassification of paleogene planktonic foraminifera. The Texas Journal of Science 23, 167–178.

Subbotina, N.N., 1958. New genera and species of foraminifera. In: Bykova, N.K. (Ed.), Microfauna of the USSR. Vsesoyznogo Neftyanogo Nauchno–Issledovatel'skogo Geologo–Razvedochnogo Instituta (VNIGRI), Leningrad, 115, Sb. 9, 58.

Svensen, H., Planke, S., Malthe–Sørenssen, A., Jamtveit, B., Myklebust, R., Eidem T.R., Rey S.S., 2004. Release of methane from a volcanic basin as a mechanism for initial Eocene global warming. Nature 429, 542–545.

Stott, L.D., Kennett, J.P., 1990. The paleoceanographic and paleoclimatic signature of the K/P boundary in the Antarctic: stable isotopic results from ODP Leg 113. Proc. Ocean Drilling Program Scientific Results 113, 829–848.

Sztrákos, K., 2005. Paleocene and lowest Eocene foraminifera from the North Pyrenean trough (Aquitaine, France). Revue de Micropaléontologie 48, 175–236.

Takano, Y., Hagino, K., Tanaka, Y., Horiguchi, T. Okada, H., 2006. Phylogenic affinities of an enigmatic nannoplankton, *Braarudosphaera bigelowii*, based on the SSU rDNA sequences. Marine Micropaleontology 60, 145–156.

Thalmann, H.E., 1932. Die Foraminiferen–Gattung Hantkenina Cushman 1924 und ihre regional–stratigraphische Verbreitung. Ecolgae Geologicae Helvetiae 25, 287–292.

Thalmann, H.E., 1942. Foraminiferal genus Hantkenina and its subgenera. American Journal of Science 240, 809–820.

Thomas, D.J., 2004. Evidence for deep–water production in the North Pacific Ocean during the early Cenozoic warm interval. Nature 430, 65–68.

Thomas, D.J., Zachos, J.C., Bralower, T.J., Thomas, E., Bohaty, S., 2002. Warming the fuel for the fire: evidence for the thermal dissociation of methane hydrate during the Paleocene–Eocene thermal maximum. Geology 30, 1067–1070.

Thomas, E., 1990. Late Cretaceous through Neogene deep–sea benthic foraminifers (Maud Rise, Weddell Sea, Antarctica). Proc. ODP, Sci. Res. 113, 571–594.

Thomas, E., 1998. Review of "Deep–sea benthic foraminifera from Cretaceous – Paleogene boundary strata in the South Atlantic – taxonomy and paleoecology". In: Widmark, J. (Ed.), Fossils and Strata, 43. Palaeogeography, Palaeoclimatology, Palaeoecology 142, 87–88.

Thomas, E., 2003. Extinction and food at the seafloor: a high–resolution benthic foraminiferal

record across the Initial Eocene Thermal Maximum, Southern Ocean Site 690. In: Wing, S.L., Gingerich, P.D., Schmitz, B., Thomas, E. (Eds.), Causes and Consequences of GloballyWarm Climates in the Early Paleogene. Geological Society of America, Special Paper 369, 319–332.

Thomas, E. 2007. Cenozoic mass extinctions in the deep sea: What disturbs the largest habitat on Earth? In: Monechi, S., et al. (eds) Large Ecosystem Perturbations: Causes and Consequences, edited by Geological Society of America, Special Paper 424, 1–23.

Thomas, E., Brinkhuis, H., Huber, M., Röhl, U., 2006. An ocean view of the early Cenozoic Greenhouse World. Oceanography 19, 63–72.

Thomas, E., Zachos, J.C., 2000. Was the late Paleocene thermal maximum a unique event? Stockholm Geological Society Transactions 122, 169–170.

Thomas, E., Foster, L., Schmidt, D., Röhl, U., Zachos, J.C. 2011. Life in the deep–sea during Eocene Hyperthermal Events. Climate Biota of the Early Paleogene, Salzburg, June 5th–8th, Berichte der Geologischen Bundesanstalt, 85, 159.

Thomas, E., Röhl, U., Monechi, S., Westerhold, T., Balestra, B., Morelli, G., 2006. An early Eocene hyperthermal event at ~52.5 Ma, in: Caballero, F., Apellaniz, E., Baceta, J.I., Bernaola, G., Orue–Etxebarria, X., Payros, A., and Pujalte, V. (eds) Climate and Biota of the Early Paleogene 2006, Bilbao, Volume of Abstracts, 136.

Thomas, E., Zachos, J. C., Bralower, T. J. 2000. Deep sea environments on a warm Earth: Latest Paleocene–early Eocene, in: Huber, B.T., MacLeod, K.G., Wing, S.L. (eds) Warm Climates in Earth History. Cambridge University Press, Cambridge, UK, 132– 160.

Tjalsma, R.C., Lohmann, G.P., 1983. Paleocene–Eocene bathyal and abyssal benthic foraminifera from the Atlantic Ocean. Micropaleontology, Special Publication 4.

Toumarkine, M., 1981. Discussion de la validité de l'espécè Hantkenina aragonensis Nuttall, 1930. Description de Hantkenina nuttalli n. sp.. Cahiers de Micropaléontologie 4, 109–119.

Toumarkine, M., Lutherbacher, H.P., 1985. Paleocene and Eocene planktonic foraminifera. In: Bolli, H.M., Saunders, J.B., Perch–Nielsen, K. (Eds.), Plankton stratigraphy. Cambridge University Press, Cambridge, 87–154.

Tremolada, F., Bralower, T.J., 2004. Nannofossil assemblage fluctuations during the Paleocene–Eocene Thermal Maximum at Sites 213 (Indian Ocean) and 401 (North Atlantic Ocean): palaeoceanographic implications. Marine Micropaleontology 52, 107–116.

Tripati, A., Zachos, J.C., 2000. Paleocene and Eocene Coastal Temperatures, Transactions of the Geological Society in Stockholm 122, 171–172.

Tripati, A., Backman, J., Elderfi eld, H., Ferretti, P., 2005,. Eocene bipolar glaciation associated with global carbon cycle changes. Nature 436, 341–346.

Tripati, A., Delaney, M.L., Zachos, J.C., Anderson, L.D., Kelly, D.C., Elderfield, H., 2003. Tropical Sea–Surface Temperature Reconstruction for the Early Paleogene Using Mg/Ca Ratios of Planktonic Foraminifera. Paleoceanography 18, 1101.

Tripati, A., Eagle, R.A., Dawber, C.F., Morton, A., Dowdeswell, J.A., Atkinson, K., Bahe, Y., Khadun, E., Shaw, R.M.H., Shorttle, O., Thanabalasundaran, L., 2008. Evidence for Northern Hemipshere glaciation back to 44 Ma from ice–rafted debris in the Greenland Sea. Earth and Planetary Science Letters 256, 112–122.

Tripati, A., Zachos, J.C., Marincovich Jr., L., Bice, K., 2001. Late Paleocene Arctic Coastal Climate as Inferred from Molluscan Stable and Radiogenic Isotope Ratios. Palaeogeography, Palaeoclimatology, Palaeoecology 170, 101–113.

Turchyn, A.V., Schrag, D.P., Coccioni, R., Montanari, A., 2009. Stable isotope analysis of the Cretaceous sulfur cycle. Earth and Planetary Science Letters 285, 115–123.

Vail, P.R., Hardenbol, J., 1979. Sea–level changes during the tertiary. Oceanus 22, 171–179.

Valdes, P.J., Glover, R.W., 1999. Modelling the climate response to orbital forcing. The Royal Society of London. Philosophical Transactions. Series A. Mathematical, Physical and Engineering Sciences. Royal Society of London 357, 1873–1890.

Van Heck, S.E., Prins, B., 1987. A refined nannoplankton zonation for the Danian of the central North Sea. In: Stradner, H., and Perch–Nielsen, K., (Eds.), International Nannoplankton Association Vienna Meeting 1985 Proceedings, Abhandlungen der Geologischen Bundesanstalt 39, 285–303.

Van Morkhoven, F.P.C.M., Berggren, W.A., Edwards, A.S., 1986. Cenozoic cosmopolitan deep–water benthic Foraminifera. Bull. Cent. Rech. Exploration–Production Elf–Aquitaine, Memoire 11, 423.

Venuti, V., Florindo, F., Caburlotto, A., Hounslow,

M.W., Hillenbrand, C–D., Strada, E., Talarico, F.M., Cavallo, A., 2011. Late Quaternary sediments from deep–sea sediment drifts on the Antartic Peninsula Pacific margin: Climatic control on provenance of minerals. Journal of Geophysical Research 116, B066104.

Venuti, V., Florindo, F., Michel, E., Hall, I.R. 2007. Magnetic proxy for the deep (Pacific) western boundary current variability across the mid–Pleistocene climate transition. Earth and Planetary Science Letters, 259, 107–118.

Verosub, K.L., and Roberts, A. P. 1995. Environmetnal magnetism: past, present, and future. Journal of Geophysical Research, 100, 2175–2192.

Via, R.K., Thomas, D.J., 2006. Evolution of Atlantic Thermohaline Circulation–Timing of the onset of Deep–water Production in the North Atlantic. Geology 34, 441–444.

Villa, G., Fioroni, C., Pea, L., Bohaty, S., Persico, D., 2008. Middle Eocene–late Oligocene climate variability: Calcareous nannofossil response at Kerguelen Plateau, Site 748. Marine Micropalaeontology 169, 173–192.

Wade, B.S., Pearson, P.N., Berggren, and W.A., Pälike, H. 2011. Review and revision of Cenozoic tropical planktonic foraminiferal biostratigraphy and calibration to the geomagnetic polarity and astronomical time scale. Earth−Science Reviews, 104, 111–142.

Walker, J.C.G., Hays, P.B., Kasting, J.F., 1981. A negative feedback mechanism for the long–term stabilization of earth's surface temperature. Journal of Geophysical Research 86, 9776–9782.

Warwick, P.D., Stanton, R.W., 1988. Depositional models for 2 tertiary coal–bearing sequences in the Powder River Basin, Wyoming, USA. Journal of Geological Society 145, 613–620.

Wei, W., Pospichal, J.J., 1991. Danian Calcareous Nannofossil Succession at Site 738 in the Southern Indian Ocean. In: Barron, J., Larsen, B., et al. (Eds.), Proceeding of Ocean Drilling Project, Scientific Results 119. College Station, TX, 495–512.

Westerhold, T., Röhl, U., 2009. High resolution cyclostratigraphy of the early Eocene–new insights into the origin of the Cenozoic cooling trend. Climate of the Past 5, 309–327.

Westerhold, T., Röhl, U., Donner, B., McCarren, H.K., Zachos, J.C., 2011. A complete high–resolution Paleocene benthic stable isotope record for the central Pacific (ODP Site 1209). Paleoceanography, PA2216.

Westerhold, T., Röhl, U., Laskar, J., Raffi, I., Bowles, J., Lourens, L.J., Zachos, J.C., 2007. On the duration of magnetochrons C24r and C25n andthe timing of early Eocene global warming events: Implications from the Ocean Drilling Program Leg 208 Walvis Ridge depth transect. Paleoceanography 22, PA2201.

Westerhold, T., Röhl, U., Raffi, I., Fornaciari, E., Monechi, S., Reale, V., Bowles, J., Evans, H.F., 2008. Astronomical calibration of the Paleocene time. Palaeogeography, Palaeoclimatology, Palaeoecology 257, 377–403.

Wing, S.L., Gingerich, P.D., Schmitz, B., Thomas, E. (eds) 2003. Causes and Consequences of Globally Warm Climates in the Early Paleocene. Geological Society of America Special Paper 369, Boulder, Colorado.

Wing, S.L., Harrington, G.J., Smith, F.A., Bloch, J.I., Boyer, D.M., Freeman, K.H., 2005. Transient floral change and rapid global warming at the Paleocene–Eocene boundary. Science 310, 993–996.

Wise, S.W., Gombos, A.M., Muza, J.P., 1985. Cenozoic evolution of polar water masses, southwest Atlantic Ocean, in Hsii, K., Weissert, H.J., (eds), South Atlantic. Paleoceanography, Cambridge (England), Cambridge University Press, 283–324.

Woodburne, M.O., Gunnell, G.F., Stuckey, R.K., 2009. Land mammal faunas of North America rise and fall during the Early Eocene climatic optimum. Denver Museum of Nature and Science Annals 1, 74.

Youssef Ali, M., 2009. High resolution calcareous nannofossil biostratigraphy and paleoecology across the Latest Danian Event (LDE) in central Eastern Desert, Egypt, Marine Micropaleontology 72, 111–128.

Zachos, J., Pagani, M., Sloan, L., Thomas, E., Billups, K., 2001. Trends, Rhythms, and Aberrations in Global Climate 65 Ma to Present. Science 292, 686–693.

Zachos, J.C., Arthur, M.A., Dean, W.E., 1989. Geochemical Evidence for Suppression of Pelagic Marine Productivity at the Cretaceous/Tertiary Boundary. Nature 337, 61–64.

Zachos, J.C., Breza, J., Wise, S. W., 1992. Earliest Oligocene Ice–sheet Expansion on East Antarctica: Stable Isotope and Sedimentological Data from Kerguelen Plateau. Geology 20, 569–573.

Zachos, J.C., Dickens, G.R., Zeebe R.E., 2008. An early Cenozoic perspective on greenhouse warming

and carbon cycle dynamics. Nature 451, 279–283.

Zachos, J.C., Kroon, D., and 25 others, 2004. Early Cenozoic extreme climates: The Walvis Ridge transect: Proc. ODP, Leg 208: http:// www–odp.tamu.edu/publications/208–IR/208ir.htm.

Zachos, J.C., Lohmann, K.C., Walker, J.C.G., Wise, S.W., 1993. Abrupt Climate Change and Transient Climates in the Paleogene: A Marine Perspective. Journal of Geology 100, 191–213.

Zachos, J.C., McCarren, H., Murphy, B., Röhl, U., and Westerhold, T. 2010. Tempo and Scale of Late Paleocene and Early Eocene Carbon Isotope Cycles: Implications for the Origin of Hyperthermals. Earth and Planetary Science Letters, 299, 242–249.

Zachos, J.C., Pagani, M., Sloan, L., Thomas, E., Billups, K. 2001. Trends, Rhythms, and Aberrations in Global Climate 65 Ma to Present. Science, 292, 686–693.

Zachos, J.C., Quinn, T.M., and Salamy, K. 1996. High resolution (104 yr) deep–sea foraminiferal stable isotope time series. Paleoceanography 11, 251–266.

Zachos, J.C., Röhl, U., Schellenberg, S.A., Sluijs, A., Hodell, D.A., Kelly, D.C., Thomas, E., Nicolo, M., Raffi, I., Lourens, L.J., McCarren, H., Kroon, D., 2005. Rapid Acidification of the Ocean During the Paleocene–Eocene Thermal Maximum. Science 308, 1611–1615.

Zachos, J.C., Schouten, S., Bohaty, S., Quattlebaum, T., Sluijs, A., Brinkhuis, H., Gibbs, S.J., Bralower, T.J., 2006. Extreme warming of mid–latitude coastal ocean during the Paleocene–Eocene Thermal Maximum: inferences from TEX86 and isotope data. Geology 34, 737–740.

Zachos, J.C., Stott, L.D., Lohman, K.C., 1994. Evolution of early Cenozoic marine temperatures. Paleoceanography 9, 358–387.

Zachos, J.C., Wara, M.W., Bohaty, S., Delaney, M.L., Petrizzo, M.R., Brill, A., Bralower, T.J., Premoli–Silva, I., 2003. A transient rise in tropical sea surface temperature during the Paleocene–Eocene thermal maximum. Science, 302, 1551–1554.

Zeebe, R.E., Zachos, J.C., 2007. Reversed deep–sea carbonate ion basin–gradient during the Paleocene–Eocene Thermal Maximum. Paleoceanography 22, 1–17.

Acknowledgements

There are a number of people without this PhD project and Thesis might not have been finished and written, and to whom I am greatly indebted.

This Thesis would not have been possible without the guidance of my promoter Prof. Rodolfo Coccioni. His sage advice, insightful criticisms, and patient encouragement aided the writing of this thesis in innumerable ways and his continuing patience, support and guidance have been invaluable to me throughout my PhD period.

Integrated analysis requires a large number of data from different sources. Hence, deep thanks and appreciation are due to many specialists without might not have been possible to integrate at high-resolution litho–, bio–, magneto–, chemostratigraphic data to discover and reveal the paleoenviromental perturbations described in previous chapters. For this reason, I wish to thank Mario Sprovieri for geochemical analyses, Rita Catanzariti and Eliana Fornaciari for calcareous nannoplankton analyses, Luigi Jovane and Jairo Savian for magnetostratigraphic and environmental magnetisms analyses.

Many thanks go to the technical staff in Urbino University. Obviously, my direct colleague working on benthic foraminifera has been of great help Dr. Fabrizio Frontalini made my working time more than a pleasure, Dr. Marianna Sideri and Dr. Carla Bucci, helped me in the office and in the lab: I could not have wished for more supportive and stimulating colleagues. I would also like to thank Dr. Sara Paletta for her practical assistance and sample preparation.

Very special thank goes to my parents, who even though they have no clue of what I am doing, always encouraged my choices and my steps of life.

Most important of all, my love and thank go to Daiana, who makes my life so beautiful.